Chapter IV

Results and Discussion

Chapter IV

RESULTS AND DISCUSSION

This chapter presents the results and discussions of the study for fulfilling the objectives of the present investigation. Also, it relates the findings to the research questions and summarizes if the findings support or nullify any hypothesis being proposed. Besides, the findings of the study are related to previous research findings and theoretical thinking.

4.1 Influence of germination conditions on malting potential of paddy and changes in enzymatic activity and physico-chemical properties

4.1.1 Malting potential of rice

The evaluation of malting potential of paddy assists in ensuring good germination during the process of malting and ensures maximum germination of grains. Thereby three parameters were investigated i.e. germination rate, germination capacity and dormancy rate.

4.1.1.1 Germination rate (GR), Germination Capacity (GC) and Dormancy rate (DR)

The germination of two paddies with different amylose content (low and intermediate amylose) was conducted at four different temperatures (25, 30, 35 and 40°C) and their malting potential is shown in Table 4.1. Embryo development which results in germination was not detected in paddy germinated at 25 and 40°C for 120h. This result was found in contradiction to the work reported by Capanzana [25] where germination was observed at temperatures less than 20°C and more than 40°C in high amylose rice of Australia.

The germination at 25 and 40°C was not visible in the paddy used, henceforth no further analysis was undertaken. The reason behind for non-emergence of radicles may be due to controlling parameters viz. synthesis of Gibberellic acid (GA) and loosening of cell wall of endosperm and testa [74].

The seeds unable to produce GA (dominating hormone for germination) are not able to complete the process of germination. The emergence of radicle from the seed indicates the completion of the germination process during which radicle breaks through the surrounding tissues such as endosperm and the testa. However, in some species the embryo growth potential is incapable of exceeding the mechanical resistance imposed by these tissues leading to physical dormancy. This literature also reported other factors which affect the radicle emergence such as gene encoding components of protein synthesis, ribosomes, photosynthetic genes, DNA synthesis, cell cycle and cell wall remodelling enzymes which are present in the embryo during germination.

Significant ($p<0.05$) changes were observed in malting potential (GR, GC and DR) for both malted rice at 30 and 35°C for 120h. The malting conditions i.e. germination temperature, time and their interaction had significant effect on malting potential of both rice. The maximum GR and GC were observed at 120h of germination for both LAR and IAR germinated at 30 and 35°C respectively. The DR decreased significantly during the period of germination at 30 and 35°C for both LAR and IAR. The GC and GR of IAR was observed to be higher than LAR at both germination temperature. Thereby, the higher decrease in DR was found in IAR as compared to LAR. In this study the germination capacity of both the LAR and IAR rice were higher than that reported by Adebowale [2] in Ofada rice of Nigeria (87.33%) and comparable to that of Sorghum (92%). This indicated high malting potential of both LAR and IAR at 30 and 35°C germination. The higher malting potential of IAR and LAR may be due to the higher synthesis of GA as already discussed in this section.

4.1.1.2 Malting yield and malting loss

Malting loss indicates the conversion of higher molecules (starch) to simpler molecules. Malting yield and loss measured for two different rice at different germination conditions are presented in Fig 4.1. The malting loss of LAR and IAR increased significantly ($p<0.05$) during 120h of germination at 30 and 35°C. The maximum malting loss in LAR and IAR was exhibited at 120h for 30 and 35°C germination respectively. The malting loss of IAR was found to be higher than LAR paddy at both the germination temperature. The malting yield conversely, decreased significantly ($p<0.05$) for both LAR and IAR during the germination period of 120h. The results revealed that the decrease in malting yield of IAR was significantly higher than LAR paddy. This may be due to the higher malting potential of IAR as observed in this study. The interaction of time and temperature was observed to have significant effect ($p<0.05$) on the malting yield and loss. The higher germination rate leads to various metabolic activities and chemical changes in the endosperm [10]. There is increase in the rate of respiration of the aleuron layer due to the development of rootlet or radical by the process of mitotic divisions which contributes to higher respiration [45]. The main respiratory substrate is initially the stored compounds such as carbohydrate and small amount of lipids present in the endosperm which is degraded by hydrolytic enzymes to smaller biomolecules to provide the necessary energy for tissue development [74]. This process along with the removal of vegetative shoots is mainly responsible for the decline in grain dry matter and hence increases in malting loss. The malting loss and yield values are in accordance with Ayernor [14] during germination of rice paddy (PSB.Rc34) where 92.81% malting yield and 25.90% malting loss was observed during 5 days of germination.

Table 4.1 Malting potential of LAR and IAR paddy germinated at 30 and 35°C for 120h

Germination Time (h)	Germination Rate (%)				Dormancy Rate (%)				Germination Capacity (%)			
	Germination Temperature (°C)				Germination Temperature (°C)				Germination Temperature (°C)			
	25	30	35	40	25	30	35	40	25	30	35	40
LAR paddy												
Native	ND	0±0.0	0±0.0	ND	ND	100±0.0	100±0.0	ND	ND	0±0.0	0±0.0	ND
24	ND	77±1.4	71±1.4	ND	ND	23±2.8	29±2.9	ND	ND	54±2.8	42±1.8	ND
36	ND	82±1.4	74±1.4	ND	ND	18±2.8	26±2.8	ND	ND	64±2.8	48±0.2	ND
48	ND	84±2.8	77±1.4	ND	ND	16±0.1	23±1.4	ND	ND	68±0.4	54±1.4	ND
60	ND	86±2.8	79±2.8	ND	ND	14±1.4	21±1.4	ND	ND	72±0.1	58±1.4	ND
72	ND	91±1.4	80±2.8	ND	ND	9±1.4	20±1.4	ND	ND	82±0.2	60±0.3	ND
84	ND	93±1.4	85±1.5	ND	ND	7±1.4	15±0.8	ND	ND	86±2.8	70±1.7	ND
96	ND	95±1.4	86±0.4	ND	ND	5±0.0	14±0.1	ND	ND	90±1.4	72±2.8	ND
108	ND	95±1.4	90±0.3	ND	ND	5±0.0	10±0.5	ND	ND	90±1.4	80±2.8	ND
120	ND	97±0.2	95±1.2	ND	ND	3±0.2	5±1.4	ND	ND	94±0.9	90±1.4	ND
IAR paddy												
Native	ND	0±0.0	0±0.0	ND	ND	100±0.0	100±0.0	ND	ND	0±0.0	0±0.0	ND
24	ND	81±0.2	81±0.08	ND	ND	19±0.3	19±0.01	ND	ND	62±0.09	62±0.4	ND
36	ND	85±0.03	85±1.4	ND	ND	15±1.4	15±0.02	ND	ND	70±0.4	70±1.4	ND
48	ND	89±1.4	89±1.4	ND	ND	14±1.4	11±1.4	ND	ND	78±1.4	78±1.3	ND
60	ND	91±1.4	91±1.6	ND	ND	9±0.5	9±1.4	ND	ND	82±1.4	82±0.2	ND
72	ND	95±0.4	94±0.04	ND	ND	5±0.01	6±0.1	ND	ND	90±0.2	88±0.9	ND
84	ND	97±1.4	96±0.2	ND	ND	3±1.4	4±0.4	ND	ND	94±0.4	92±0.2	ND
96	ND	98±0.0	97±0.0	ND	ND	2±0.0	3±0.0	ND	ND	96±0.0	94±0.0	ND
108	ND	98±0.0	97±0.0	ND	ND	2±0.0	3±0.0	ND	ND	96±0.0	94±0.0	ND
120	ND	98±0.0	99±0.0	ND	ND	2±0.0	1±0.0	ND	ND	96±0.0	98±0.0	ND

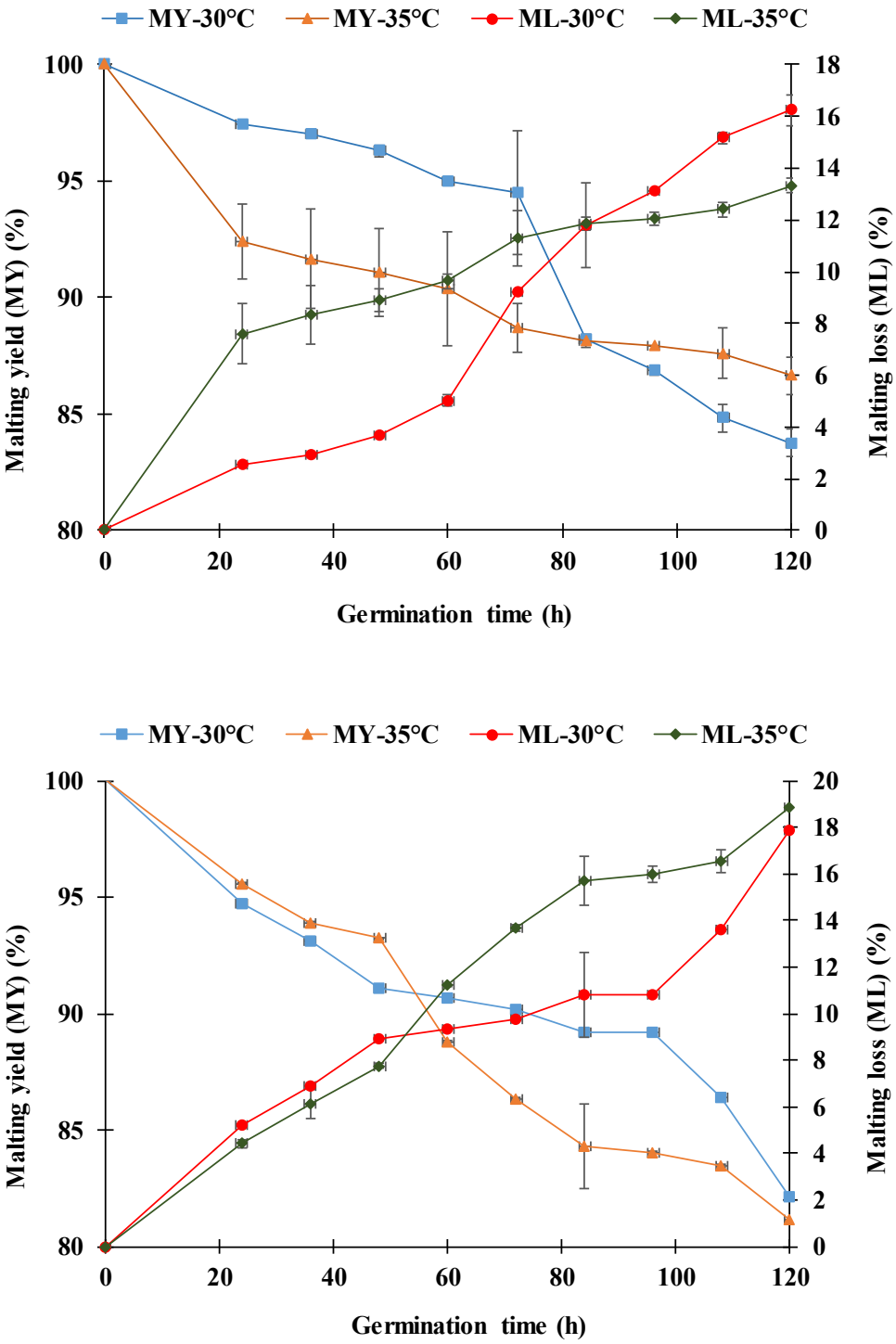

Fig 4.1: Malting yield (MY) and Malting loss (ML) of LAR (top) and IAR (bottom) native and malted rice

4.1.1.3 Thousand Kernel Weight

Thousand kernel weights of cereal are used to determine the suitability of the grain for malting. The results of thousand kernel weight are presented in Fig 4.2. A weight loss of 14% and 6% was observed in rice kernel of LAR grains germinated at 30 and 35°C respectively. The thousand-kernel weight of IAR rice was also observed to decrease by 13 and 15% respectively when incubated at 30 and 35°C. A higher weight loss in IAR malted rice was found as compared to the LAR malted rice. This may be due to the higher malting loss in case of IAR malted rice during the process of germination. Both germination time, temperature and their interaction showed a significant ($P<0.05$) effect on the thousand-kernel weight of both LAR and IAR malted rice. Ayernor [14] reported a similar decrease in thousand kernel weights during germination of PSB. Rc 34 rice paddy. This is due to the utilization of the reserve compounds such as starch and proteins to provide the required energy for the growth and development of the embryo which is also mentioned earlier in the section3.2.2 for decrease in the malting loss. Moreover, leaching of certain compound occurs such as minerals and other constituents during steeping which further leads to decrease in weight [75].

4.1.2 Enzyme activity

4.1.2.1 Total Amylolytic Activity

The total amylolytic activity plays an important role in seed germination and maturation. The results of the amylolytic activity are presented in Fig 4.3. The results revealed that the amylolytic activity of both malted rice increased significantly ($p<0.05$) from the native rice during the process of germination. The interaction between germination time, temperature and A-AR had significant effect on total amylolytic activity. The change in activity was found steeper upto 72h and becomes plateau thereafter. The maximum amylolytic activity for LAR and IAR was observed at germination temperature of 30 and 35°C respectively. Moreover, a higher activity for IAR was observed as compared to LAR at both germination temperatures. This higher level of amylolytic activity causes rapid starch degradation during the process of germination. Dziedzoave et al. [35] during the malting process reported higher levels of endogenous gibberellins in some barley varieties. Gibberellins are the principle hormones involved in the stimulation of enzymes during germination. This difference in the levels of the endogenous gibberellins might have contributed to the higher level of amylolytic activity in IAR malted rice as compared to LAR at both germination temperature. However, apart from presence of GA other controlling factors are temperature, moisture, nature of additives used, genotype and environmental conditions [66].

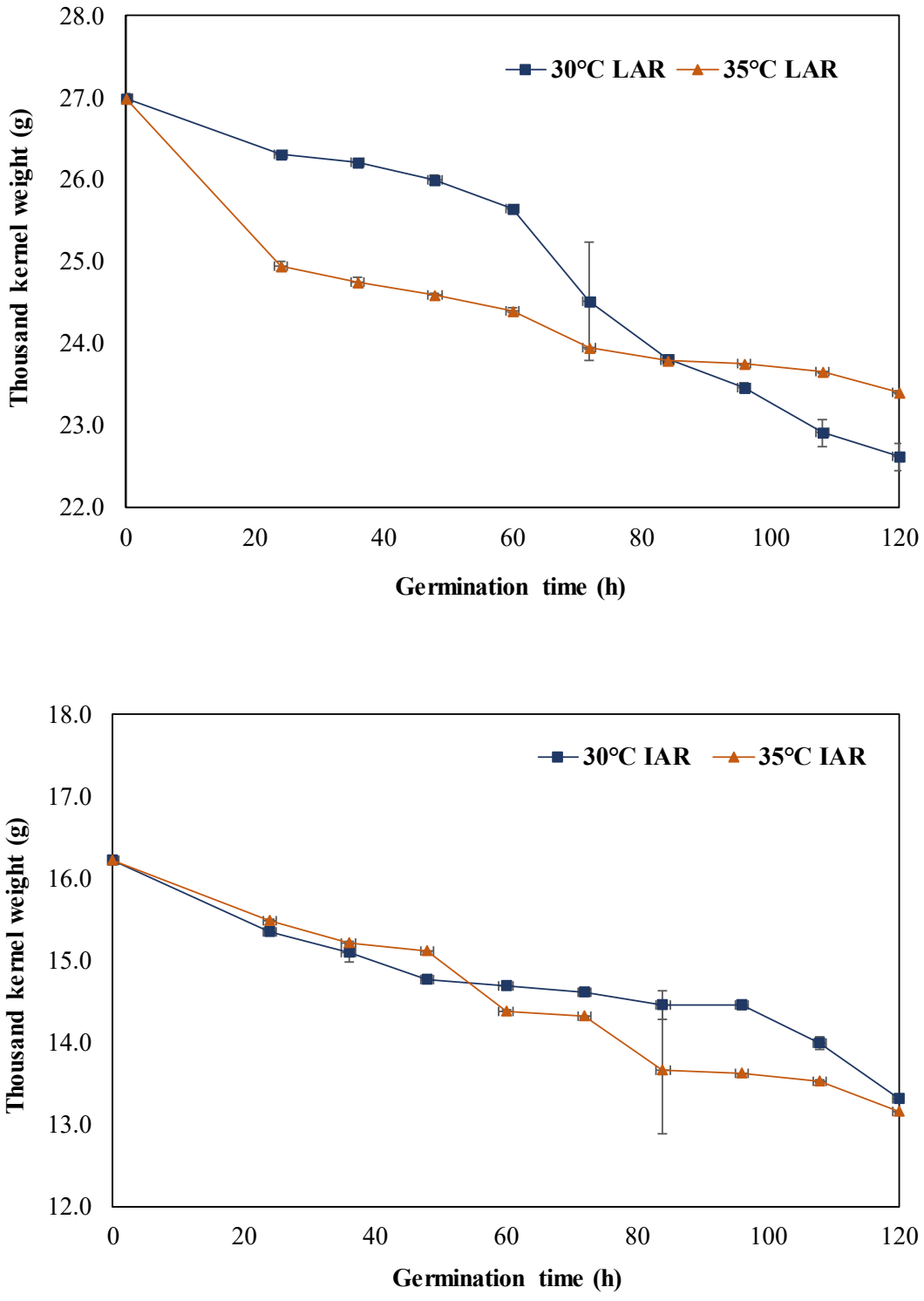

Fig 4.2: Thousand kernel weight of LAR and IAR native and malted rice

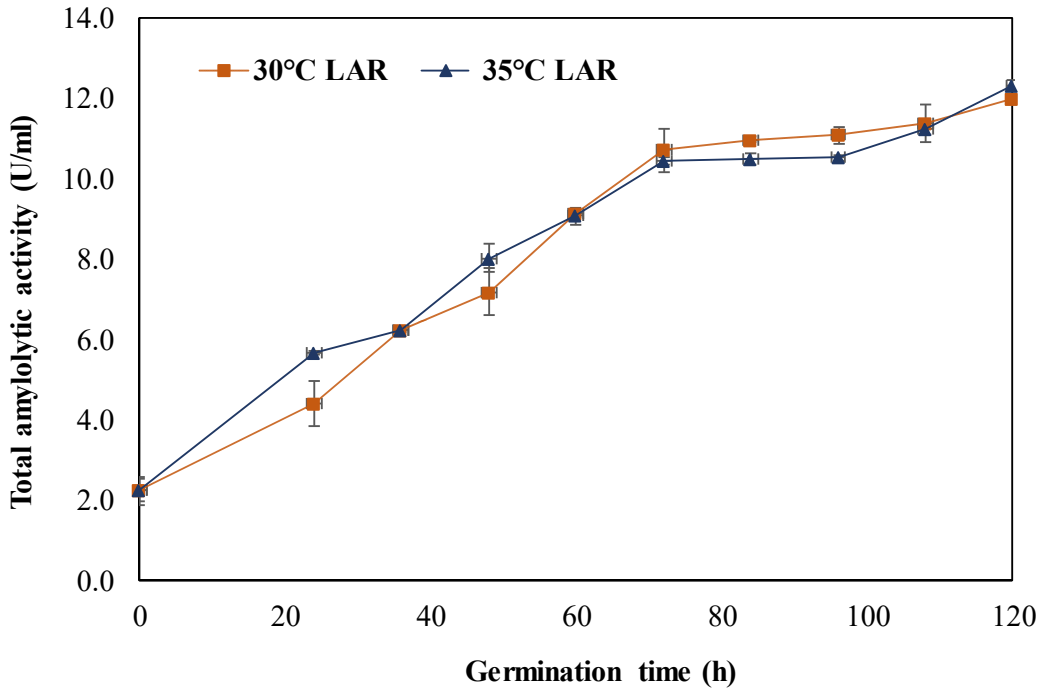

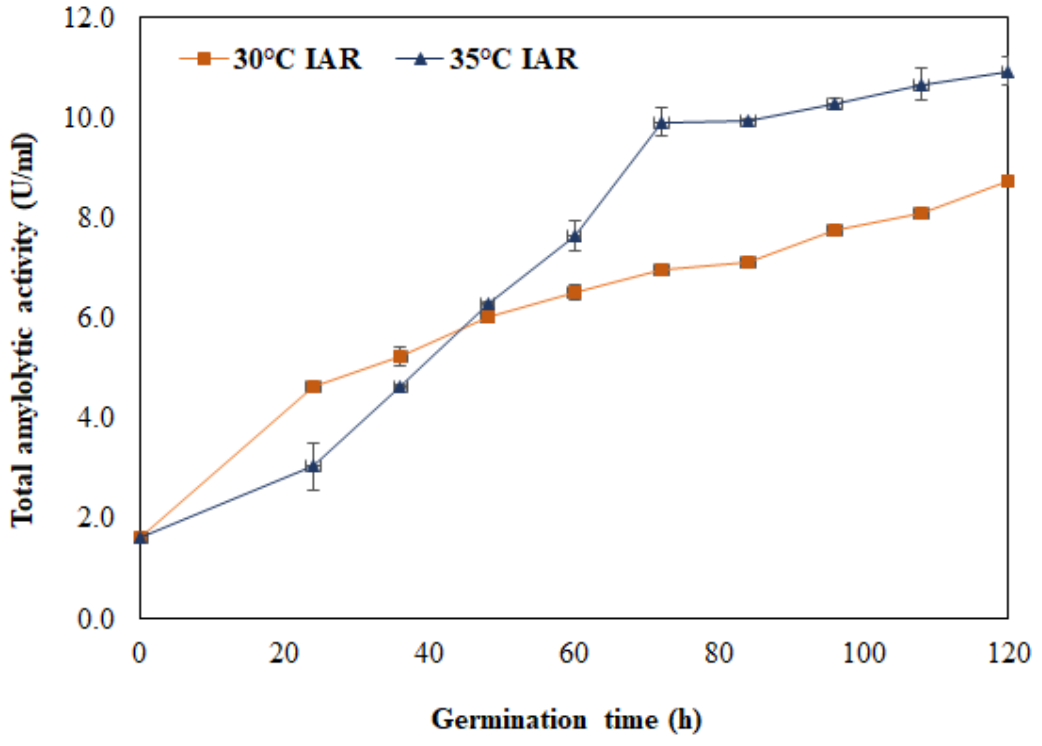

Fig 4.3: Total amylolytic activity of LAR and IAR native and malted rice

4.1.2.2 Alpha amylase activity

Alpha amylase mainly acts as a liquefying enzyme during the process of germination. In this study the change in amylase activity with time and temperature is presented in Fig 4.4. The alpha amylase activity was observed to be incipient in native rice which increased significantly up to 96 h of germination and became constant thereafter in both rice samples. LAR malted rice germinated at 30 and 35°C showed 3 and 2-fold increase in α- amylase activity up to 96h of germination. The IAR malted rice exhibited 4 and 5-fold increase up to 96 h of germination when germinated at 30 and 35°C respectively. Similar to amylolytic activity, a higher level of α-amylase activity was exhibited by IAR malted rice at both germination temperature as compared to LAR malted rice. This variation in activity may be again attributed to the variation in the level of endogenous GA in different rice varieties as discussed earlier. The interaction between time, temperature and A-AR was observed to have significant effect on the α-amylase activity. It is reported that α-amylase constitute approximately 30% of the total protein synthesized during germination [70]. Thereby, this endo amylase played a major role in starch hydrolysis during the process of germination. Therefore, rice may be considered as a source of α-amylase production for its utilization in various industries.

4.1.3 Chemical changes during malting

4.1.3.1 Total starch content

The changes in starch of malted rice are presented in Fig.4.5. The germination conditions significantly affected the starch content of both LAR and IAR. An exponentially decreasing trend in starch content of the LAR and IAR malted rice was observed during period of germination. Temperature was also found to have significant effect ($p<0.05$) on the starch content of both LAR and IAR malted rice. The interaction between different time, temperature and A-AR of both types of rice were also observed to have significant ($p<0.05$) effect on the total starch content. A degradation level of 58% and 62% in starch were observed in LAR malted rice during germination at 30°C and 35°C respectively. In case of IAR malted rice, higher starch degradation (74%) was observed at 35°C when compared to 30°C (65%). Moreover, it was also observed that starch degradation of IAR malted rice was comparatively higher than LAR malted rice at both germination temperature. This may be due to the high malting potential of IAR as already observed in this study. Wu et al. [101] reported that the higher degradation of starch may be attributed to the presence of higher amylose content (IAR of present study) that gets rapidly degraded by hydrolytic enzymes than amylopectin.

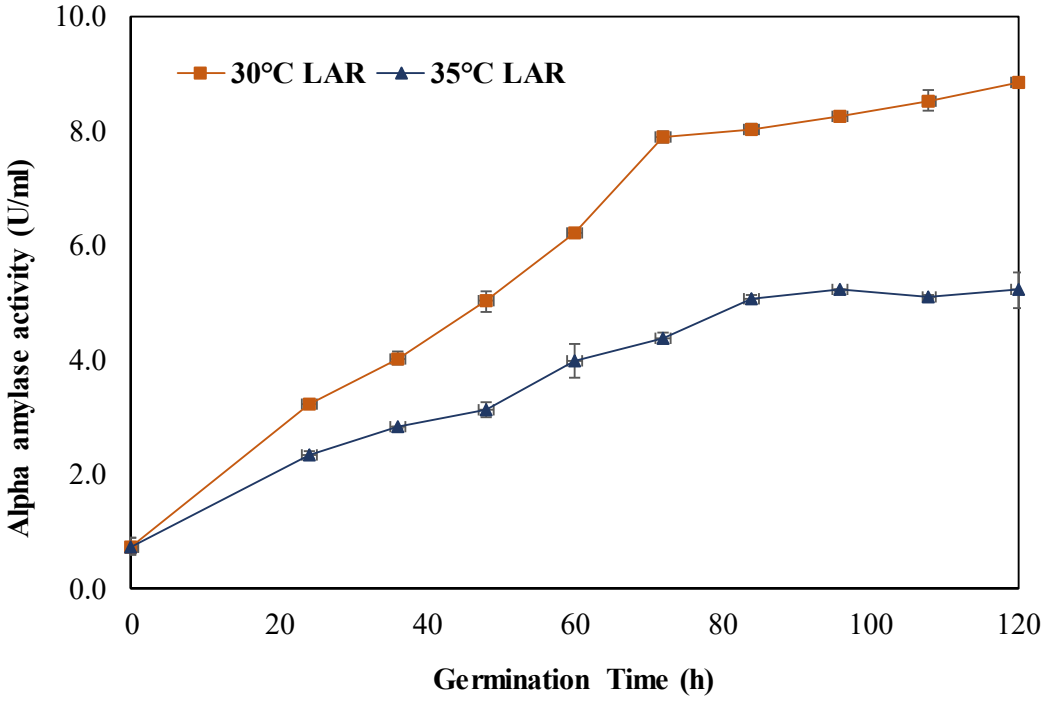

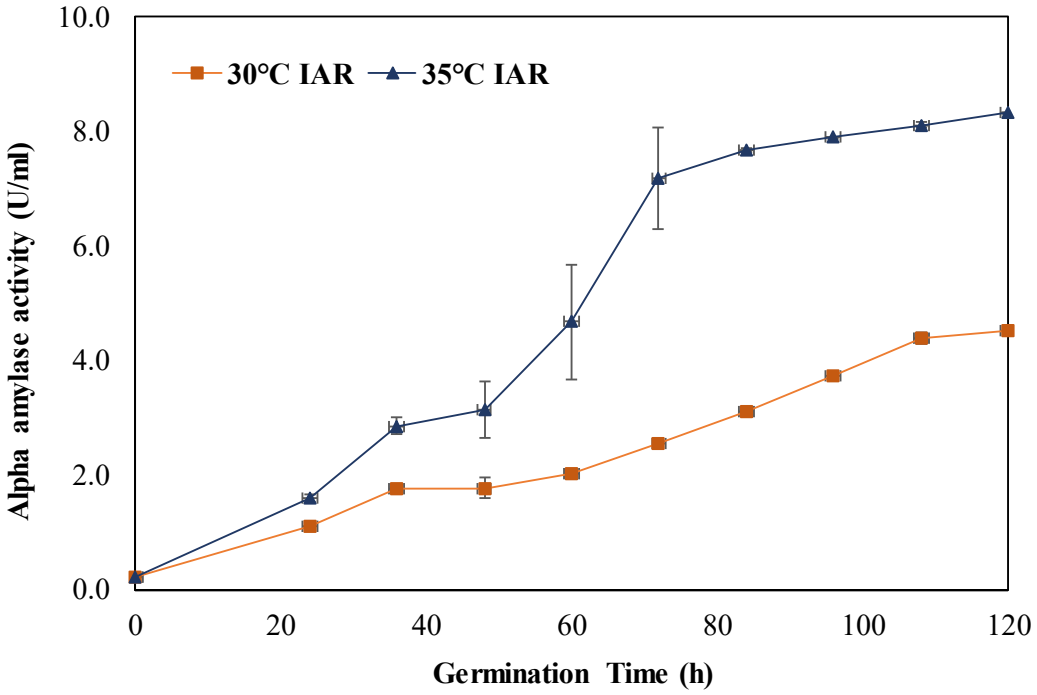

Fig 4.4: Alpha amylase activity of LAR and IAR native and malted rice

The starch degradation was also evident from the SEM micrographs (Fig 4.7) of malted rice where pins and holes were observed in the starch granules due to hydrolysis (detailed discussion given in section 4.1.4.2). Mohan et al. [2010] reported approximately 10% decrease in starch content in both *Indica* and *Japonica* rice in five days germination with more than 95% GC which was comparatively much lower than that observed in this study with similar range of GC for both types of rice. The major factor for starch degradation can be attributed to the action of various hydrolytic enzymes such as amylases and debranching enzymes produced during germination that converts starch into simpler compounds as reported by various authors.

4.1.3.2 Reducing sugar

The change in reducing sugar content during malting of rice was estimated by the dinitrosalicyclic acid method (87] which is shown in the Fig 4.5. The reducing sugar increased significantly and exponentially up to 14 and 20 times in LAR malted rice germinated at 30 and 35°C respectively. In case of IAR, the higher reducing sugar content was exhibited by malted rice germinated at 35°C (34 times) rather than malted rice germinated at 30°C (29 times). Moreover, a significant difference was also observed between the two types of rice as IAR showed higher reducing sugar content as compared to LAR. This variation in reducing sugar content may be attributed to higher level of starch degradation in IAR malted rice as compared to LAR by the various hydrolytic enzymes during germination. Moreover, the interaction between time, temperature and A-AR was observed to have significant effect on the reducing sugar. The hydrolytic enzymes such as amylases (α and β) cause degradation of starch during the process of germination. α-amylase (endoenzyme) being a liquefying enzyme acts on its own and cleaves the inner α-1, 4 linkages at random points and stops at α-1, 6 linkages leading to decrease in viscosity. β-amylase (exoamylase) in another hydrolytic enzyme which is a saccharifying enzyme and acts on the α-1, 4 linkages of both amylose and amylopectin from the non-reducing end but cannot degrade α- 1, 6 linkages. This degradation of starch leads to formation of mixture of simple sugars [70]. Moongngarm [67] reported made similar observations for increase in reducing sugar during five days germination of rough and brown rice of RD-6. Saman [85] reported higher reducing sugar content with decrease in starch during the process of germination due to higher hydrolytic enzymes.

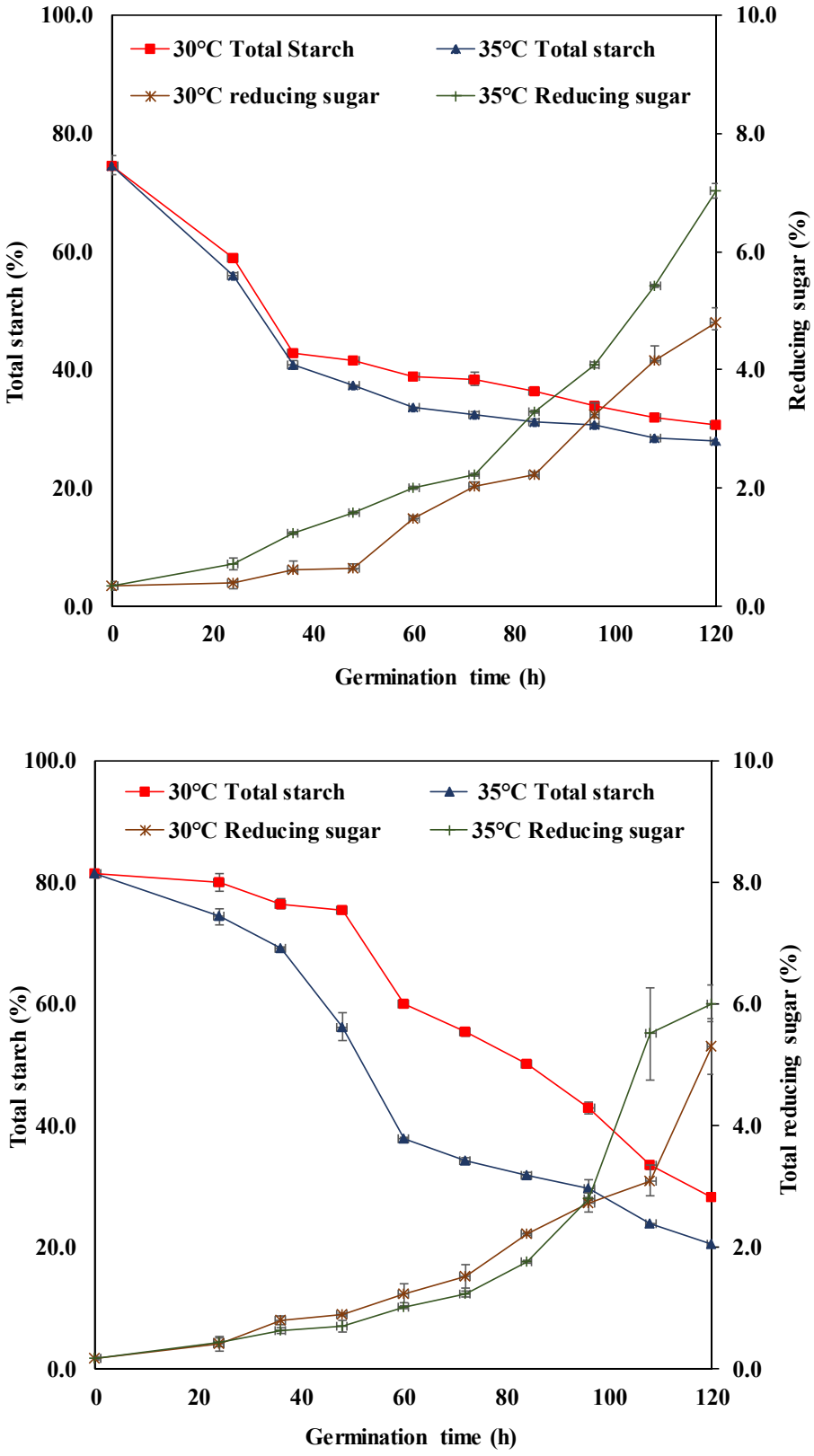

Fig 4.5 Total starch content of LAR and IAR malted rice

4.1.4 Physical, morphological and structural properties affected by malting

4.1.4.1 Bulk and tapped densities

Bulk and tapped densities indicate the packing characteristics of solids. The bulk and tapped densities of the malted rice are presented in Fig 4.6. The bulk density of LAR malted flour decreased significantly by 10 and 8% when germinated at 30 and 35°C respectively for 120h. The bulk densities of IAR malted flour germinated at 30 and 35°C also decreased by 12 and 13% respectively during the process of germination. In this case the interaction of germinating temperature and time was not significant ($p<0.05$). The tapped densities of LAR and IAR malted flour germinated at two different temperatures (30 and 35°C) were also significantly affected by germination as it decreased gradually with germination time. The IAR malted flour exhibited higher decrease in bulk and tapped density as compared to LAR malted flour during the germination process at both germination temperature.

The decrease in bulk and tapped density for both LAR and IAR malted flour with increase in germination time may be due to the various physico-chemical activities occurring during germination such as starch hydrolysis. Moreover, leaching of inorganic compounds and total solids during steeping and germination also contributed to the decrease in density [81].

4.1.4.2 Morphological changes

The Scanning electron micrographs of both malted rice germinated at 30 and 35°C for 120h is shown in Fig 4.7. The rice granules in micrographs of native rice showed regular surface without any modification. However, the granules lost its smoothness and appeared rough and eroded in the micrographs of both malted rice germinated at 30 and 35°C respectively. In some starch granules pin holes were also formed during germination. This surface modification in both types of rice may be attributed to the hydrolysis of starch by hydrolytic enzymes produced during germination. The uneven surface modification may be attributed to variation in susceptibility to the hydrolytic enzymes activity during germination. The enzymatic activity for hydrolysis of starch is a sequential step. Firstly, enzyme diffuses towards the solid surface and adsorbed through sites and finally catalytic reaction take place [29]. The adsorption can be influenced by granule size, surface characteristics and minor constituents such as proteins and lipids on the surface [70]. After adsorption during catalytic reaction, starch granules are hydrolysed either by exo-corrosion or endo-corrosion. Exo-corrosion mainly involves the erosion of entire starch granules or a part of it by hydrolytic enzymes whereas endo-corrosion involves activity of α-amylase which hydrolyses the linkages present in the inner region of the substrate leading to creation of pores or cavities

[29]. This pores or cavities increase in cross section which aids to the diffusion of more enzymes through it, eventually leading the enzymes to the centre of the granule.

The surface modification due to the enzyme action may be recognized by five different patterns in micrograph viz. pin holes, sponge-like erosion, numerous medium-sized holes, distinct loci leading to single holes in individual granules, and surface erosion [101]. The modification of surface and development of pores, which is evident in micrographs of the both malted rice during germination may be correlated to the above mechanism of starch degradation. SEM provides mainly the information on sample's surface topography and therefore degree of starch degradation in both malted rice which is evident from analytical values in this study, could not be concluded from the micrographs.

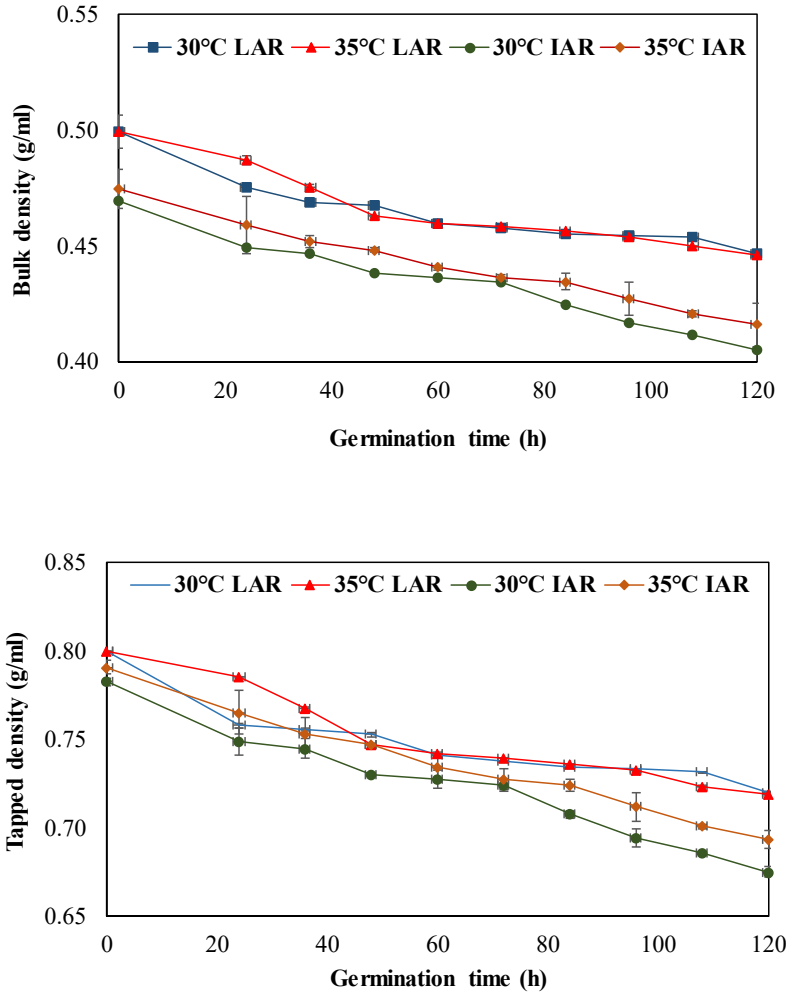

Fig 4.6 Bulk and tapped density of LAR and IAR native and malted rice

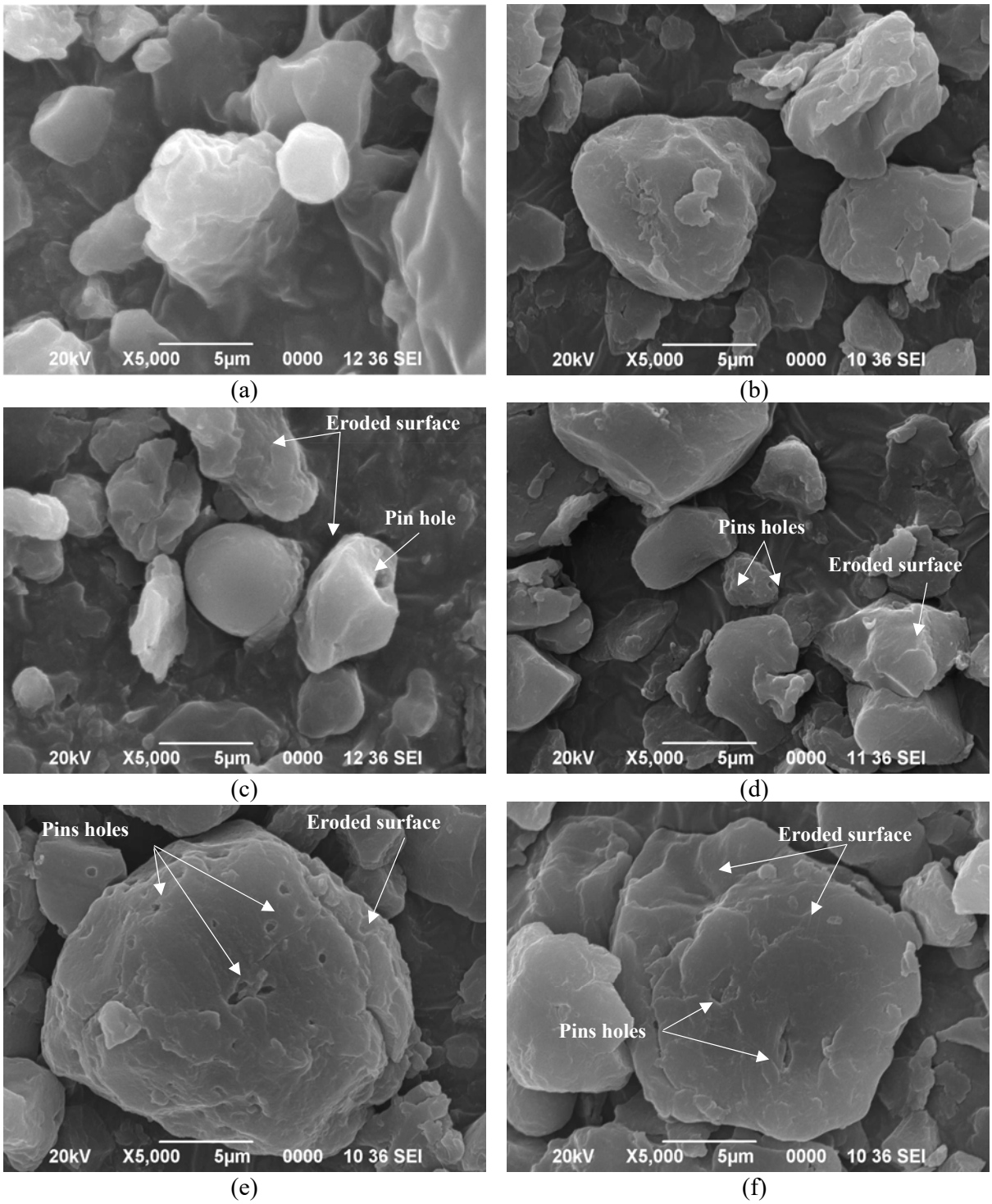

Fig 4.7. Scanning Electron Micrograph of rice : a. Native LAR rice; b. Native IAR rice c. 30°C LAR (120h); d. 35°C LAR (120h); e. 30°C IAR (120h) and f. 35°C IAR (120h)

4.1.4.3 Phase identification by XRD

X-ray diffractogram is widely used to study the crystallinity pattern of starch granules. Starch granules which are semi-crystalline in nature and mainly known to exist in three crystalline structures such as A, B and C types [71]. The diffractograms of malted rice are shown in Fig 4.8. From the diffractogram it was observed that the native rice showed five major peaks at Bragg angle 15.2, 17.8, 18.85, 20.1 and 23.05. The major peaks of native IAR rice were found at Bragg angle 15.05, 17.5, 18.1, 20.45 and 22.7. Similar major peaks were also observed after malting for both rice incubated at 30 and 35°C for 120h. In case of IAR malted rice decrease in the intensities of the peaks were observed during the process of germination at both temperatures which may be due to the higher rate of starch degradation in IAR as already discussed. All malted rice showed mainly A-type diffraction peak which is a characteristic of cereal starches.

The highest crystallinity was observed in the native LAR (54.03%) and IAR (52.60%) rice but the both malted rice showed gradual decrease in crystallinity with increase in germination time as compared to native rice. The % crystallinity of LAR malted rice germinated at 30 and 35°C was observed to decrease upto 36.49% and 49.41% respectively during 120h of germination. The higher decrease in crystallinity in LAR germinated at 30°C may be due to the high starch degradation. The % crystallinity of IAR malted rice germinated at 30 and 35°C was observed to decrease upto 35.30% and 46.50% respectively. The IAR malted rice showed comparatively higher decrease in % crystallinity than LAR malted rice which may be due to the enzymes that caused rapid damage to amylose and partly to amylopectin. This is similar to the results observed by Sun et al. [93] and reported that degree of starch crystallinity depends on the content of amylose and the molecular structure of amylopectin such as chain length, the extent of branching and molecular weight. However, crystallinity of malted rice might have also been affected by other parameters such as proteins and lipids present in rice [106].

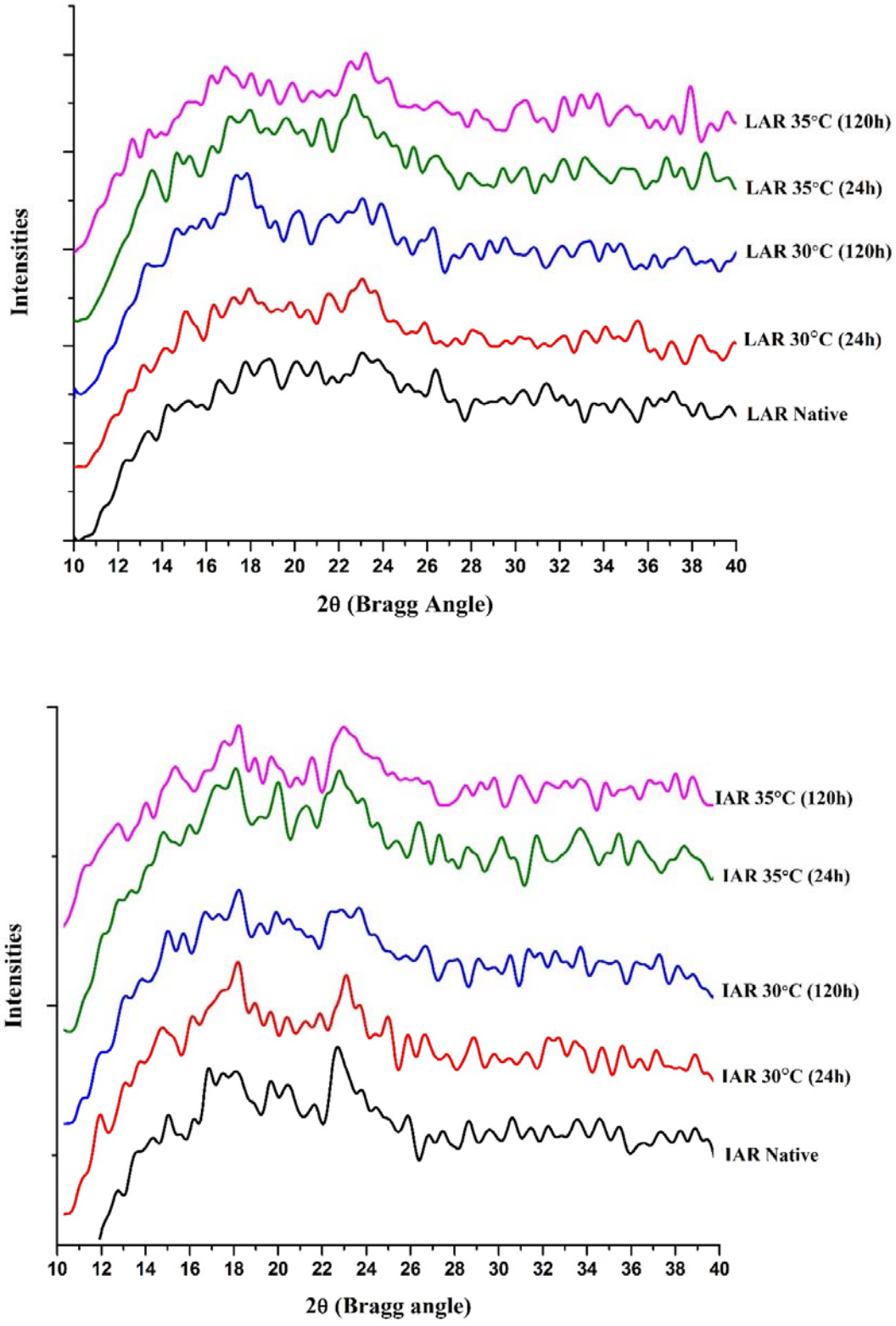

Fig 4.8 X-ray diffractograms of LAR and IAR rice: A. Native rice; B. 30°C (24h); C. 30°C (120h); D. 35°C (24h) and E. 35°C (120h)

4.2 Modelling of enzyme reaction rate and germination process using ANN approach

Germination is a complex process in which the gibberellin hormone is triggered which stimulates the release of amylolytic enzymes into the endosperm. These enzymes play a very important role in the various biochemical and physiological reactions that occur in the endosperm. Starch is the major reserved compound in the endosperm and the amylolytic enzymes (α and β amylases) causes partial degradation of the structural components i.e. glycosidic linkages in the starch molecule resulting formation of glucose, maltose and dextrins [22]. During germination process, simultaneously two phenomenon occurs the synthesis of amylolytic enzyme and enzyme reaction on substrate i.e. starch. The Michaelis-Menten enzyme reaction kinetics is well verse proven by the researcher for almost all enzyme reactions. The Michaelis-Menten kinetics explains the dependence of the initial rate of enzyme-catalyzed reactions on concentration. However, in the present study, unlike other enzyme-substrate reactions, there is a continuous production of hydrolytic enzymes that act on starch and simultaneous release of reducing sugar is observed during germination. In such varying conditions, model equations and corresponding reaction constants should be investigated and re-estimated for its usability and adequacy. Thereby, with a change in the reaction conditions, the usability of the model equation in those reaction conditions should be investigated and the kinetic constants in the model need to be re-estimated. An alternative method i.e. Boltzmann function may be applied to estimate the reaction rate. According to Bas [19] most of the time course data of the biochemical reactions could be fitted to Boltzmann equation with a high accuracy. Boltzmann function (Eq. 3.12 and 3.13) was selected as an alternative method because of its high accuracy for most of the time course data of biochemical reactions [19]. Moreover, since germination is a complex process the enzymes kinetics may not obey the Michaelis–Menten description.

4.2.1 Estimation of enzyme reaction Rate by Boltzmann function

The substrate (starch) and product (reducing sugar) concentrations were estimated at regular intervals of time during germination which was affected by the action of hydrolytic enzymes. The time course concentration and germination time were fitted to the Boltzmann function. In the model, the width of Boltzmann function (dx) was considered to total change in substrate concentration. Model parameters and its R^2 value were obtained for both LAR30 and LAR35 and IAR 30 and IAR35 are presented in Table 4.2. The R^2 values of the all predicted model equations were found within the acceptable limit i.e. from 0.871 to 0.947

and these values indicated that time courses of the hydrolysis reaction of starch can be potentially explained by the Boltzmann function (BF). An equation, obtained by the derivation of the predicted model equation, was used for determining the enzymatic reaction rate for the period of reaction time. The predicted reaction rates for all samples are presented in Fig. 4.9. From the plot, it was evident that the change in substrate concentration and reaction rates followed a similar trend.

Table 4.2 Boltzmann function (BF) model parameters

Sample	Width of BF (dx)	A1	A2	R^2	RMSE
LAR30	43.887	120.2	22.58	0.893	5.097
LAR35	46.613	125.0	15.51	0.879	5.945
IAR30	53.196	163.8	23.50	0.871	7.478
IAR35	61.062	170.4	$8.52x10^{-9}$	0.947	5.135

4.2.2 Modelling Michaelis-Menten enzyme kinetics

The Michaelis-Menten kinetics explains the dependence of the initial rate of enzyme-catalyzed reactions on concentration. The enzyme reaction rate which was obtained from the Boltzmann function was employed in Michaelis-Menten equation to determine the model parameters (K_m and V_{max}). The estimated parameters are presented in Table 4.3. The observed and predicted values of velocity or reaction rate are presented Fig. 4.10. The K_m represents the substrate concentration at which the reaction rate is half its maximum value. The estimated parameters were not in accordance with the Michaelis-Menten enzyme kinetics. The statistical parameters were also not found in acceptable range. Thus, the experimental data were not following the traditional Michaelis-Menten enzyme kinetics because in paddy germination process the enzyme concentration/ activity and substrate concentration were dynamic with respect to time of germination.

Table 4.3 Michaelis-Menten Equation parameters with their statistical parameters

Samples	V_m	K_m	R^2	RMSE
LAR30	40.44	5070.0	0.723	0.0853
LAR35	2.434	217.3	0.723	0.0855
IAR30	39.81	5071.0	0.982	0.0217
IAR35	1.11	47.65	0.955	0.0315

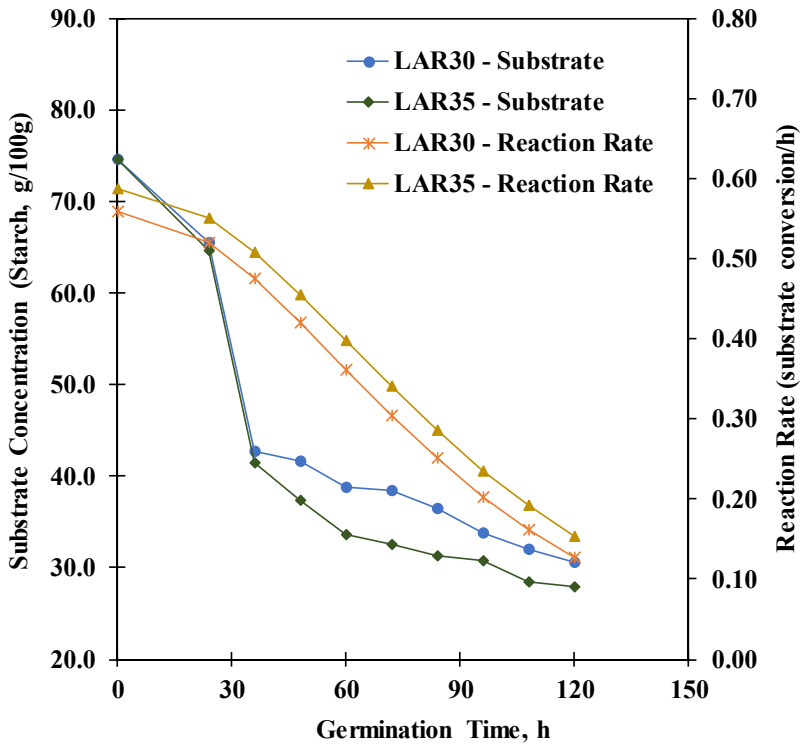

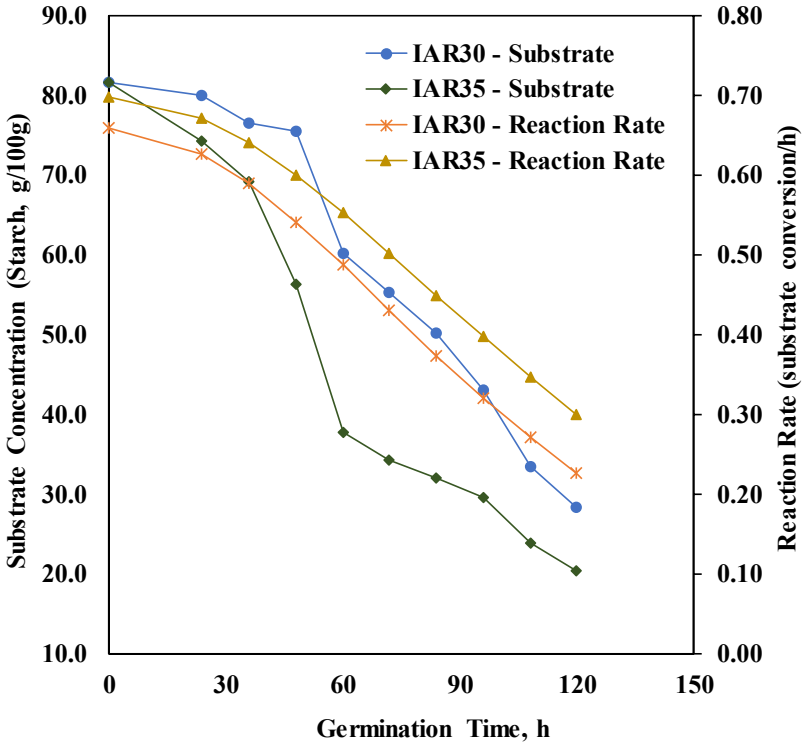

Fig. 4.9 Time courses for a change in starch content and reaction rate for LAR and IAR rice during malting

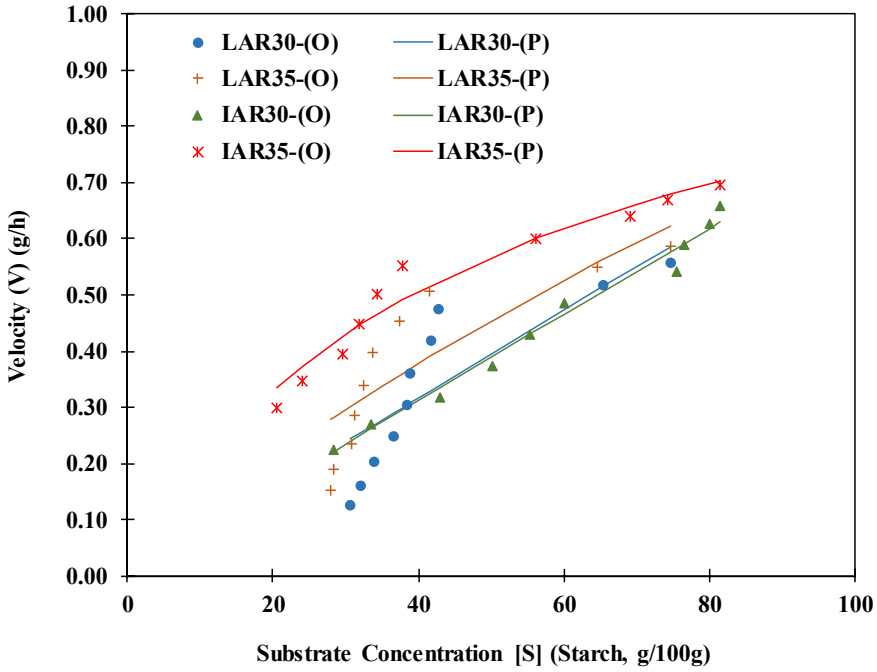

Fig. 4.10 Observed vs Predicted values for Michaelis-Menten equation

4.2.3 Stochastic Model

During germination process, simultaneously two phenomenon occurs the synthesis of amylolytic enzyme and enzyme reaction on substrate i.e. starch. Thus, a different approach was applied in developing the modified enzyme reaction kinetics. The reaction order of the time course enzyme activity and substrate utilization was estimated based on the experimental data of present study (Eq. 4.1).

$$V = \frac{K_1|E_t|_m|[S]_t|_n}{(K_4 + |[S]_t|_n)} \qquad \text{Eq. 4.1}$$

Where, E_t is the m^{th} order function for time course function of enzyme activity and $[S]_t$ is the n^{th} order function for time course function of substrate concentration and K1 and K4 are the empirical constants.

The experimental data for all samples (the enzyme activity and starch concentration) were fitted to zero, first and second order reaction kinetics. The statistical parameters along with the reaction order are presented in Table 4.4. From the Table 4.4, it is evident that the phenomenon of simultaneous synthesis of enzyme and action of enzyme followed the zeroth order reaction kinetics whereas, change in the substrate concentration followed the second order for LAR rice and the first order for IAR rice for both temperatures.

According to literature, when reaction rate becomes independent of substrate concentration, the reaction behaves as a zero-order reaction with respect to substrate. Further, in this study, it is observed that during the process of germination, amylopectin content decreased rapidly as compared to amylose. In case of LAR, the substrate concentration followed second order reaction which might be due to the sharp decrease in substrate concentration (starch). In LAR, amylopectin content was higher as compared to amylose and amylopectin due to shorter branch structure gets degraded faster. On the other hand, in case of IAR, first order reaction was observed which means that the reaction rate and substrate concentration are directly proportional to each other. This trend can also be observed from the Fig 4.9.

Table 4.4 Order of reaction for time course change for enzyme and substrate

Rice	E_0 U/ml	$[S]_0$ (g/100g)	Reaction Order					
			Enzyme			Substrate		
			m	R^2	RMSE	n	R^2	RMSE
LAR30	0.750	74.580	0	0.905	0.841	2	0.913	4.342
LAR35	0.750	74.580	0	0.883	0.517	2	0.914	4.738
IAR30	0.214	81.519	0	0.979	0.204	1	0.888	6.565
IAR35	0.214	81.519	0	0.936	0.774	1	0.911	6.686

After incorporating the ordered function for enzyme activity and substrate concentration in Eq. 4.1 the proposed mathematical expressions are as follows:

For LAR sample (zeroth and second order) (Eq. 4.2)

$$V = \frac{K_1(E_0+K_2*t)\left(\frac{[S]_0}{1+K_3*[S]_0*t}\right)}{\left(K_4+\left(\frac{[S]_0}{1+K_3*[S]_0*t}\right)\right)} \qquad \text{Eq. 4.2}$$

For IAR samples (zeroth and first order) (Eq. 4.3)

$$V = \frac{K_1(E_0-K_2*t)\left([S]_0\exp(-K_3*t)\right)}{\left(K_4+\left([S]_0\exp(-K_3*t)\right)\right)} \qquad \text{Eq. 4.3}$$

Where, K_1; K_2; K_3 and K_4 are the empirical constants, t is the germination time and E_0 and $[S]_0$ are the enzyme activity and substrate concentration at t=0.

The coefficients of Eq. 4.2 and Eq. 4.3 were estimated using non-linear regression analysis by CFTOOL toolbox of Matlab R2014a and presented in Table 4.5. The statistical parameters with a higher coefficient of correlation (R^2) and lower SSE reveal that the proposed model predicts the enzyme reaction kinetics during germination.

Table 4.5 Parameters of proposed model with their statistical parameters

Samples	K_1	K_2	K_3	K_4	R^2	SSE	RMSE
LAR30	1.422	0.0258	$-8.89x10^{-3}$	6.107	0.943	0.012	0.045
LAR35	1.429	0.0285	$-2.86x10^{-3}$	21.75	0.970	0.006	0.033
IAR30	$1.12x10^{-3}$	-7.132	0.012	3.41	0.979	0.004	0.027
IAR35	$8.89x10^{-3}$	-1.960	0.031	7.81	0.934	0.008	0.036

4.2.4 Process modeling of starch hydrolysis by using the artificial neural network (ANN)

Process modeling of starch hydrolysis was performed by using ANN modeling technique. The analysis was carried out in MATLAB R2014a with the help of a developed code. In order to develop ANN model, Levenberg-Marquardt back-propagation algorithm was used. The number of neurons in the input and output layer was decided depending on independent and dependent variables. In this study, independent variables for the ANN modeling were germination temperature and time, whereas Starch, amylase, reducing sugar and α-amylase were dependent variables. This modeling was conducted for low amylase (LAR) and intermediate amylose rice (IAR).

The number of neurons in the hidden layer was decided on the basis of trial and error approach. Total no of data for the ANN modeling was 60. Each run of the ANN algorithm consisted of 2000 iterations. Transfer function used for the ANN modeling was a sigmoid function. The experimental data after dividing into three parts (75% for training, 15% for testing and 15% for validation respectively) were fitted with the help of the developed MATLAB code.

For each run of a particular ANN network architecture, mean square error (MSE) and coefficient of determination (R^2) were determined. The best network was selected on the basis of highest R^2 and lowest MSE values. Fig. 4.11 shows the selection of best ANN architecture.

From Fig. 4.11, it can be observed that best ANN architecture for both LAR and IAR was 2-neurons in the input layer, 6-neurons in the hidden layer and four neurons in the output layer (2-6-4). Fig. 4.12 shows the best ANN architecture for both rice.

Weight and bias value of the best ANN architecture ('u', 'w', 'Th' and 'To') was determined by random number generations in the developed code. These values can be used for determining production output on the basis of known input. Besides that, these values along with transfer function of the ANN model can be used for controlling the production of reducing sugars during starch hydrolysis of both rice within the mentioned temperature range. The weight and bias values of the best ANN architecture for both the varieties of rice are shown in Table 4.6.

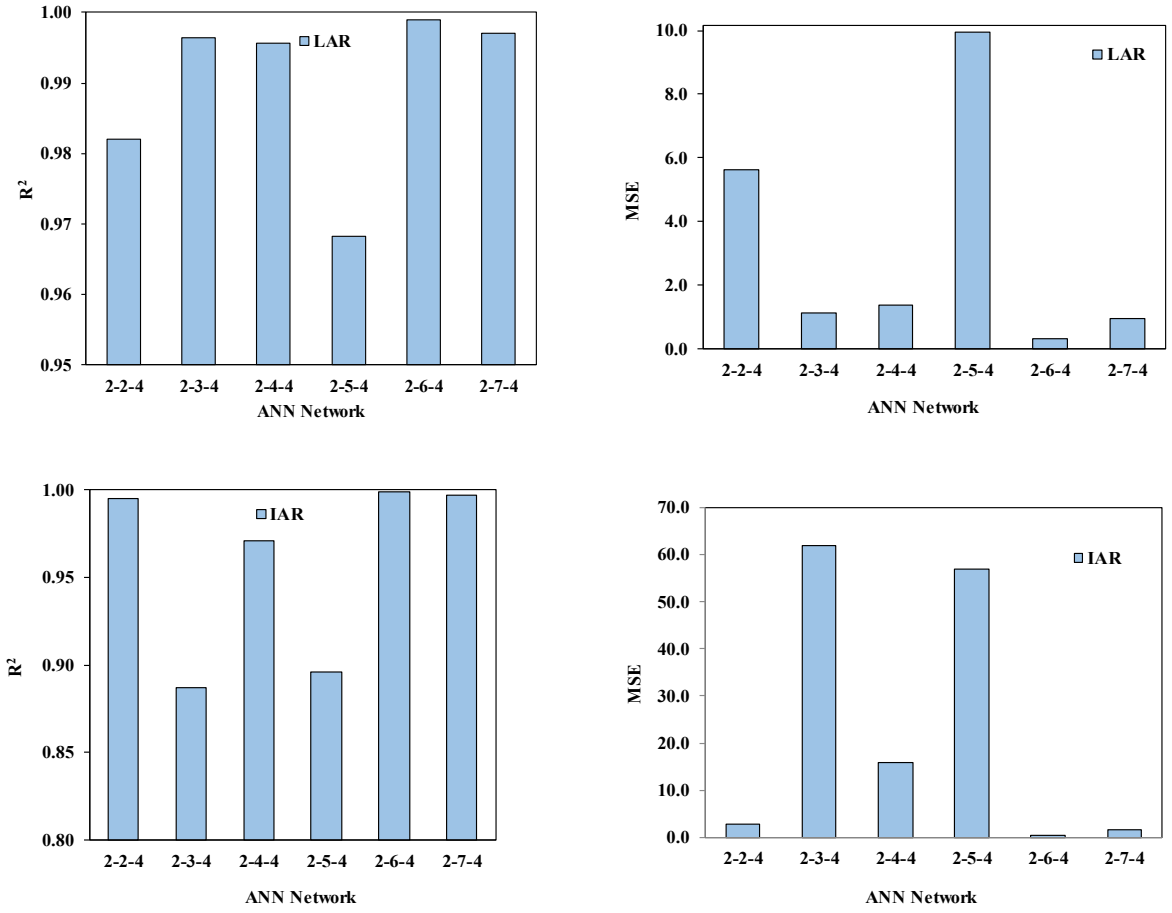

Fig. 4.11 Selection of ANN architecture for LAR and NAR

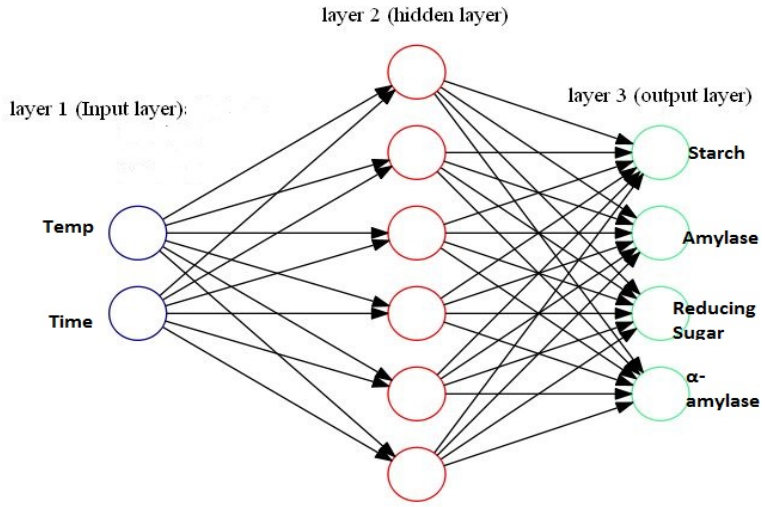

Fig. 4.12 Best ANN architecture for both LAR and NAR

Table 4.6 Weight and bias value of best ANN network for LAR and IAR

Samples	u		w						Th	To
LAR	0.15787	-7.3998	2.7475	0.4218	-2.0856	-0.0482	-2.2237	0.2923	-5.2247	1.5856
	-2.2023	-3.057	-0.4321	-0.6197	0.4017	1.261	1.8324	0.4459	1.6304	-0.6069
	3.5501	0.2538	-0.7564	-0.6977	2.1189	0.0885	2.5453	-0.4601	-0.5393	-0.8206
	2.2029	1.9415	-0.3666	-0.5064	-1.2565	1.7213	0.7768	0.6092	1.553	-1.0688
	-3.3655	3.4938							-0.3135	
	0.88503	-3.7989							2.8527	
IAR	2.6418	2.4672	0.8701	1.9088	-1.3928	-0.7086	0.0449	-0.5499	-3.8218	0.2899
	-1.6968	-1.367	0.0519	-1.5325	0.8414	0.1950	-0.4939	0.6370	1.6796	0.9224
	-2.2852	3.8903	0.3087	-0.5161	1.33	0.9745	-0.9760	0.5657	-1.1222	-0.0101
	2.2596	2.5772	0.6587	-1.2826	0.7080	0.2784	0.1518	1.4527	0.2343	-0.4458
	2.1492	1.0529							2.8339	
	1.9442	1.1193							4.4747	

Fig. 4.13 and 4.14 show the plot of predicted values obtained from ANN modeling and experimental values of the dependent variables for both low amylose (LAR) and intermediate amylose rice (IAR). The coefficient of determination (R^2) value for both LAR and IAR model was 0.999.

The statistical performance parameters for both developed models i.e. the enzyme reaction kinetics and ANN based germination process model were found to be acceptable. Thus, the approach made for modelling of enzyme reaction kinetics and germination process may be tested for other germination processes too.

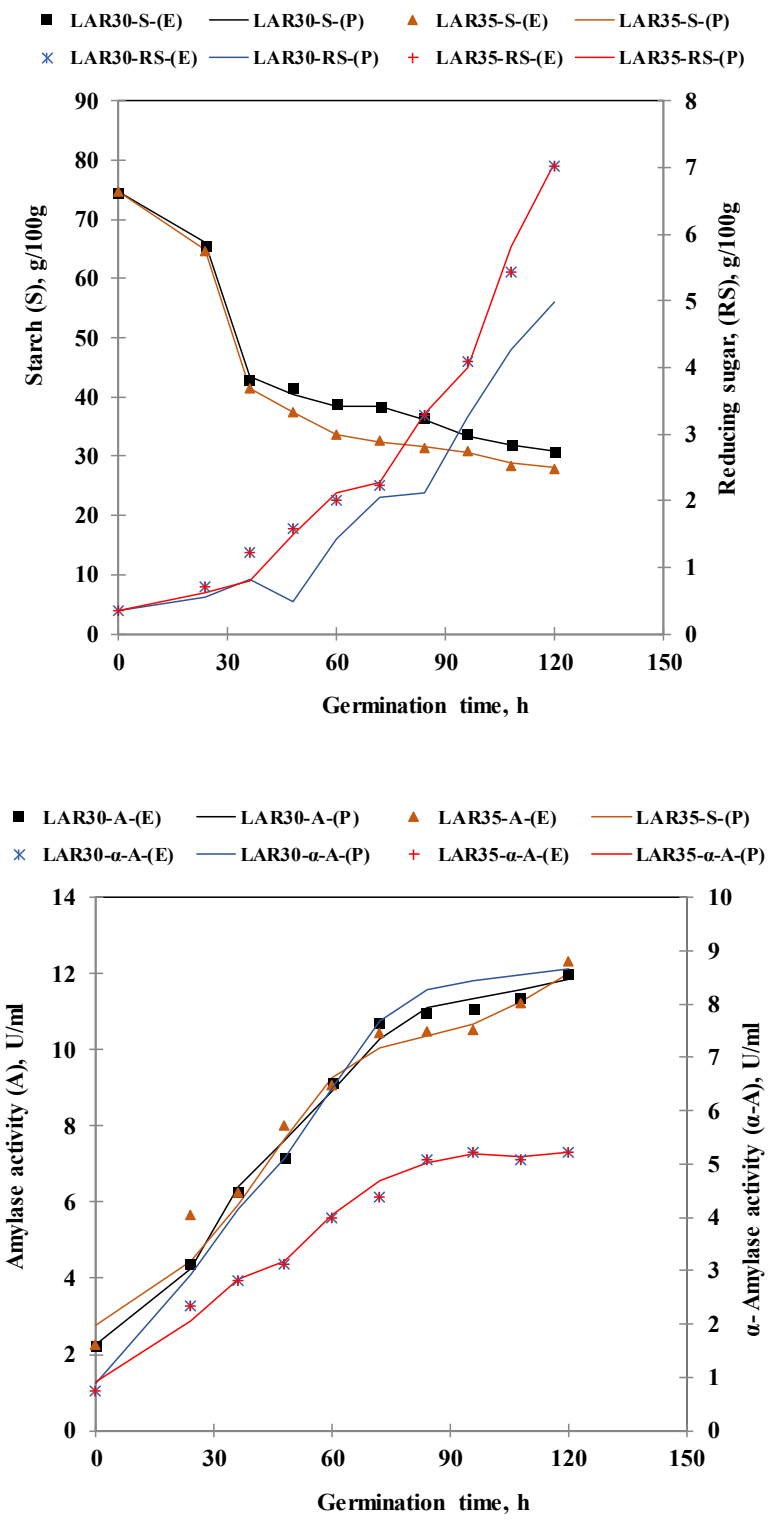

Fig. 4.13 Graph between experimental and ANN predicted values of LAR rice; Starch and Reducing sugar (Top); Amylase and α-amylase (Bottom)

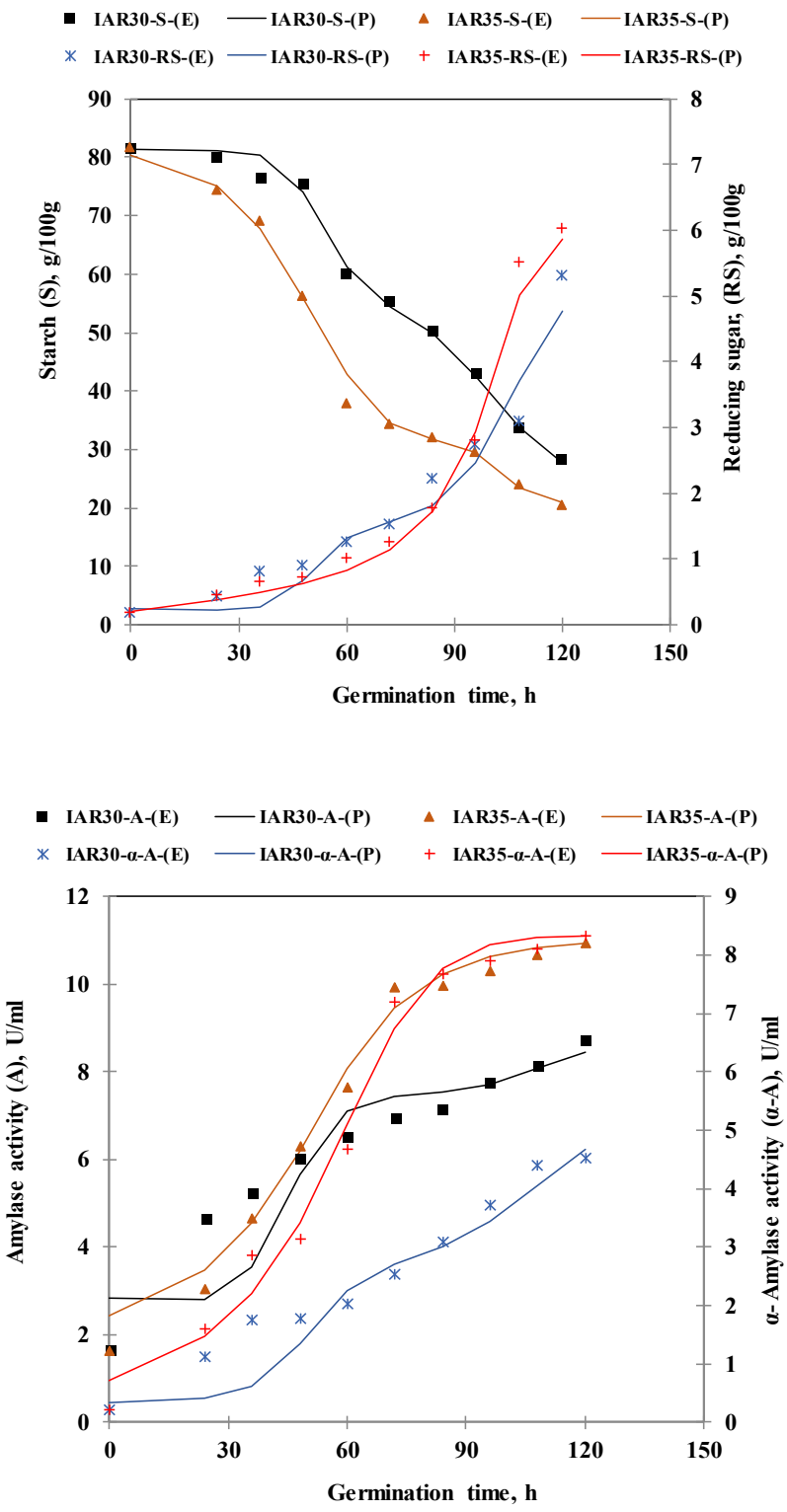

Fig. 4.14 Graph between experimental and ANN predicted values of IAR rice; Starch and Reducing sugar (Top); Amylase and α-amylase (Bottom)

4.3 Predicting enzymatic starch hydrolysis mechanism during paddy malting by vibrational spectroscopy and multivariate calibration analysis

The enzymatic starch hydrolysis mechanism was predicted during malting of paddy (low amylose and intermediate amylose) under different germination conditions (temperature and time) based on the structural change obtained from the spectra of vibrational spectroscopy. Further, multivariate calibration analysis model had been developed to quantify amylose, amylopectin, total starch and reducing sugar content during the process of malting by employing the PLS algorithm, and thereafter compare the results with those obtained from the standard calorimetric method.

4.3.1 Time and temperature dependent change in amylose and amylopectin during malting of paddy

Several biochemical changes take place in paddy during germination (Table 4.7). An increasing trend of amylose content was observed in LAR malted rice at both temperatures whereas the amylopectin content decreased significantly ($p \leq 0.05$). This might be due to the action of amylolytic enzymes on the branched structure of amylopectin leading to the formation of small-branched oligosaccharides. On the other hand, the amylose content and amylopectin of IAR malted rice decreased significantly ($p \leq 0.05$) during the 120 h of germination. However, higher extent of decrease occurred in amylopectin as compared to amylose in both varieties of paddy. The changes in of LAR and IAR were different due to the variation in amylose and amylopectin contents. The variation in the size of the substrate during hydrolysis played an important role and higher amylase action might have occurred on amylopectin [13]. Germination temperature had a significant effect on amylose and amylopectin contents of malted paddy (LAR and IAR) as higher change was noticed at 35°C compared to that at 30°C. Moreover, both malted paddy germinated at 35°C exhibited higher extent of decrease in amylopectin as compared to that at 30°C (Table 4.7). Amylose and amylopectin are the two glucopolysaccharide components of starch [58] and thereby a similar trend in changes was observed for starch degradation during germination which was indicated in our earlier section 4.1.3.1 [54].

Table 4.7 Amylose and amylopectin composition of low amylose (LAR) and intermediate amylose (IAR) malted paddy during germination

Time (h)	Amylose		Amylopectin	
	30°C	35°C	30°C	35°C
Low Amylose rice				
0	12.32±0.35	12.32±0.35	62.12±0.93	62.12±0.93
24	12.23±0.21	12.20±0.25	53.23±1.01	52.34±0.80
48	13.03±0.67	13.79±0.21	28.64±0.39	23.51±1.21
72	14.61±0.28	14.73±0.42	23.78±0.78	17.82±1.13
96	15.46±0.21	17.69±0.33	18.40±0.73	13.10±0.85
120	16.53±0.21	21.10±0.28	14.15±0.12	6.86±0.61
Intermediate Amylose rice				
0	20.2±0.70	20.20±0.70	61.32±0.74	61.32±0.74
24	19.67±0.22	20.01±0.70	60.28±1.06	54.33±0.31
48	20.22±1.41	19.98±0.49	55.21±1.29	36.29±0.76
72	16.41±0.35	18.27±0.42	38.95±1.04	16.09±0.71
96	15.68±0.14	17.32±0.70	27.30±0.73	12.27±0.50
120	13.73±0.49	14.64±0.37	14.58±0.65	5.81±0.29

4.3.2 Starch hydrolysis mechanism during malting by vibrational spectroscopy

4.3.2.1 Raman spectroscopy

Germination of paddy brings about important biochemical changes in the endosperm. The main mechanism involved during germination is the hydrolysis of starch by various amylolytic enzymes to provide energy to the growing embryo. Both LAR and IAR varieties showed a decrease in total starch and a significant increase in amylolytic activity which resulted in the formation of reducing sugars.

Raman spectroscopy is based on scattering of light which is sensitive to skeletal vibrational modes, such as C–C symmetric vibration and pyranoid ring vibration [38]. This technique along with FTIR may help to understand the structural mechanism of paddy germination. The band assignments are listed in Table 4.8 and the Raman spectra of LAR and IAR paddy varieties under different germination conditions are shown in Fig. 4.15 and 4.16.

Four spectral regions were analyzed for the interpretation of the structural mechanism that were: below 800 cm^{-1}, 800-1500 cm^{-1} (the fingerprint region), 1600-1800 cm^{-1} (C=O) and the region between 2800 and 3000 cm^{-1} (C-H stretch region). In Raman spectroscopy,

vibrations in the 800–400 cm^{-1} region are generally due to CCO and CCC deformations, and very strong coupling was noticed which could be related to the glycosidic ring skeletal deformations.

Table 4.8: Band Assignment of FTIR and Raman spectrum listed from literature (Fan et al. [38], Almeida et al. [4])

FTIR		Raman	
Wavenumber (cm^{-1})	**Assignment**	**Wavenumber (cm^{-1})**	**Assignment**
532	Skeletal mode of pyranose ring	442	Skeletal modes of pyranose ring
576		474	
608		652	
710	C-C stretching	710	
857	C(1)-H, CH_2 deformation	864	
930	Skeletal mode vibrations of alpha, 1-4 linkage	888	C(1)-H, CH_2 deformation
1020	Amorphous	918	α-1→6 glycosidic linkage
1054	Crystalline	948	α-1→4 glycosidic linkage
1082	C–O–H bending	1054	(C-O), (C-C), (C-O-H)
1160	C–O, C–C stretching	1000	α-D-glucose
1200	Open chain α-D-glucose	1022	β-D-glucose
1244	CH_2OH (side chain) related mode	1086	C–O–H bending
1342	C-O-H bending, CH2 twisting	1122	C–O stretching, C–O–H bending
1420	CH_2 bending, C–O–O stretch	1158	C–O, C–C, C–H relate mode
1458	C–H bending of –CH2	1200	α-D-glucose
1650	Amide I	1230–1240	Amide III
1550	Amide II	1280	CH_2OH (side chain) related mode
2854	C-H stretching mode	1258	CH_2OH (side chain) related mode
2926	CH_2 stretching	1372	CH_2 scissoring, C–H and C–O–H deformation
		1458	CH_2 bending
		1667–1673	Amide I
		2908	C–H stretching

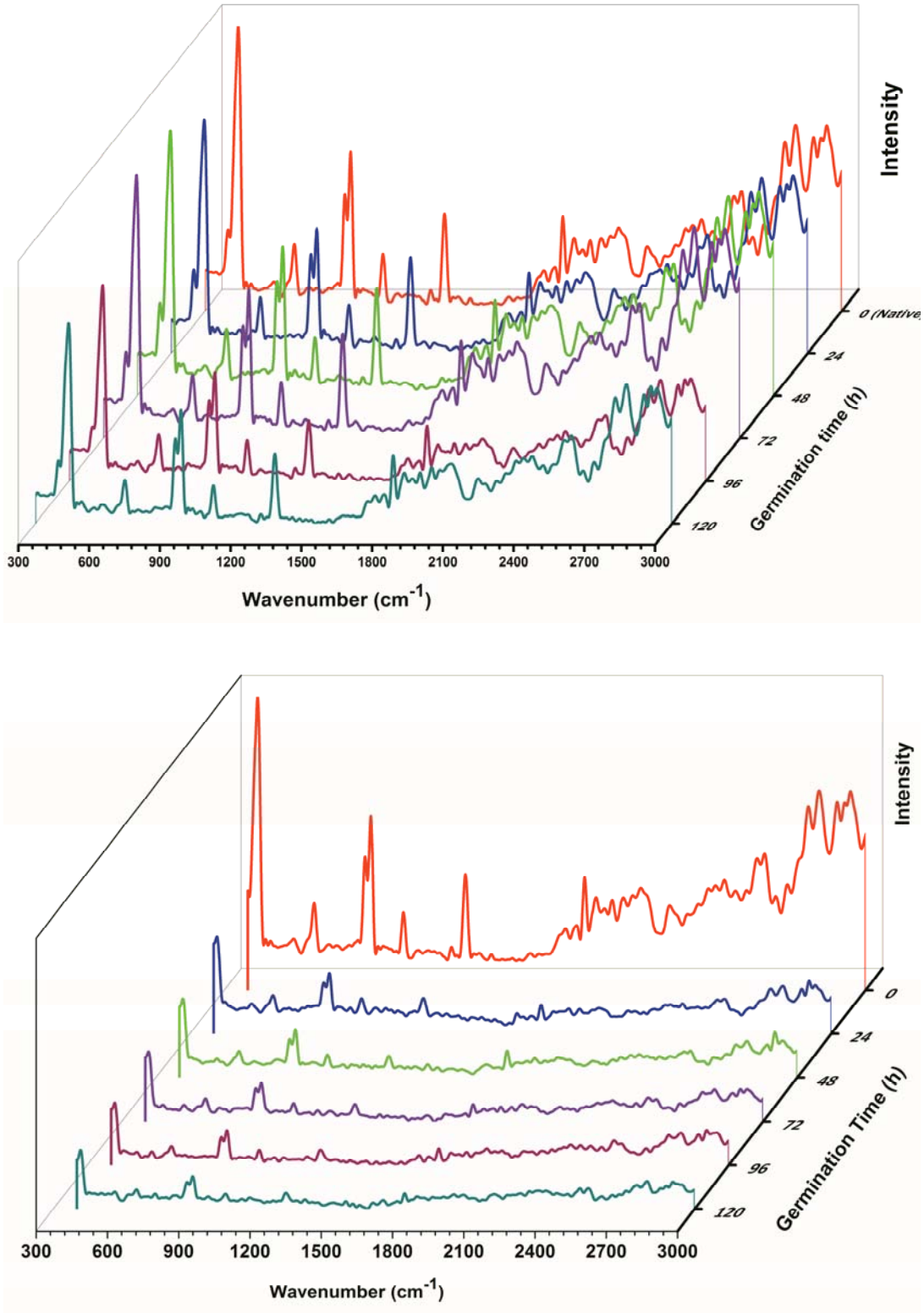

Figure 4.15: Raman spectra of malted paddy varieties at different germination times: (a) LAR 30°C (b) LAR 35°C

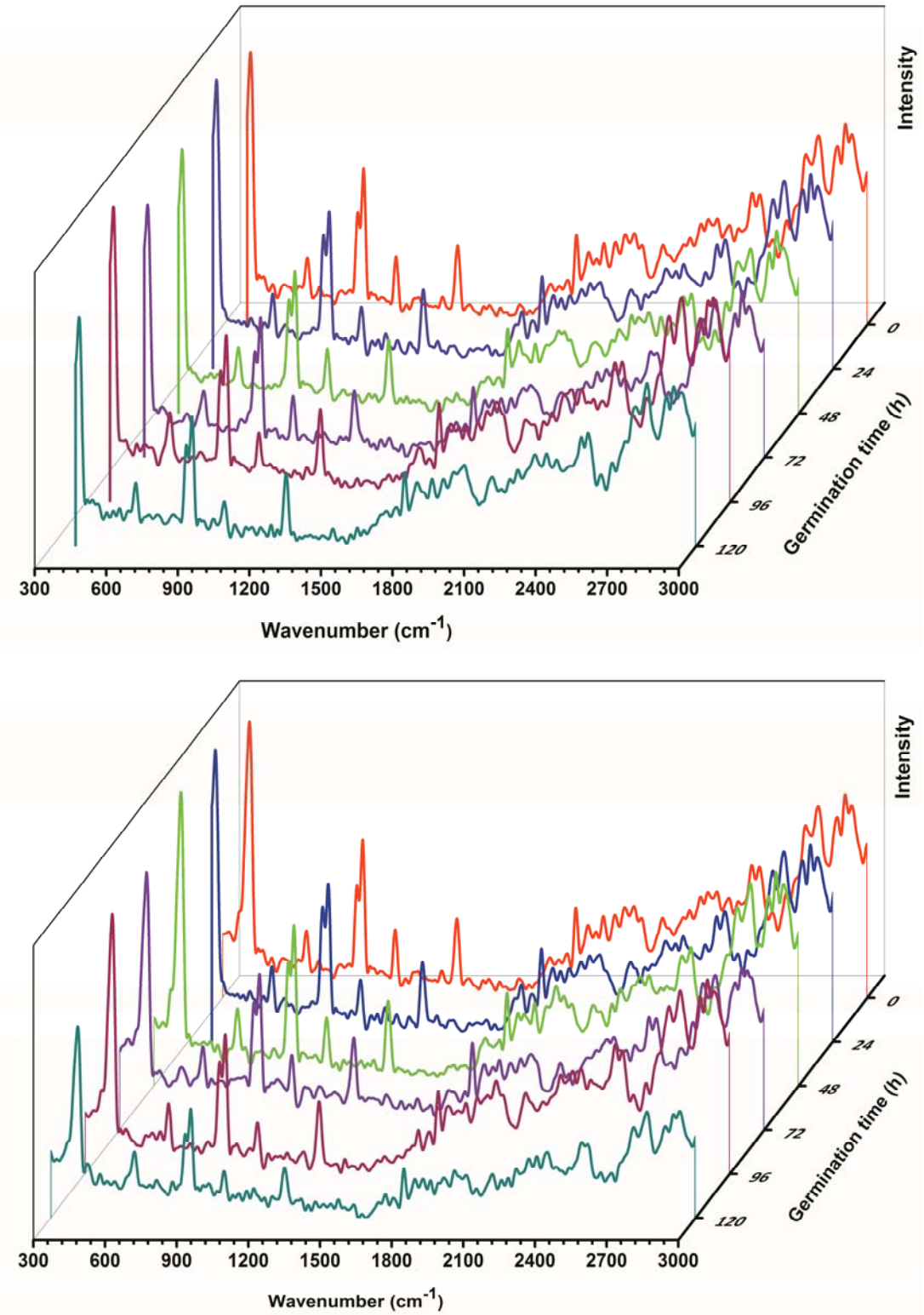

Figure 4.16: Raman spectra of malted paddy varieties at different germination times: (a) IAR 30°C (b) IAR 35°C

In LAR paddy, bands at 442, 474, 678 and 864 cm^{-1} and for IAR paddy bands at 652, 710 and 864 cm^{-1} were observed. These bands might be attributed to the skeletal vibrations of the pyranose ring in the glucose units of starches [56]. Starch is composed of amylose and amylopectin and its variation in LAR and IAR samples might have resulted in different band wavelengths corresponding to the skeletal vibrations. The intensity of these bands decreased significantly with germination time and disappeared at 120 h of germination at both temperatures. It indicated that the skeletal structure of pyranose ring had been degraded during germination and the connection between the chemical bonds were broken down leading to a decrease in vibrational energy.

The region between 1,200 and 800 cm^{-1} is characteristic of the CO and CC stretching and COC deformation modes. The region is mainly known as the fingerprinting or anomeric region [4]. In this anomeric region, the distinction between α and β configurations of the polysaccharide molecules can be made. The vibrations originating from C-O-C of α-1→4 glycosidic linkages were observed near 920-960 cm^{-1} [56]. The Raman spectra of LAR and IAR paddy showed a band at 948 cm^{-1} and 938 cm^{-1}, respectively which might be assigned to the α-1→4 glycosidic linkage. This band decreased significantly ($p \leq 0.05$) after 24 h of germination till 120 h. It might be attributed to the synthesized endo-amylase (such as α-amylase) during germination which cleaved the α-(1→4) linkage [20]. Amylopectin is a major component of starch and the band at 920– 960 cm^{-1} might be attributed to the presence of α- (1→6) glycosidic linkages [4]. In the present study, a band at 918 cm^{-1} was observed for the LAR native rice sample which might be assigned to α- (1→6) linkage present in amylopectin. The spectra showed that the intensity of this band also decreased significantly ($p \leq 0.05$) with germination time indicating starch hydrolysis process which was supported by chemical analysis. In the case of native IAR paddy, the band at 918 cm^{-1} appeared negligible which might be due to its lower amylopectin content compared to LAR. The starch hydrolysis was also observed from SEM micrographs (Fig 4.7) during germination; the micrographs of native rice (LAR and IAR) appeared smooth and homogeneous. Some errosions and indentations were observed from the micrographs of both malted rice at 24 h of germination while cavities were noticed in 120 h sample indicating hydrolysis of the interior of the granules by the mechanism of exocorrosion.

The Raman spectra of carbohydrates showed several vibration spectra in the region between 1500 and 1200 cm^{-1}. The hydrolysis of the glycosidic linkages led to the formation of reducing sugars such as glucose, maltose, dextrins, etc. The Raman spectra of LAR paddy indicated that the intensity of the band at 1054 cm^{-1} (C-O-H bending) showed an increasing

trend with germination time at 30°C. This was due to higher concentration of free hydroxyl groups as glucose contains five free OH groups.

A new band at 1000 cm^{-1} was observed in the LAR paddy after 24 h of germination at 30°C and the intensity increased during the process. This band might be attributed to the formation of α-D-glucose during germination [8, 24]. The Raman spectra of LAR paddy germinated at 35°C showed three new bands at 1025, 1080 and 1126 cm^{-1} after 24 h of germination which might be ascribed to α-D-glucose and β-D-glucose [24]. Similarly, in IAR paddy, new peaks were observed at 1064 and 1087 cm^{-1} that again could be attributed to α-D-glucose and β-D-glucose. Schuster et al. [89] reported a marked increase in the band of 1128 cm^{-1} (C-O-H bend) during saccharification. In the native IAR paddy, a band was observed at 1118 cm^{-1} which was assigned to C-O-H bending. This band shifted to higher wavenumber (1122 cm^{-1}) and the intensity increased during the 120 h of germination at both 30 and 35°C indicating the presence of higher concentrations of free hydroxyl groups. The band at 1158 cm^{-1}, assigned to C–O, C–C and C–H related mode, decreased with germination time in LAR paddy at both temperatures of germination. In the region between 1340 and 1,200 cm^{-1} bands, the contributions of several vibrational modes were observed, such as CO and CC-stretching and CCH, COH, and CCH deformations [4]. The Raman spectra of LAR germinated paddy at both temperatures showed a band at 1200 cm^{-1} indicating the formation of α-D-glucose due to amylolytic activity on starch.

The amylases synthesized during germination is a protein that was identified by Raman spectroscopy for amide-I at 1670 cm^{-1}, amide-III at 1230–1240 cm^{-1} while amide II band appeared to be negligible. Moreover, amide I and amide III bands at different ranges of band wavenumber represented different protein conformations (α-helix, β-sheet and random coil). In the present study, the sample germinated at 30 and 35°C showed a peak at 1670 cm^{-1} after 24 h of germination (Figure 4.15 and 4.16) which increased with germination time. This band might be attributed to the predominance of β-sheet structure of amylase enzyme [83]. Moreover, a new band near 1230–1240 cm^{-1} was observed after the onset of germination (24 h), which increased with germination time indicating the presence of amide III band of protein.

The region at 1260-1280 cm^{-1} of starch in Raman spectra is assigned to CH_2OH (side chain) related mode which is the characteristics of V form amylose [56] and a band close to this region i.e. at 1258 and 1280 cm^{-1} was observed for LAR and IAR paddy, respectively during the germination. The intensity of these band decreased with an increase in the germination

time indicating a degradation of the amylose structure. According to Kizil et al. [56], the vibrational bands (bending and deformation) related to the carbon and hydrogen atoms could be observed in the region 1500-1300 cm^{-1}. The band observed at 1372 cm^{-1} in LAR paddy could be assigned to CH_2 scissoring; during the process of germination, the intensity of this band increased gradually. Similarly, a band at 1458 cm^{-1} was observed for IAR paddy that could be attributed to CH_2 bending. However, this band disappeared during the 120 h of germination at both germination temperatures. Raman spectra of starches showed C-H stretching modes in 2800-3000 cm^{-1}. The intensity of the band at 2908 cm^{-1} decreased which might be due to the variation in the amylose-amylopectin ratio during germination as reported in irradiated starch [56]. Schuster et al. [89] also reported a decrease in the intensity of this band during gelatinization of starch.

4.3.2.2 FTIR

Infrared spectroscopy can provide more information about the chemical groups containing highly polar bonds, or heteronuclear functional groups. A strong vibration of chemical groups is associated with the sharp changes in dipole moment, which in turn leads to a strong IR absorption and a higher peak height in FTIR spectroscopy [38]. The chemical shift in Raman and FTIR spectra for the same chemical group was similar but the intensity and peak numbers of Raman and FTIR varied due to the varietal difference and different vibration modes [38].

Like FT-Raman, four main regions obtained from IR spectra of both native and germinated paddy (LAR and IAR) were analyzed for the interpretation and prediction of structural mechanism of malting in paddy. These regions were: below 800 cm^{-1}, 800-500 cm^{-1} (the fingerprint region), 1600-1800 cm^{-1} (C=O) and the region between 2800 and 3000 cm^{-1} (C-H stretch region). In the present study (Fig. 4.17 and 4.18), the skeletal mode vibrations of the glucose pyranose ring for native LAR and IAR paddy were observed at 528, 576, 608 and 710 cm^{-1}. Unlike in Raman spectra, these bands showed very subtle changes during the 120 h of germination for both the paddy varieties at 30 and 35°C. This might be due to the fact that FTIR spectroscopy was less sensitive towards skeletal vibrational modes, such as C–C symmetric and pyranoid ring vibrations. In FTIR

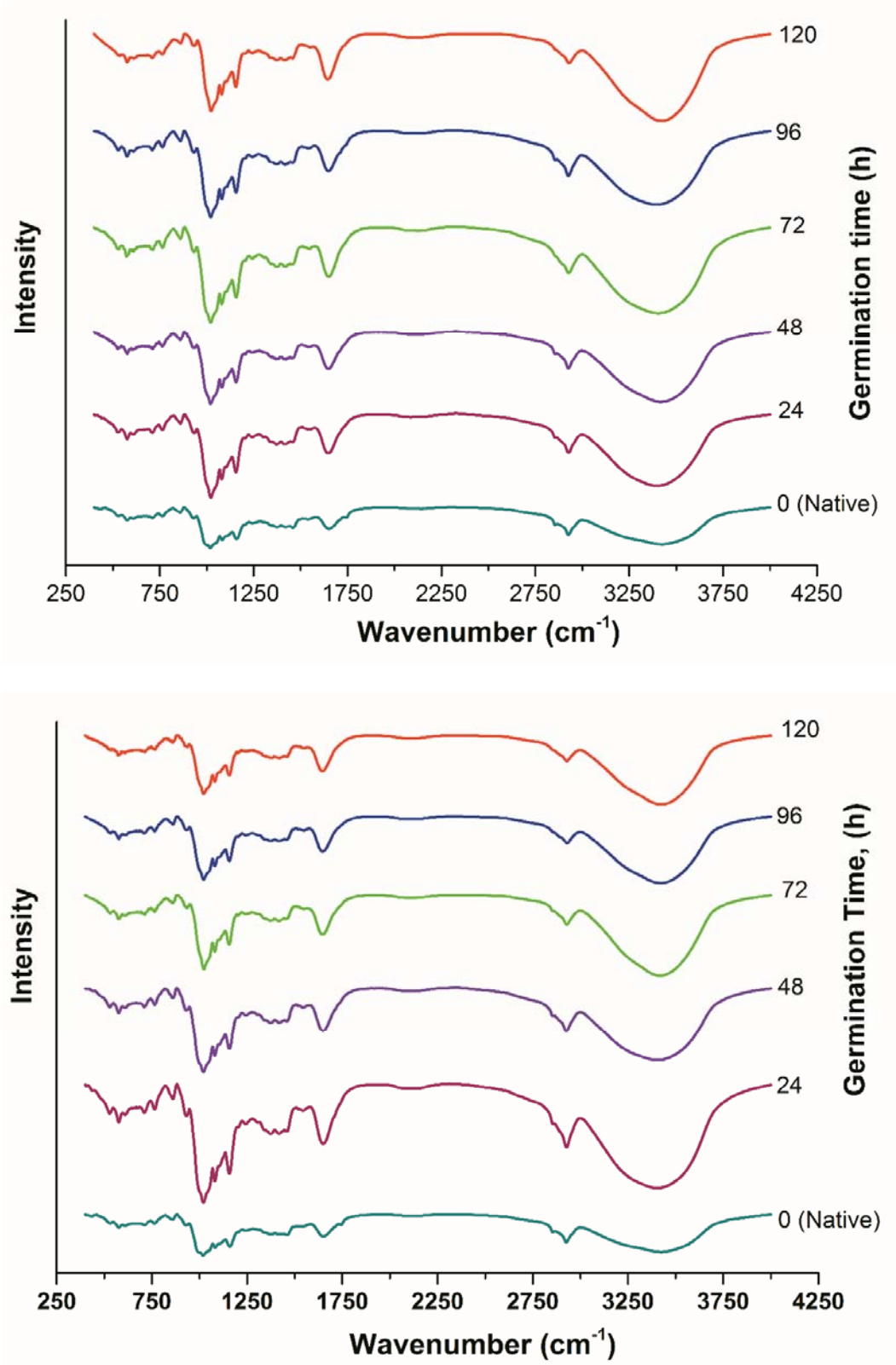

Fig. 4.17 FTIR spectra of malted paddy varieties: (a) LAR 30°C (b) LAR 35°C

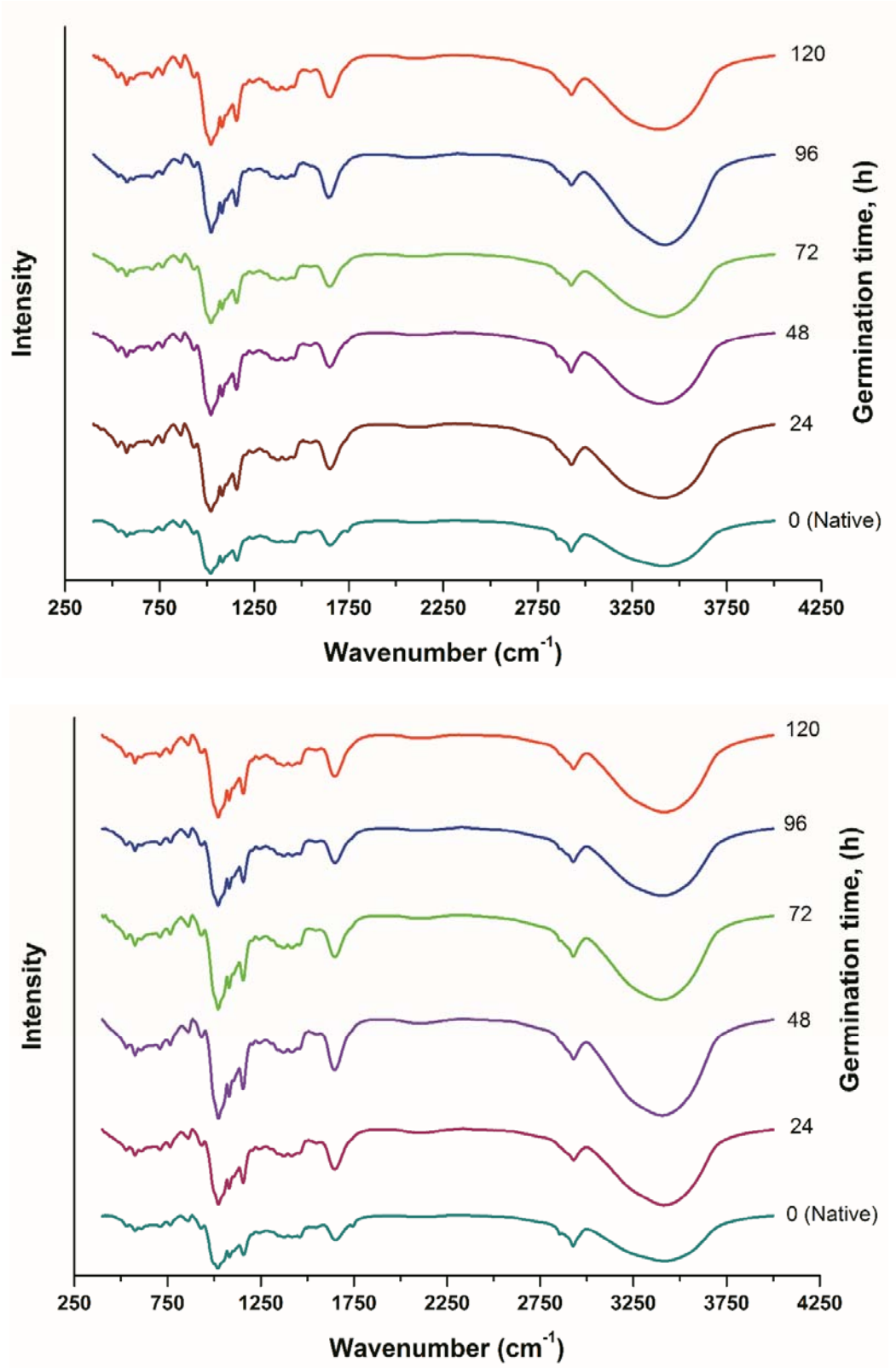

Fig. 4.18 FTIR spectra of malted paddy varieties: (a) IAR 30°C (b) IAR 35°C

spectra, the α,1→4 glycosidic linkage was observed in the band of 931 cm^{-1} and 934 cm^{-1} for both varities of native paddy. After 24 h of germination, a marginal change in location and intensity of the bands were noticed. The change in location might be due to the presence of α-1,6 linkage of the amylopectin that shifted the band to higher wavenumbers [56]. The intensity of the bands decreased after 24 h of germination which was due to the action of the hydrolytic enzymes on the glycosidic linkages. The IR absorbance band at 1022 cm^{-1} was associated with amorphous structure in starch and a band at 1047 cm^{-1} was sensitive to ordered or crystalline structure of starch [102,99]. It was observed that after 24 h of germination, the band at 1022 cm^{-1} increased gradually up to 120 h of germination. However, the intensity of the band at 1047 cm^{-1} corresponding to crystalline region decreased from 24 h of germination and eventually disappeared at 120 h of germination. This result can be correlated with the XRD diffractograms (Fig 4.8) which showed that the crystallinity decreased with the germination time. The native rice showed major peaks at the Bragg angle 15, 18, 20 and 23 which was characteristics of A-type starch. However, with the process of starch hydrolysis during germination the intesity of peak at 15, 18 and 20 2θ were observed to decrease and the peak at 23 2θ became broader during 120 h of germination. The IAR malted rice showed higher decrase in crystallinity as compared to LAR sample which might be due to the higher amylopectin content. Amylopectin is maily considered as the crystalline region in starch and amylopectin content showed higher degradation than amylose. Thus, it could be concluded that the crystalline region degraded faster as compared to amorphous region during germination. Similar results were also reported by Man et al. [63] during hydrolysis of high amylose starch residue by amyloglucosidase. This indicated that a liquefying enzymes like α-amylase, synthesized during germination, cleaved the α, 1→4 glycosidic linkage and being an endo-amylase, it hydrolyzed the bonds located in the inner region of the substrate. The exoamylases, also known as saccharifying enzymes, cleaved α, 1→4 glycosidithec linkage from the non-reducing ends by successive removal of maltose/glucose by the process of multiple- or multi-chain attacks as discussed earlier in the present study. The products of α- and β-amylase hydrolysis are the oligosaccharides of varying chain length having α- and β-configurations, respectively at the C_1 of the reducing glucose unit [70]. These changes were observed in the FTIR spectrum as the intensity of the band 1080 cm^{-1}, corresponding to β-D-glucose, increased from 24 h to 120 h of germination when compared to native paddy. Two new peaks were observed at 1200 and 1342 cm^{-1} after the onset of germination which corresponded to open chains of α-D-glucose and β-D-glucose [46, 47].

It was observed that the amylase enzyme which remains dormant in the native paddy was synthesized during the process of germination at 30 and 35°C [54]. The synthesis of this enzyme was also investigated by FTIR; it was based on the vibrational bands of protein in native form. The amide I vibration, absorbing near 1650 cm^{-1}, increased mainly from the C=O stretching vibration with minor contributions from the out-of-phase CN stretching vibration, the CCN deformation and the NH in-plane bend [17]. This amide I band was particularly known to be associated with secondary structure. In the present study, a small peak was observed at 1650 cm^{-1} for both native paddy. The intensity of the peak increased with the germination time for both the paddy indicating an increase in the synthesis of amylase enzyme. Moreover, amylase enzymes might had a α-helix configuration and a characteristic of unordered structure. According to Barth [17], α-helices gave rise to a main absorption band close to 1650 cm^{-1}. A new peak at 1550 cm^{-1} was observed during 120 h of germination for both the malted paddy which was absent in the native paddy. This phenomenon might be attributed to the amide II band involving C-N stretching vibrations in combination with N-H bending and the band was hardly affected by the side chain vibrations.

The band at 1160 cm^{-1} was identified for the native rice which might be assigned to C-O and C-C stretchings; during germination, a shift of the band was observed and the intensity increased during germination. The FTIR absorption band at 1242 cm^{-1} was attributed to the CH_2OH related mode as well as the C-O-H deformation mode [56]; the intensity of these bands increased marginally during germination. The vibrational bands (bending and deformation) related to the carbon and hydrogen atoms could be observed in the region 1500-1300 cm^{-1} [56]. The native LAR and IAR paddy showed a band at 1376 cm^{-1} which might be assigned to C–H symmetric bending of CH_3, and a shifting towards lower wavenumber was observed between 24 and 120 h. FTIR spectra of starch showed the C-H stretching modes at 2800-3000 cm^{-1}. A small shoulder peak, observed at 2854 cm^{-1} for both the native varities, disappeared gradually during 120 h of germination. The FTIR absorption band at 2926 cm^{-1} shifted to higher wavenumber after 24 h of germination. Intensity changes in this range could be attributed to the variations in the amount of amylose and amylopectin present in starches [56].

4.3.3 Proposed mechanism of starch hydrolysis

A mechanism of starch hydrolysis could be depicted based on structural changes in spectra at different germination times. Germination process induced various biochemical changes in the endosperm by the action of synthesized enzymes. In the present study, based on the

vibrational spectra of malted rice flour, the amylase enzymes (α and β) were synthesized with the onset of germination, which otherwise remained dormant. The amylase enzyme, as observed from the spectrum (amide I, II and III) existed in the α-helical or β-sheet forms during germination. The starch hydrolysis process commenced with the action of amylase on the CCO and CCC bonds which was associated with pyranose ring structure of the glucose units of starch. In the next step, enzyme acted on the CO, CC and COC bonds which indicated to the cleavage of glycosidic linkages in amylose and amylopectin by the process of multiple- and multi- chain attacks. The breakdown of the gycosidic linkages led to a decrease in the crystalline region of strach. The significant increase in the intensity of the bands in the region 1200-1500 cm^{-1} indicated the formation of α and β-D-glucose. The CH_2 bonds in paddy increased with the germination time which was probably due to the changes in the pyranose ring structutre of the glucose units. On the other hand, the C-H stretching mode decreased possibly due to the formation of simple sugars during germination; the formation of simple sugars completed the process of starch hydrolysis.

4.3.4 Multivariate analysis to correlate changes during malting

4.3.4.1 Principle component analysis (PCA)

The PCA biplot (Figure 4.19 and 4.20) shows the inter-relationship among the independent variables (germination time and intensities at different wavelengths obtained from Raman spectra) and dependent variables (amylose, amylopectin, total starch and reducing sugar contents) of LAR and IAR malted samples germinated at 30 and 35°C. In LAR germinated at 30°C shown in Fig. 4.19 (top), the principal components PC1 and PC2 accounted for 64 and 27% of the variation and thus explained 93% of the total variance, and thereby only the plot of PC1 versus PC2 is presented here. The Raman bands at 442, 678, 918, 948, 1054, 1158, 1258 and 2908 cm^{-1} corresponding to skeletal vibrations of the pyranose ring in the glucose unit of starches, amylopectin, α, 1-4 glycosidic linkage, CH_2OH (side chains) mode and C–O, C–C, C–H relate mode formed a group that behaved in a similar manner. This group was present in the vicinity of starch and amylopectin contents, and Raman bands at 864 and 474 cm^{-1}. Both these groups decreased during malting which was observed earlier in the present study due to starch hydrolysis. However, both these groups were inversely related to the time of germination and reducing sugar and amylose contents. The Raman bands at 894, 1000, 1200 and 1372 cm^{-1} was associated with C-O-H modes, α-D-glucose, and CH_2 scissoring were observed to increase with germination time. This was attributed to the action of α- and β-amylases on starch which produced oligosaccharides of varying lengths with an increase in germination time.

The PCA biplot of LAR malted paddy germinated at 35°C (Fig. 4.19 (bottom)) represented the relation between Raman bands and the contents of amylose, amylopectin, total starch and reducing sugar. The PC1 and PC2 together accounted for 94% of the total variation. The time of germination, amylose content, reducing sugar content and bands at 1054 and 1200 cm^{-1} associated with C-O-H mode and α-D-glucose formed a group which indicated that these bands also increased with germination time. This group was in proximity to the Raman bands associated with α and β-D-glucose present in the LAR malted sample. However, both these groups were observed to have an inverse relation with amylopectin and starch contents, and Raman bands corresponding to skeletal vibrations of pyranose ring, C-O modes, CH_2OH relate modes and CH stretching.

In IAR 30°C (Fig. 4.20 (top)), the principal components could explain 90.8% of the variation. The contents of amylose, amylopectin, and starch, and the band at 888, 941 and 1022 formed a cluster. However, the components of the group were inversely related to reducing sugar content and time of germination. It indicated that an increase in germination time decreased the amylose and amylopectin contents but increased the reducing sugar content. In addition, the wave numbers 888, 941 and 1022 bonds representing the CH_2 deformation, skeletal mode vibrations of α-1,4 glycosidic linkage, respectively also decreased. Schuster et al. [89] also observed similar results during on-line monitoring of starch hydrolysis by FT-Raman spectroscopy. It might be possible that the hydrolytic enzymes acted on starch during germination which cleaved the glycosidic linkages in amylose and amylopectin. The time of germination was in the neighborhood of reducing sugar and band at 1087 cm^{-1}, representing β-D-glucose. It indicated that the action of enzymes acted on the starch present in the rice kernels to produce the low molecular compounds like the reducing sugars. An increase in the time of germination exhibited a decrease in the bands at 710, 864 and 1458 corresponding to glycosidic ring skeletal deformations and CH_2 bending, respectively which again indicated degradation of starch.

The PCA biplot of IAR malted rice germinated at 35°C is shown in Fig. 4.20 (bottom). The PC1 and PC2 accounted a variation of more than 94%. The germination time was closely related to Raman bands associated with α and β-D-glucose; these bands increased with germination time. On the other hand, similar to earlier study, amylose, amylopectin and starch contents and bands related to skeletal modes of pyranose ring and CH_2 bending showed the inverse relationship with germination time.

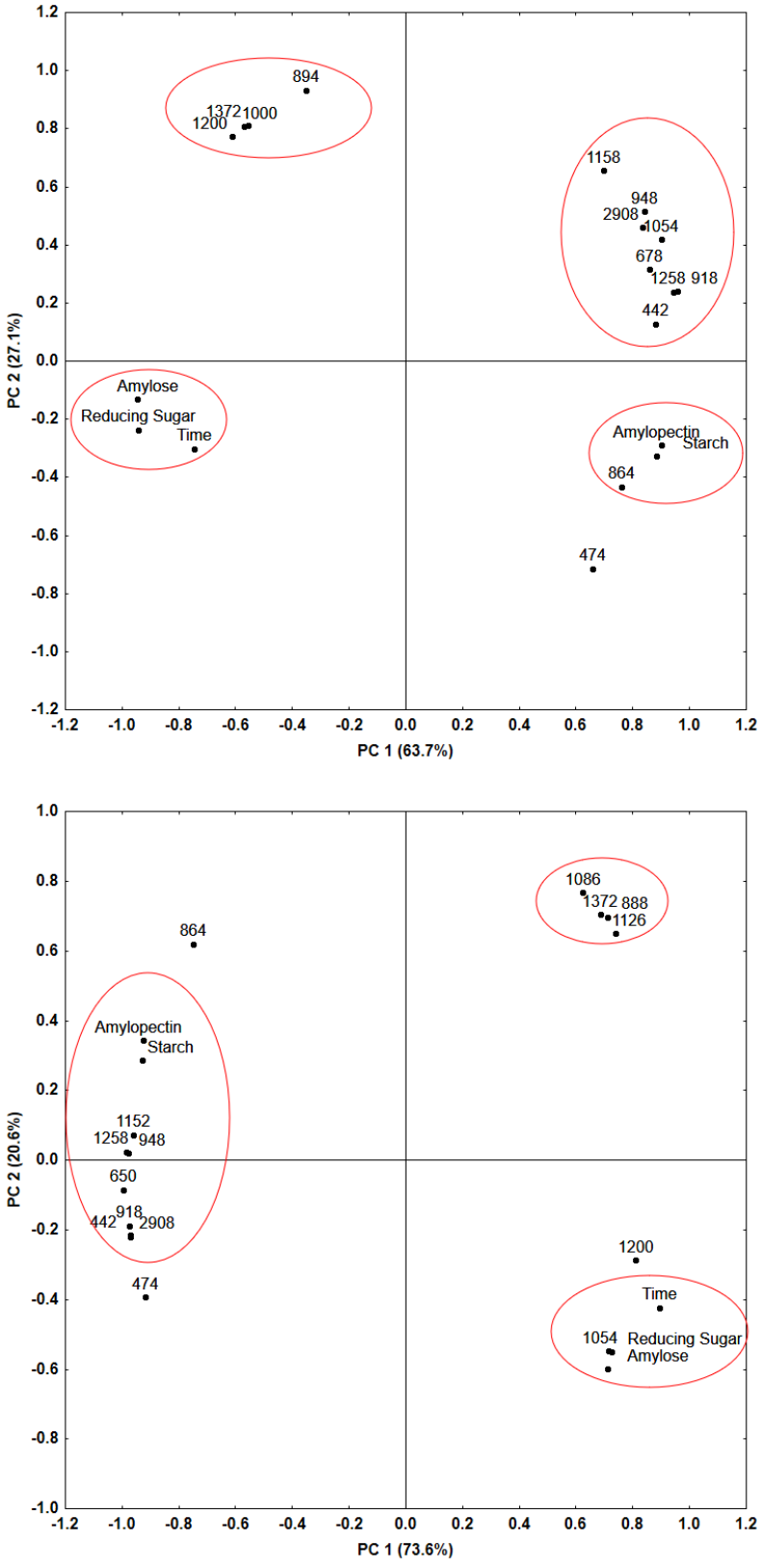

Fig. 4.19 PCA biplots of malted paddy varieties: LAR 30°C (top); LAR 35°C (bottom)

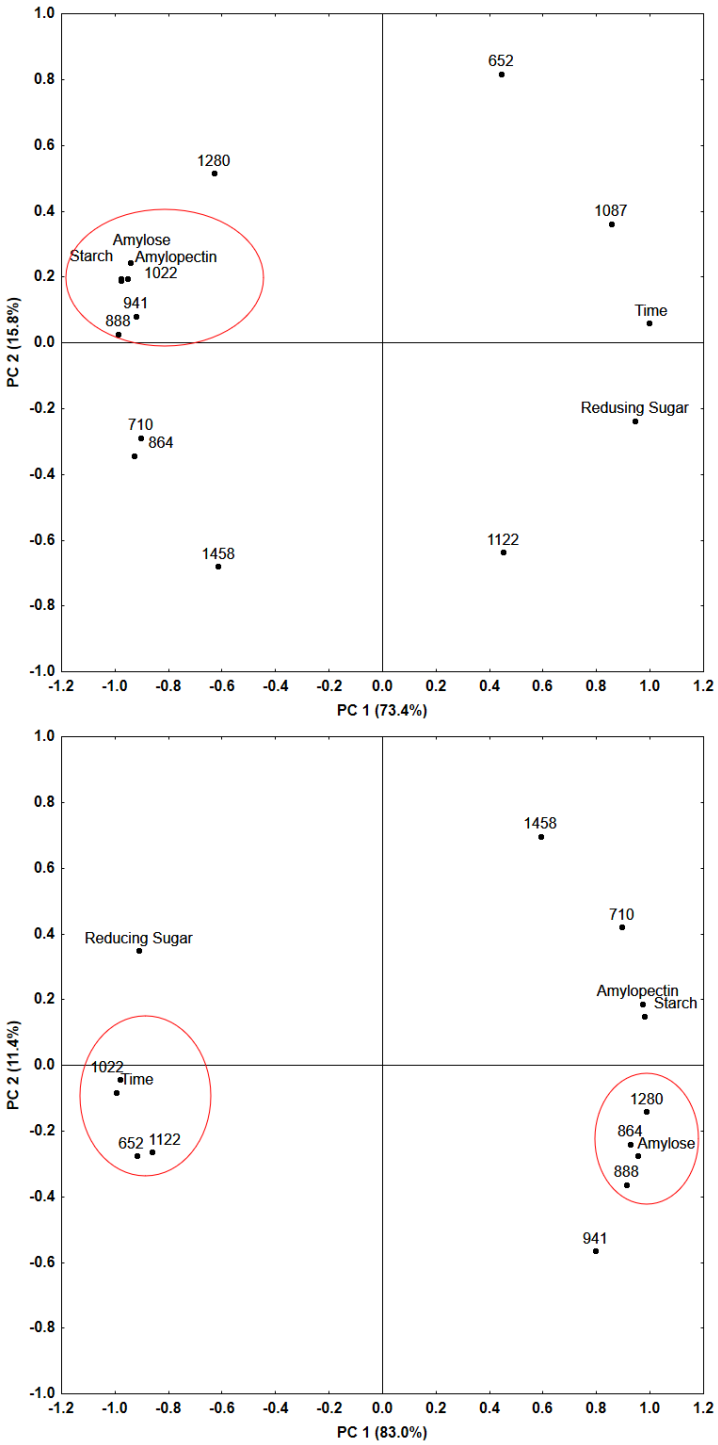

Fig. 4.20 PCA biplots of malted paddy varieties: IAR 30°C (top); IAR 35°C (bottom)

4.3.4.2 Partial least squares (PLS)

The method of PLS can be employed for multivariate calibration [4]. It first extracts a set of latent factors that may explain as much of the covariance as possible between the independent and dependent variables; latter, a regression step predicts values of the dependent variables. In the present study, the relevant information contained in the Raman

spectra were concentrated in a few latent variables, which were then optimized to produce the best correlation with amylose, amylopectin, total starch and reducing sugar contents of LAR and IAR samples. The PLS model was constructed with the data obtained from the Raman intensity (variable X) and the amylose, amylopectin, total starch and reducing sugar contents (variable Y), and the data were arranged in a matrix form. The number of components to be used in the study model was chosen by cross validation method. The correlation coefficients obtained for both LAR and IAR paddy at both germination temperatures were between 0.981 and 0.998 (significant at $p \leq 0.01$). The actual versus predicted plot of different parameters are shown in Fig 4.21 and it can be observed that the actual and predicted values are close to each other. The accuracy of the model could also be judged by the root mean square error of prediction (RMSEP) and a high value of RMSEP leads to a poor predictive ability of the model. In the present study, the RMSEP values were found to be low (0.043-0.568) for all the analysis. This indicated that the Raman spectroscopy can be applied for quantification of amylose, amylopectin, total starch and reducing sugar in germinated paddy.

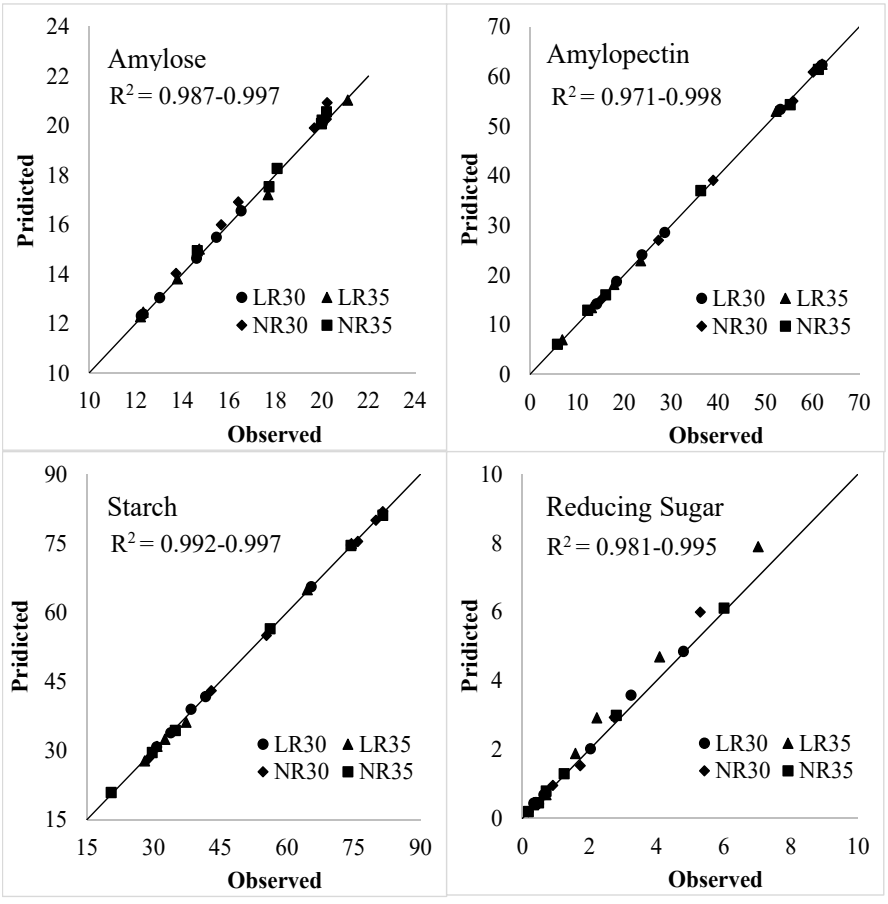

Fig. 4.21 Actual value versus Raman predictions of different parameters of LAR and IAR malted paddy

4.4 Interrelation between pasting properties and thermal behaviour of malted rice

The process of germination brings about various modifications due to decomposition of high molecular weight compounds. An increase in reducing sugars occurs while the viscosity of the malted rice slurry decreases due to the amlyolytic effect on starch [75]. However, the understanding of the effect of amylose and amylopectin ratio on the pasting properties and thermal behaviour of malted rice at different germination conditions are still inadequate. Moreover, the correlation among pasting properties and thermal behaviour of malted rice during the process of germination also requires detailed investigations. The pasting properties of the malted rice was carried out by rapid visco analyser (RVA) while thermal properties were measured in a differential scanning calorimeter (DSC) at a temperature range from 20 to 150°C. The results are expected to provide an insight into the changes occurring during the process of germination in the endosperm and assist in the development of malted rice flour based weaning food formula, and bakery and confectionery products.

4.4.1 Pasting properties

A rapid visco-analyser (RVA) is a tool to monitor the changes during cooking. The pasting behaviour of malted LAR and IAR varieties is shown in Fig. 4.22 and Table 4.9.

4.4.1.1. Pasting temperature

The pasting temperature (PT) indicates the minimum temperature required to gelatinise/cook a starch-rich sample. During gelatinization, water is absorbed by the sample which involves granular swelling, melting of the crystalline zone of starch, exudation of the molecular components from the granular portion and eventually total distribution of the granules. The native LAR showed a lower PT compared to IAR (Fig. 4.22) which might be due to a variation in the amylose content. Jang et al. [49] reported that higher amylose content of rice starch had higher PT. The LAR and IAR showed a decrease in PT as germination time increased indicating a faster swelling and gelatinization of the germinated starch granules. Similar results were also observed by Musa [71] for germinated brown rice which swelled faster than the brown rice and white rice. Germination caused enzymatic hydrolysis of starch which felicitates the swelling of granules. The independent variables amylose/amylopectin content and germination time had significant effects ($p<0.05$) though germination temperature did not have a significant effect. However, the interaction between independent variables did not have a significant effect ($p\leq0.05$) on PT.

4.4.1.2. Peak viscosity

Peak viscosity (PV) of a starch-rich sample reflects the water binding capacity; the magnitude also indicates the energy required for mixing and transferring of viscous sample [27]. The native IAR exhibited higher PV than native LAR which might be attributed to the higher amylose content in IAR. A similar result was also reported by Noda et al. [73]. The ANOVA indicated the significant effect of amylose-amylopectin content, time and temperature on PV.

Table 4.9 Pasting properties of malted LAR and IAR rice at different germination conditions

Time (h)	PT	PV1	PV2	HPV	BDV	SBV	CPV
LAR30	°C	mPa-s	mPa-s	mPa-s	mPa-s	mPa-s	mPa-s
0	71 ± 1^{c}	0 ± 0^{a}	1757 ± 3^{e}	1092 ± 1^{f}	665 ± 5^{d}	686 ± 2^{b}	1785 ± 1^{e}
24	69 ± 2^{b}	226 ± 1^{f}	255 ± 1^{d}	200 ± 2^{e}	55 ± 0^{c}	175 ± 2^{ab}	374 ± 4^{d}
48	68 ± 0^{b}	92 ± 0^{e}	100 ± 1^{c}	83 ± 0^{d}	17 ± 1^{b}	78 ± 0^{ab}	160 ± 1^{c}
72	65 ± 0^{a}	33 ± 1^{d}	40 ± 0^{b}	30 ± 1^{c}	10 ± 1^{a}	19 ± 0^{a}	51 ± 0^{b}
96	65 ± 0^{a}	28 ± 1^{c}	30 ± 1^{a}	21 ± 0^{b}	9 ± 1^{a}	13 ± 1^{a}	36 ± 1^{a}
120	65 ± 0^{a}	25 ± 1^{b}	28 ± 1^{a}	20 ± 1^{c}	8 ± 2^{a}	12 ± 1^{a}	32 ± 2^{a}
LAR35							
0	71 ± 1^{a}	0 ± 0^{a}	1757 ± 3^{e}	1092 ± 1^{e}	665 ± 5^{c}	686 ± 2^{b}	1785 ± 1^{e}
24	70 ± 7^{a}	305 ± 7^{d}	320 ± 6^{d}	258 ± 12^{d}	62 ± 4^{b}	212 ± 8^{c}	471 ± 1^{d}
48	70 ± 7^{a}	67 ± 0^{c}	82 ± 0^{c}	68 ± 0^{c}	15 ± 0^{a}	53 ± 1^{b}	121 ± 2^{c}
72	66 ± 6^{a}	32 ± 2^{b}	44 ± 0^{b}	38 ± 0^{b}	6 ± 0^{a}	20 ± 2^{a}	57 ± 2^{b}
96	66 ± 3^{a}	25 ± 0^{b}	32 ± 0^{a}	24 ± 1^{a}	7 ± 1^{a}	11 ± 0^{a}	35 ± 0^{a}
120	66 ± 2^{a}	22 ± 1^{b}	27 ± 1^{a}	22 ± 1^{a}	5 ± 0^{a}	10 ± 1^{a}	32 ± 0^{a}
Time (h)	**PT**	**PV**	**HPV**	**BDV**	**SBV**	**CPV**	
IAR30	°C	mPa-s	mPa-s	mPa-s	mPa-s	mPa-s	
0	75 ± 0^{b}	3041 ± 2^{f}	806 ± 3^{f}	2235 ± 5^{e}	2113 ± 2^{e}	2919 ± 4^{e}	
24	72 ± 1^{b}	987 ± 1^{e}	407 ± 4^{e}	583 ± 2^{d}	821 ± 1^{d}	1228 ± 3^{d}	
48	71 ± 1^{b}	157 ± 3^{b}	47 ± 1^{c}	111 ± 3^{c}	79 ± 2^{c}	126 ± 6^{c}	
72	70 ± 0^{a}	146 ± 1^{d}	45 ± 0^{d}	142 ± 1^{b}	64 ± 0^{b}	118 ± 1^{b}	
96	70 ± 0^{a}	79 ± 1^{b}	41 ± 1^{b}	41 ± 0^{a}	24 ± 1^{a}	61 ± 0^{a}	
120	68 ± 1^{a}	73 ± 1^{a}	31.5 ± 2^{a}	38.5 ± 1^{a}	20 ± 3^{a}	55 ± 1^{a}	
IAR35							
0	75 ± 0^{b}	3041 ± 2^{e}	806 ± 3^{e}	2235 ± 5^{f}	2113 ± 2^{f}	2919 ± 4^{e}	
24	72 ± 1^{b}	624 ± 6^{d}	241 ± 6^{d}	383 ± 0^{e}	442 ± 1^{e}	683 ± 4^{d}	
48	72 ± 1^{a}	151 ± 4^{c}	45 ± 1^{c}	106 ± 2^{d}	35 ± 0^{d}	76 ± 4^{c}	
72	70 ± 0^{a}	132 ± 3^{b}	45 ± 1^{c}	87 ± 2^{c}	32 ± 1^{c}	81 ± 2^{c}	
96	70 ± 0^{a}	79 ± 0^{a}	34 ± 0^{b}	45 ± 0^{b}	24 ± 1^{b}	58 ± 1^{b}	
120	68 ± 1^{a}	75 ± 0^{a}	32 ± 0^{a}	43 ± 0^{a}	15 ± 0^{a}	42 ± 0^{a}	

Values in the same column with different subscripts are significantly different at $p\leq0.05$

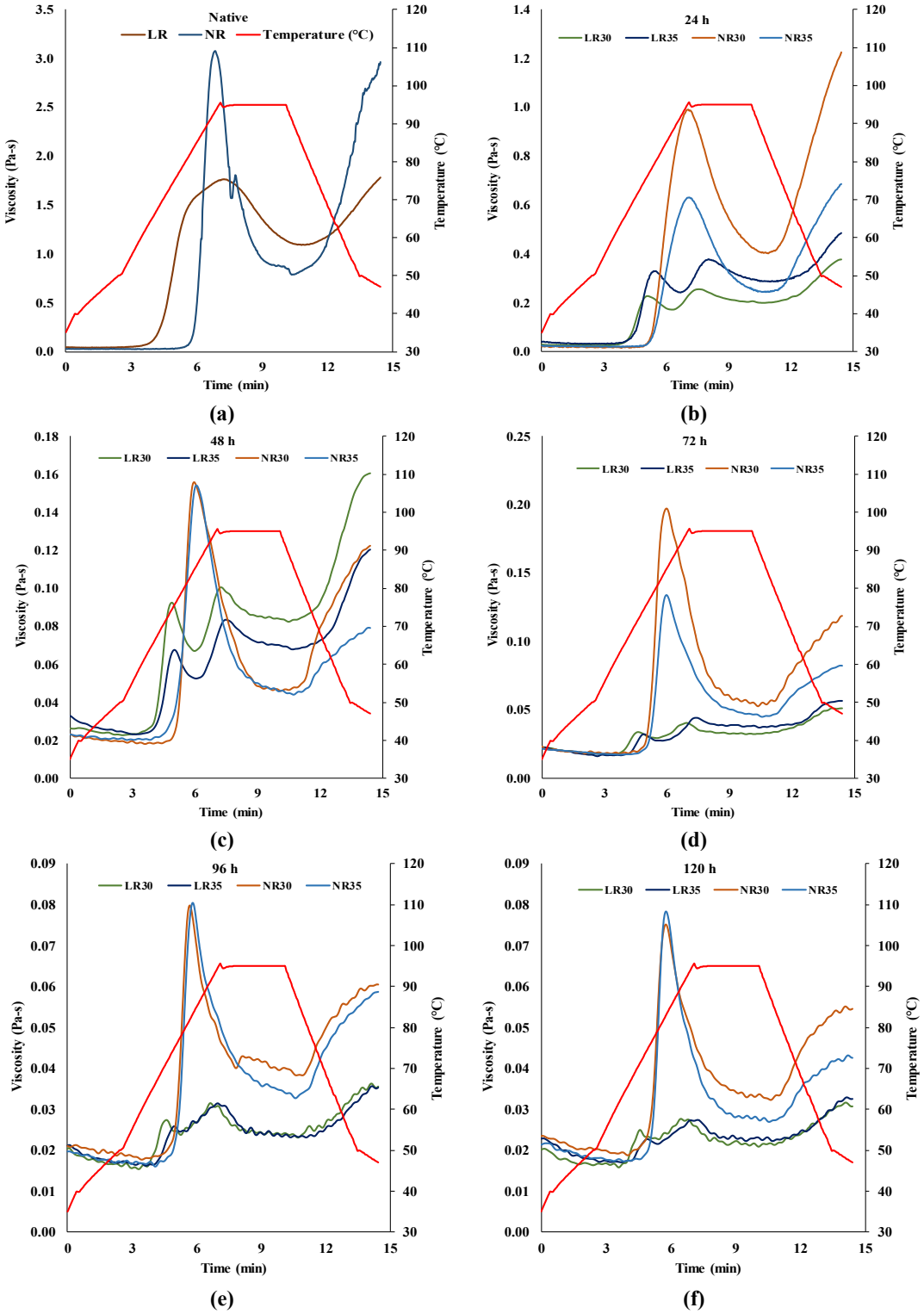

Fig 4.22: Pasting properties of LAR and IAR malted rice at different germination conditions: (a) Native rice, (b) 24 h germination, (c) 48 h germination, (d) 72 h germination, (e) 96 h germination, and (f) 120 h of germination

Two peak viscosities were observed in LAR30 and LAR35 (Fig 4.22). A steep rise in viscosity was noticed from the pasting point and the first peak appeared at about 4 min which was followed by a decrease in viscosity. Unlike IAR, a second PV was observed after a few minutes followed by a decrease in viscosity before setback viscosity. The biphasic peak observed for malted LAR samples was possibly due to the formation of starch-lipid complex. It was reported that in cereal starches, lipids are present both on the surface and inside the granule, and they may be in the free or bound state to starch components [15]. As amylopectin content is higher in LAR, its outer branches might assist in the formation of a helical inclusion complex with lipid [36]. However, it was observed that the complex did not survive for a long time as dissociation occurs due to the shearing action in the viscoamylograph in addition to the heating process which eventually caused a fall in viscosity. The magnitude of the second peak was higher than that of the first peak viscosity but both the peaks decreased significantly during the phase of germination due to breakdown of amylopectin. A similar biphasic pasting curve due to the formation of amylose-lipid inclusion complexes was reported by Nelles et al. [72] for maize starch during prolonged holding time when subjected to viscoamylographic testing.

Germination process hydrolyses starch to smaller molecules by the secreted hydrolytic enzymes. The α-amylase being an endo-amylase cleaves the α-1, 4 glycosidic bonds from the inner regions of starch which results in decreases viscosity. On the other hand, exo-amylases also known as saccharifying enzymes, hydrolyse starch from the non-reducing ends to yield maltose and glucose. However, both α- and β-amylases cannot cleave the α-1→6 glycosidic linkages which produce α- and β-dextrins; these dextrins of sufficient degree of polymerization (DP) might have complexed with endogenous lipids present in starch during the process of gelatinization through ionic or hydrogen bonding to exhibit the second PV [68]. Wu et al. [101] reported a similar decrease in PV during the germination of brown rice. It was attributed to a decrease in starch content by the amylase activity. In the case of IAR samples, a higher degradation of starch was observed; conversion to simple reducing sugars was expected by various hydrolytic enzymes without amylose-lipid complex formation. The change in PV during germination might also be attributed to the loss of crystallinity of starch granules which was reported in section 4.1.4.3.

4.4.1.3. Hot paste viscosity

The peak viscosity is followed by the hot peak (paste) viscosity (HPV), and it is the viscosity of the system at the end of cooking/heating time at 95ºC. The HPV primarily indicates the fragility of the swollen grains towards shear treatment. During the holding period at 95°C, disruption of granules occurs due to shearing offered by the rotating paddle and bowl. This phenomenon resulted in the formation of a viscous mass/paste; the cooked starch paste consisted of a continuous phase of solubilized starch fraction and a discontinuous phase of granule remnants (outer portion of the granule) [32]. The germination time had a significant effect on HPV compared to amylose-amylopectin content and temperature.

The native LAR showed higher HPV compared to IAR (Fig. 4.22). It is possible that a variation in the amylose and amylopectin contents had a significant effect on HPV. Amylopectin is usually responsible for swelling of starch granules whereas amylose and lipids impede granular swelling and maintain the integrity of the swollen granules during pasting [49]. Therefore, higher swelling of LAR granules increased its susceptibility to shear damage resulting in high HPV. Comparable results were also reported by Ashogbon [11] who studied the pasting properties of starch from different cultivars of rice from Nigeria.

The HPV of LAR and IAR samples decreased with germination time due to the action of amylolytic enzymes; the amylose-amylopectin content showed significant effect. IAR showed a higher decrease of HPV compared to LAR at both germination temperatures which might be due to its high amylopectin content that affected the swelling of granules and their disintegration.

4.4.1.4. Breakdown viscosity

Breakdown viscosity (BDV) measures the susceptibility of cooked starch towards disintegration during continuous stirring and heating; it is calculated as the difference between the PV and HPV. During heating in the viscoamylograph, the swelled granules had a less space to expand further, and the Brownian movement made the swollen granules to collide each other, and thus disintegrated to a high extent. However, the breakdown depended on the rigidity and structural integrity of the swollen granules.

The BDV of native IAR was higher than that of LAR (Fig 4.22). The high breakdown indicated the sensitivity towards heat and stress during cooking [37]. This result was not in agreement with the previous studies which had suggested a less breakdown of IAR due to

the presence of amylose that hindered granule swelling [49, 97]. Park et al. [78] indicated that although IAR was resistant to gelatinization, they broke down easily once they had been gelatinized.

The BDV for both LAR and IAR decreased drastically after 24 h of germination whereas it further decreased at a slower rate which was also observed by Juhasz et al. [52]. However, a significant effect ($p \leq 0.05$) was observed between amylose-amylopectin content, time and. The malted IAR showed a higher decrease (about 20%) compared to malted LAR (about 10%) at both germination temperatures.

4.4.1.5. Setback viscosity

Setback viscosity (SBV) or retrogradation index refers to the process of cooling of a heated starch dispersion in which the exuded amylose molecules re-associate and the swollen starch granules are united to provide an ordered structure resulting in an increase of the system viscosity. This phenomenon is also known as the recrystallization process of amylopectin and amylose during which the formation and aggregation of double helices takes place. A high SBV implies a high extent of re-crystallization of gelatinized starch during the phase of cooling of starch-rich samples [37]. Higher SBV values were observed for native LAR compared to IAR. Ashogbon [11] and Kong et al. [57] reported that the amylose component in the starch had the higher retrogradation tendencies. The higher SBV of native LAR sample might be attributed to the longer chain length of amylopectin which helped the development of retrograded fractions.

The SBV of malted LAR and IAR samples increased during the initial 24 h of germination. This was expected due to the hydrolysis of amylose and amylopectin molecules which matched the earlier results of Musa et al. [71] for germinated brown rice. This phenomenon is related to chain length and contents of amylose and amylopectin in starch. The interaction between amylose-amylopectin content, time and temperature showed a significant difference ($p<0.05$) in setback. The IAR30 and IAR35 showed the higher decrease compared to LAR30 and LAR35 samples which might be attribute to the higher extent of hydrolysis of starch granules by amylolytic enzymes.

4.4.1.6. Final or cold paste viscosity

Cold paste viscosity (CPV) or final viscosity is the viscosity of the system at the end of the cooling phase at 50°C; the increase in viscosity is due to retrogradation or re-association

characteristic of amylose due to a decrease in the system temperature. The viscosity measured at 50°C might be linked to the eating quality of foods. The native IAR showed a higher CPV compared to LAR which might be attributed to the linear chain structure of amylose to aid the formation of hydrogen bonds resulting in the development of firm gels [57].

The CPV of the malted LAR and IAR for both temperatures decreased significantly as germination time increased. IAR30 and IAR35 exhibited higher decrease in CPV compared to LAR30 and LAR35. The interaction between amylose-amylopectin content, time and temperature showed significant effects ($p<0.05$) on CPV. The decrease in CPV with germination time was mainly due to amylase activity; the enzyme activity increased with germination time to enhance the breakdown of starch into small fragments and exhibited a decline in CPV. The pasting property had been reported to be affected by the presence of proteins and lipids, and the formation of amylose-lipid complexes [68].

4.4.2 Thermal behaviour

The measured thermal properties of samples in terms of the onset temperature (T_O), peak temperature (T_P) and completion temperature (T_C) are shown in Table 4.10 and Fig. 4.23 (sample graph). These indices were affected by the amylose-amylopectin content, germination time and temperature. The onset temperature (T_O) reflects the initiation of gelatinization phenomenon and corresponds to PT of RVA. The T_O values of non-germinated samples (65.7-66.0°C) were lower than that of PT values (71.0-75.0°C). Woo et al. [100] reported the T_O of starches from 10 rice cultivars to be between 57.9 and 64.4°C which was lower than those obtained in the present investigation. These differences might be attributed to the differences in the principle of measurement. The gelatinization temperatures (T_O and T_P) of the native IAR were higher compared to LAR. This might be attributed to the variation in the amylose and amylopectin contents. In high amylose rice, the chain association between amylose decreases the hydration of the amorphous region of the starch granules and thereby retards swelling and gelatinization [49]. Park et al. [78] also reported similar observations where non-waxy rice showed higher T_O and T_P as compared to waxy rice which were attributed to the presence of the crystalline region in the waxy rice which required less energy for melting. The onset temperature (T_O) and peak temperature (T_P) of malted LAR and IAR samples increased till 24 h of germination. This might be attributed to the *in-situ* formation of starch-lipid complex as reported earlier in the present

study. It is reported that in excess water, as in case of DSC, a total dispersion of amylose molecules in aqueous phase occurs which makes them readily available for complexing with the dispersed liquids. Moreover, crystalline amylose–lipid complexes can be obtained especially when crystallization occurs at a high temperature.

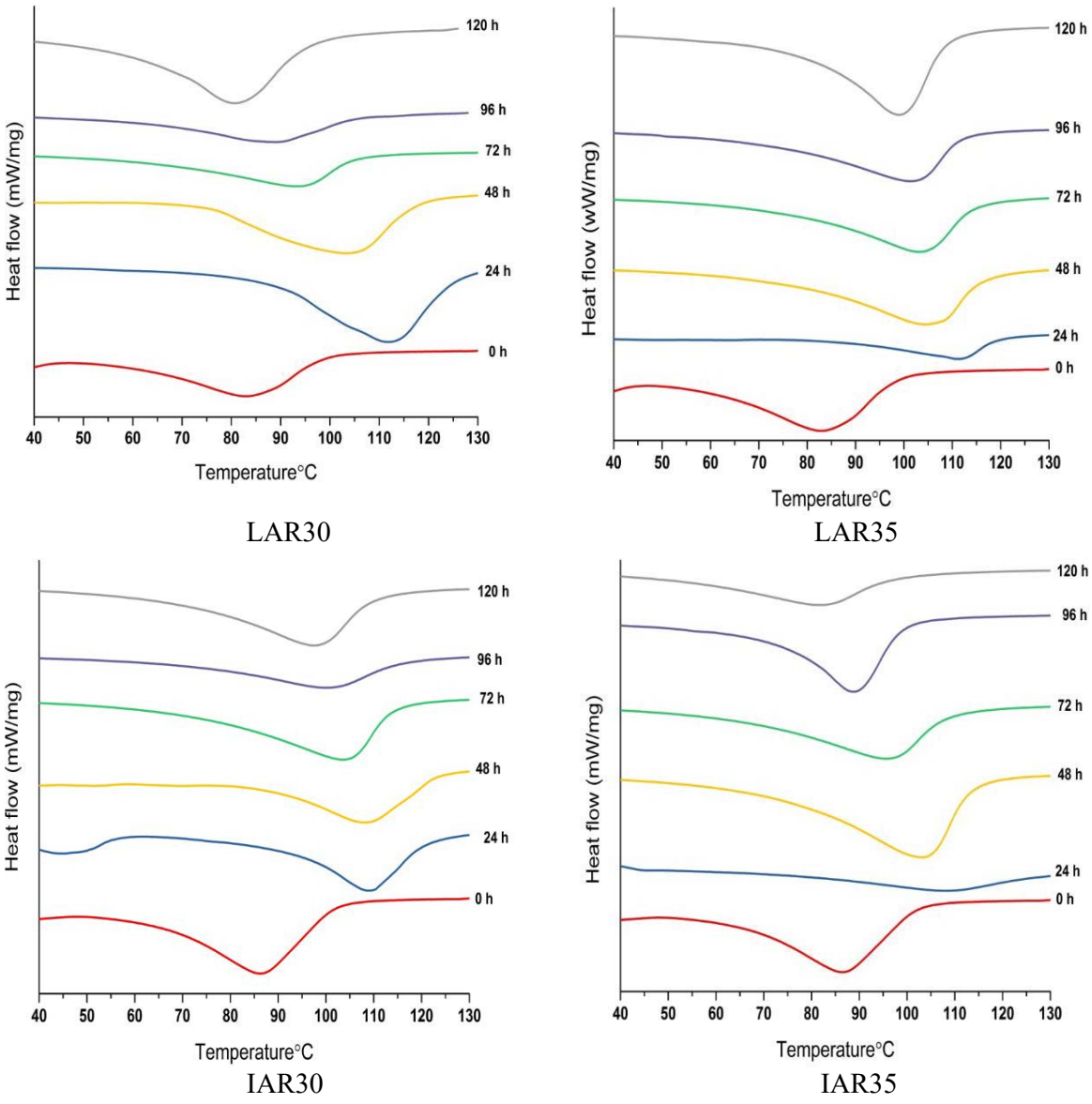

Fig. 4.23 Thermal properties of LAR and IAR malted rice at different germination conditions

Table 4.10: Thermal properties of malted LAR and IAR varieties at different germination conditions

Germination time (h)	Onset temperature (T_O)	Peak temperature (T_P)	Endset temperature (T_C)
LAR30			
0	64.08±0.34^{a}	83.20±1.45^{a}	100.10±0.16^{a}
24	98.73±1.26^{f}	117.4±1.59^{f}	129.87±2.45^{f}
48	92.37±0.56^{e}	115.49±2.78^{e}	128.23±0.98^{e}
72	90.37±2.68^{d}	114.39±0.38^{d}	123.68±1.67^{c}
96	87.27±0.89^{b}	111.67±2.98^{c}	124.95±0.23^{d}
120	82.18±0.98^{b}	99.46±0.29^{b}	112.02±1.78^{b}
LAR35			
0	64.08±0.81^{a}	83.20±0.18^{a}	100.10±0.93^{a}
24	95.81±1.25^{f}	111.49±2.76^{f}	118.04±1.89^{e}
48	88.90±0.87^{e}	104.49±1.75^{e}	113.12±0.27^{d}
72	85.27±2.13^{d}	104.03±0.34^{d}	112.39±0.56^{d}
96	83.80±0.15^{c}	102.38±1.36^{c}	109.65±0.99^{c}
120	82.35±2.67^{b}	98.95±0.19^{b}	108.02±1.78^{b}
IAR30			
0	65.73±1.34^{a}	86.09±0.29^{a}	100.13±1.14^{a}
24	98.56±0.97^{f}	108.98±1.48^{e}	118.52±2.38^{e}
48	92.54±1.56^{e}	108.49±0.23^{e}	120.03±0.45^{f}
72	83.083±0.38^{d}	103.52±1.29^{c}	112.94±1.78^{d}
96	82.18±2.67^{c}	100.36±0.18^{b}	111.12±0.15^{c}
120	79.26±1.53^{b}	97.49±0.33^{b}	107.65±2.13^{b}
IAR35			
0	65.73±0.98^{a}	86.09±0.98^{b}	100.13±0.76^{b}
24	83.54±2.59^{d}	109.19±1.45^{f}	127.54±1.34^{e}
48	78.99±0.31^{c}	103.54±2.98^{e}	112.90±0.34^{d}
72	71.73±1.76^{b}	96.63±0.17^{d}	105.37±1.78^{c}
96	71.00±2.67^{b}	88.81±0.45^{c}	99.00±2.89^{b}
120	66.06±0.56^{a}	82.27±1.67^{a}	91.73±1.41^{a}

Values in the same column with different subscripts are significantly different at $p \leq 0.05$

According to Bail et al. [15], cereals with high amylose content contained a greater amount of lipid (starch–lipid complexes) might result in a high final gelatinization temperature. However, T_O and T_P decreased between 24 and 120 h of germination which might be due to the breakdown of gylocosidic linkages in amylose leading to the formation of smaller molecular weight compounds such as glucose, maltose and maltodextrins. Thus, only a small amount of amylose was leached that could not complex with lipids leading to a decrease in the T_O and T_P values. The T_O of native LAR and IAR was not statistically different ($p \leq 0.05$) but malted IAR showed lower values than LAR as germination progressed; the effect of germination temperature was not statistically different ($p \leq 0.05$) for

LAR but T_O was lower for IAR35 compared to IAR30. This might be due to the higher starch degradation by various hydrolytic enzymes in malted IAR which was also observed in our study [54]. The end set or conclusion temperature (T_C) reflects the thermal status of the sample when the crystalline structure gets transformed into amorphous phase. The T_C followed the same trend as T_O and T_P in malted LAR and IAR samples and thereafter decreased up to 120 h of germination.

4.4.3 Kinetics of pasting properties and thermal behaviour

The second-order kinetic model was best suited (R^2 between 0.721 and 0.970; significant at $p \leq 0.01$) for the pasting properties followed by the first-order model (R^2 between 0.698 and 0.99) though the zero-order model was unsuitable (R^2 between 0.115 and 0.862); the model parameters are shown in Table 4.11. The root means square error (RMSE) values also followed the same trend. Similarly, the rational function (Eq. 3.9) employed for the thermal properties (Table 4.12) showed high R^2 ranging from 0.95 to 0.99 (significant at $p \leq 0.05$). It is thus inferred that the model second-order kinetic was best suited for the pasting properties while the complex rational model was applicable for the thermal properties.

Table 4.11 Model parameters related to pasting properties

Sample	RVA parameter	A_0	k (h^{-1})	R^2	RMSE
RLA30	PT	71	1.31×10^{-05}	0.865	2.06×10^{-04}
	PV2	1757	3.05×10^{-04}	0.946	3.56×10^{-03}
	HPV	1785	2.52×10^{-04}	0.925	3.65×10^{-03}
	CPV	1092	4.21×10^{-04}	0.930	5.74×10^{-03}
RLA35	PT	71	1.02×10^{-05}	0.829	2.14×10^{-04}
	PV2	1757	3.01×10^{-04}	0.970	2.58×10^{-03}
	HPV	1785	2.53×10^{-04}	0.937	3.33×10^{-03}
	CPV	1092	3.73×10^{-04}	0.955	3.99×10^{-03}
RNA30	PT	75	1.17×10^{-05}	0.883	1.59×10^{-04}
	PV	3041	1.13×10^{-04}	0.941	1.37×10^{-03}
	HPV	2919	1.47×10^{-04}	0.930	2.00×10^{-03}
	CPV	806	2.65×10^{-04}	0.884	4.26×10^{-03}
RNA35	PT	75	7.00×10^{-06}	0.721	1.54×10^{-04}
	PV	3041	1.14×10^{-04}	0.958	1.11×10^{-03}
	HPV	2919	1.88×10^{-04}	0.928	2.44×10^{-03}
	CPV	806	2.80×10^{-04}	0.894	4.15×10^{-03}

4.4.4 Inter-relationships

The inter-relation between thermal behaviour and pasting properties was established based on correlation matrix (Table 4.13) and principle component analysis (PCA) (Fig. 4.24 and 4.25). The correlation coefficient matrix showed that the amylose content was negatively correlated to pasting and thermal properties for LAR30 and LAR35. On the other hand,

amylopectin was positively correlated to the pasting properties but negatively correlated with the thermal behaviour. This was due to the breakdown of crystalline region of starch into amorphous state by various hydrolytic enzymes. PT showed positive correlation with HPV, SBV and CPV (r=.0.827, 0.868 and 0.842, respectively, p ≤0.05) for LAR30. PT decreased with germination time a while a high gelatinization onset temperature was observed in 24 h of germination indicating resistance towards granule swelling; it later decreased with germination time. The first peak viscosity in LAR30 showed positive correlation with T_O (r=0.94, p≤00.01). In LAR30 and LAR35, PV2 positively correlated with HPV, BDV, SBV and CPV (p≤0.01).

Table 4.12 Model parameters related to pasting and thermal properties

	Thermal properties	a	b	c	d	R^2	RMSE
LAR30	T_O	64.080	6.45E+05	6267	12.62	0.994	1.462
	T_P	83.250	7.75E+05	4968	20.56	0.968	3.780
	T_C	100.100	1.07E+06	6878	19.65	0.946	4.230
LAR35	T_O	64.080	8.07E+05	8230	14.55	0.982	2.271
	T_P	83.200	8.38E+05	7416	8.83	0.979	2.163
	T_C	100.100	2.20E+06	8400	17.26	0.982	1.276
IAR30	T_O	65.730	6.78E+05	6486	18.71	0.975	2.819
	T_P	86.090	1.71E+05	1406	2.85	0.996	0.899
	T_C	100.100	1.06E+06	7883	1.661	0.971	1.959
IAR35	T_O	65.730	6.63E+05	7431	21.71	0.975	1.768
	T_P	86.090	1.05E+05	7755	4.22	1.000	0.375
	T_C	100.100	8.66E+05	6210	27.26	0.990	2.049

In IAR30 the amylose and amylopectin contents had higher positive correlations with pasting properties rather than the thermal properties which indicated that amylose played an important role in pasting properties. The amylose and amylopectin contents showed positive correlations with PT (r=0.896 and r=0.905, respectively, p≤0.05). The PT positively correlated with PV, HPV, BDV, SBV and CPV (p≤0.05). Similarly, the PV exhibited positive correlations with HPV, BDV, SBV and CPV (r=0.983, 0.998, 0.997 and 0.998, respectively, p≤0.01). Similarly, IAR35 showed that amylose and amylopectin contents had positive correlations with pasting and thermal properties. In IAR35, PV showed higher positive correlations with HPV, BDV, SBV and CPV (p≤0.01). Moreover, a positive correlation was observed between PT and T_O but negatively correlated with T_P and T_C. On the other hand, T_O T_P and T_C showed negative correlations with PV, HPV, BDV, SBV and CPV.

Table 4.13 Lower-half correlation matrix among pasting and thermal properties

	PT	PV1	PV2	HPV	BDV	SBV	CPV	T_O	T_P	T_C	Amys	Amylp
LAR30												
PT	1**											
PV1	0.315											
PV2	0.806	-0.277										
HPV	0.827*	-0.242	0.999**									
BDV	0.771	-0.332	0.998**	0.995**								
SBV	0.868*	-0.166	0.993**	0.997**	0.985**							
CPV	0.842*	-0.215	0.998**	1**	0.992**	0.999**						
T_O	0.197	0.949**	-0.413	-0.380	-0.465	-0.307	-0.354					
T_P	-0.442	0.603	-0.835*	-0.819*	-0.859*	-0.784	-0.808	0.753				
T_C	-0.359	0.650	-0.789	-0.771	-0.816*	-0.730	-0.757	0.795	0.991			
Amys	-0.895*	-0.511	-0.561	-0.588	-0.516	-0.642	-0.607*	-0.489	0.050	-0.024	1**	
Amylp	0.966**	0.346	0.797	0.818*	0.761	0.858*	0.833**	0.193	-0.396	-0.329*	-0.889*	1**
LAR35												
PT												
PV1	0.710											
PV2	-0.023	-0.143										
HPV	0	-0.012	1**									
BDV	-0.059	-0.182	0.999**	0.998**								
SBV	0.074	-0.020	0.992**	0.995**	0.987**							
CPV	0.029	-0.080	0.998**	0.999**	0.995**	0.998**						
T_O	0.532	0.690	-0.799	-0.783	-0.823*	-0.720	-0.760					
T_P	0.483	0.674	-0.811	-0.796	-0.834*	-0.735	-0.773	0.995**				
T_C	0.608	0.745	-0.716	-0.698	-0.744	-0.630	-0.672	0.984	0.982**			
Amys	-0.686	-0.421	-0.552	-0.569	-0.525	-0.614	-0.587	0.058	0.066	-0.100		
Amylp	0.451	0.419	0.825*	0.839*	0.801	0.886*	0.858	-0.321	-0.339	-0.198	-0.836	1**

	PT	PV	HPV	BDV	SBV	CPV	T_O	T_P	T_C	Amys	Amylp
IAR30											
PT	1**										
PV	0.877*										
HPV	0.904*	0.983**									
BDV	0.861*	0.998**	0.970**								
SBV	0.894*	0.997**	0.995**	0.989**							
CPV	0.861*	0.998**	0.970**	1**	0.989**						
T_o	0.155	-0.282	-0.152	-0.325	-0.228	-0.325					
T_p	-0.318	-0.708	-0.604	-0.739	-0.665	-0.739	0.873*				
T_c	-0.205	-0.638	-0.539	-0.667	-0.596	-0.667	0.898	0.987**			
Amys	0.896*	0.587	0.627	0.568	0.608	0.568	0.496*	0.080	0.211		
Amylp	0.905*	0.628	0.680	0.605	0.653	0.605	0.519*	0.069	0.180	0.982**	1**
IAR35											
PT	1**										
PV	0.636										
HPV	0.701	0.996**									
BDV	0.611	0.999**	0.992**								
SBV	0.657	1**	0.998**	0.998**							
CPV	0.669	0.999**	0.999**	0.997**	1**						
T_o	0.167	-0.355	-0.289	-0.378	-0.346	-0.331					
T_p	0.195	-0.249	-0.188	-0.270	-0.244	-0.229	0.969*				
T_c	0.439	-0.075	-0.001	-0.101	-0.064	-0.047	0.944	0.964*			
Amys	0.430	0.492	0.523	0.480	0.489	0.498	0.539	0.658	0.700	1**	
Amylp	0.742	0.749	0.790	0.733	0.754	0.764	0.349	0.430	0.586	0.857*	1**

* Significant at p=0.05 ** Significant at p=0.01 All other are non-significant at p=0.05

The principle component analysis (PCA) is a powerful tool for visualization of the inter-relationships between/among the independent variables and dependent parameters that may be used to explain the maximal variance of the data [79]. The principle components (PC), as biplots, which explained the variance in the pasting and thermal properties of LAR and IAR are presented in Fig 4.24 and 4.25 respectively. The biplot of pasting properties and thermal behaviour of LAR30 showed that the first (PC1) and second (PC2) principal components accounted for 71.7% and 25.5% of the variance, respectively, explaining a total of 97.2% of the variation. The pasting properties (PV2, SBV, CPV, HPD and BDV) could be grouped together and thus they behaved in the similar manner. This group was observed in the vicinity of PT and amylopectin content exhibiting a high correlation among them. Both the group parameters showed significant decrease with germination process due to breakdown of starch by amylolytic enzymes. On the other hand, PV1 and thermal properties (T_O, T_P and T_C) were loaded away from these two groups and was expected to have an inverse relationship among them. The amylose content was loaded on the opposite quadrant of that of amylopectin meaning an inverse relationship. In LAR30, amylose content increased significantly due to the breakdown of crystalline region to amorphous region. Thereby, amylose content showed a negative correlation with the thermal and pasting properties. Woo et al. [100] had also reported that no correlation was observed between amylose content and any thermal parameter measured by DSC. Their results were also in accordance with earlier reports that showed weak correlation between amylose content and thermal characteristics of starches [73].

The PCA biplot of LAR35 (Fig 2.24) showed that PC1 and PC2 accounted for about 96% of the total variation. Here, similar correlation among pasting properties, thermal properties and amylose and amylopectin contents was observed as exhibited by LAR30.

The biplot of pasting properties and thermal behaviour of IAR30 is shown in Fig 4.25. The PC1 and PC2 jointly explained 97.5% of the total variation. The pasting properties (PV, SBV, CPV, HVD and BDV) formed a group and thus expected to behave in the same manner. This group was in the vicinity of PT, amylose and amylopectin contents exhibiting higher correlation among them. These group parameters decreased during 120 h of germination due to the action of amylolytic enzymes on starch. Significant linear correlations were observed between amylose content, lipid content, gelatinization temperature and gelatinization enthalpies for rice starches [68].

On the other hand, T_O, T_P and T_C were close by and had an inverse relationship with the above-mentioned groups. This was due to an increase in these temperatures during the germination process.

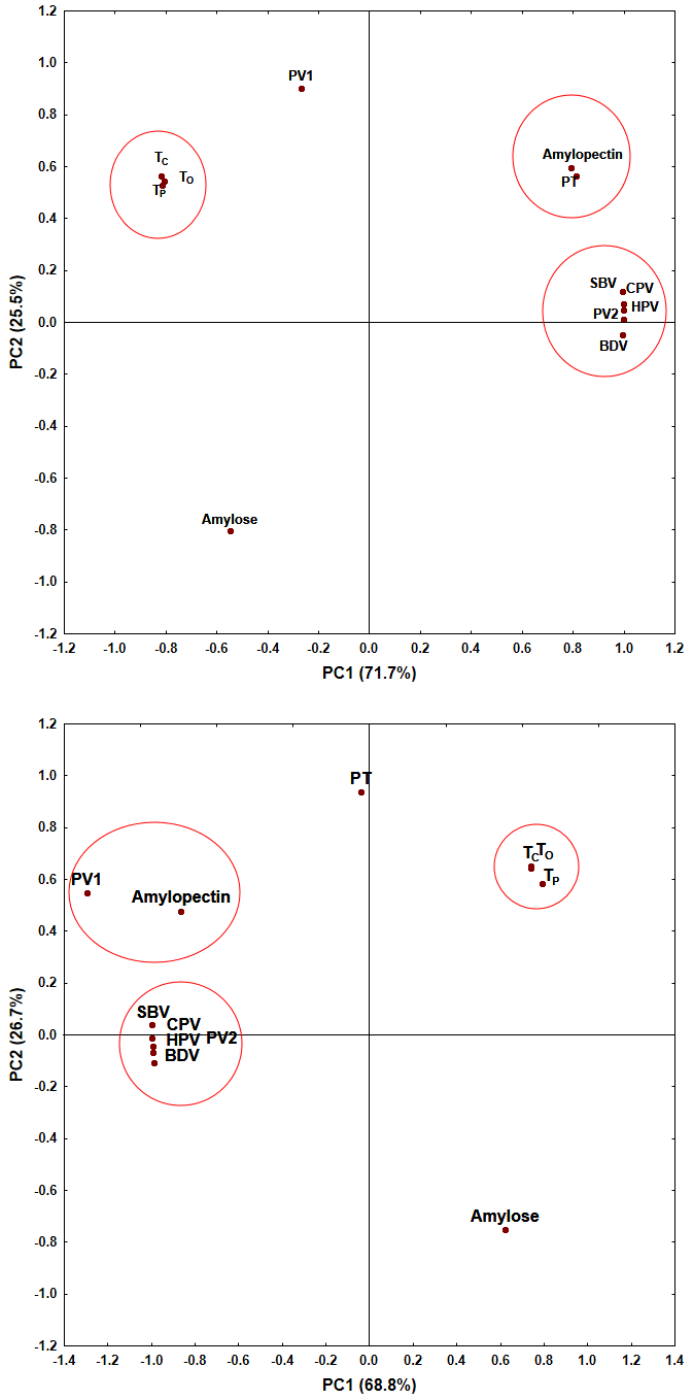

Fig 4.24 PCA biplots of pasting and thermal properties of malted LAR variety germinated at 30°C (top) and 35°C (bottom)

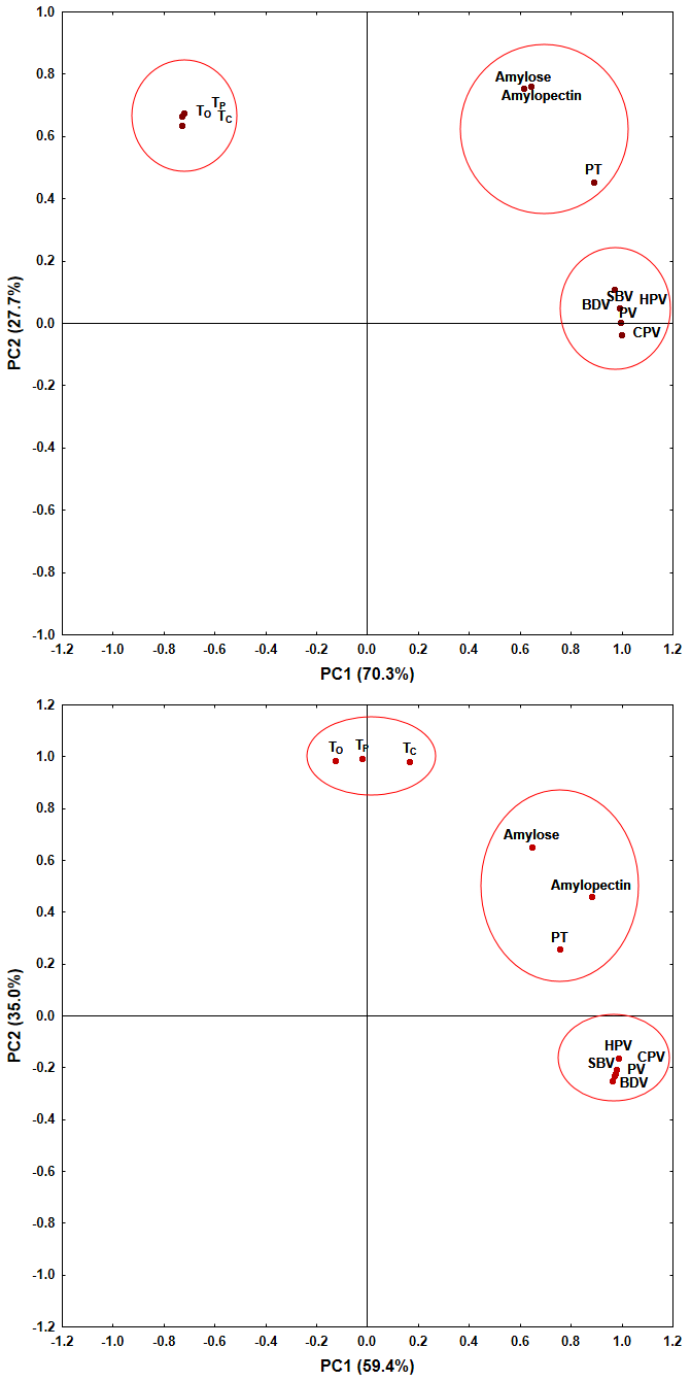

Fig 4.25 PCA biplots of pasting and thermal properties of IAR malted paddy germinated at 30°C (top) and 35°C (bottom)

The biplot of pasting properties and thermal behaviour of IAR30 explained 94.5% of the total variation. Similar correlations were observed among pasting and thermal properties for IAR30. Ye et al [103] examined the thermal and rheological properties of brown flours from four *Indica* rice subspecies with varying amylose contents. The results showed an increase in peak, final and setback viscosities ($p \leq 0.05$) with an increase in amylose content while the phase transition temperatures of brown rice flour ($p \leq 0.05$) decreased.

4.5 Optimization of weaning formula based on its physico-chemical and nutritional properties

4.5.1 Selection of ingredients for weaning formula

The weaning period is one of the most crucial time for the infants as it represents a period of dietary transition when the nutritional requirements for growth and brain development are maximum [84]. The ingredients were selected based on the recommended dietary allowances as reported by [84]. The ingredients selected were whole wheat flour, rice flour, Bengal gram flour, whole milk powder, *Bhim kol* and malted rice flour. The malted rice flour was added to reduce the bulk density and increase the calorific value of the weaning formula. *Bhim kol* is considered one of the most nutritious fruit from ancient time as it is a rich source of energy, amino acids, vitamins and minerals. It is reported that 100 g of mature fruit pulp would provide 16.8 % of the energy RDA for infants [18].

4.5.2 Modification of ingredients

The ingredients such as whole wheat flour, rice flour, Bengal gram flour and malted rice flour were modified by the process of dry heat treatment i.e. roasting. The purpose of roasting was to improve colour, extends shelf life, enhances flavour and reduces the antinutrient factors of cereals and legumes [91]. Moreover, roasting of grains results in gelatinization of starch and denaturation of proteins which improves the digestibility of cereals and legumes. The moisture content, calorific value and crude protein of all ingredients are shown in Table 4.14.

Table 4.14 Moisture content (%), calorific value and crude protein on dry basis

SN	Ingredients	Moisture Content (%)	Calorific Value (Kcal/100g db)	Crude Protein (g/100g db)
1.	Roasted whole wheat flour	6-7%	482.80	13.55
2.	Roasted rice flour		425.81	4.28
3.	Roasted pulse flour		465.59	24.65
4.	Whole milk powder		578.95	28.58
5.	Malted rice flour		455.914	4.40
6.	Fruit (Bhim Kol)	75-80%	1340.00	3.95

4.5.3 Effect of roasting on pasting properties of ingredients

Roasting of cereals involves physical modification of starch which improves the grain characteristics. The pasting properties of the ingredients are shown in Table 4.15 and Fig. 4.26 and 4.27. From the results it was observed that the roasting of the ingredients caused significant decrease in the pasting temperature (PT), peak (PV), hot paste viscosity (HPV), Breakdown viscosity (BDV) cold paste viscosity (CPV) and setback viscosity (SB) when compared to native flour. This is due to the fact that roasting causes partial gelatinization of the starch granules which gets easily hydrated and swell rapidly in presence of heat leading to lower viscosity [91]. The roasted malted rice showed lower pasting properties than roasted rice flour. Higher decrease in roasted malted rice flour is due to the synthesis of hydrolytic enzymes during germination such as α and β amylase which breakdown starch to lower molecular compounds. Sun et al. [93] reported that millet flour showed higher pasting properties after roasting as compared to the native flour and this was contradictory to our results. However, Sharma [91] showed similar decrease in pasting properties of roasted barley.

Table 4.15 Pasting properties of the native and roasted ingredients

	Wheat flour		Rice flour		Pulse flour		Malted rice flour	
	Unroasted	**Roasted**	**Unroasted**	**Roasted**	**Unroasted**	**Roasted**	**Unroasted**	**Roasted**
PT	81.1±0.09	68.9±0.97	88.6± 0.5	78.6±0.02	75.1±0.08	70.5±0.98	72±1.0	68.9±0.034
PV	1182±1.78	251±1.69	3119±1.34	348±0.13	767±1.69	40±0.71	624±6.0	177± 0.46
HPV	683±1.68	200±2.98	2603± 0.67	300±1.56	758±1.56	35±0.44	241±0.0	166±0.98
BDV	499±0.07	51±0.01	516±0.71	48±0.24	9±0.87	5±0.16	383±1.0	11±1.57
CPV	1396±1.68	458±0.98	5159±0.98	537±0.45	914±1.49	61±1.06	442±1.0	280±0.95
SB	897±2.89	407±0.18	4643±1.13	489±1.67	905±0.28	56±1.97	683±4.0	269±1.57

4.5.4 Formulation of weaning food using D-optimal mixture design

The D-optimal mixture design was used to develop weaning formulations for baby's (6-12 months) daily requirement to meet the daily nutrient recommendation. As per the standard design procedure (section 3.4.5.1) total 31 numbers of mixtures were prepared with different portions of all ingredients as shown in Table 3.2. The responses viz. crude protein content, energy content, water absorption index (WAI) and water solubility index (WSI) for combinations were estimated and presented in Table 4.16.

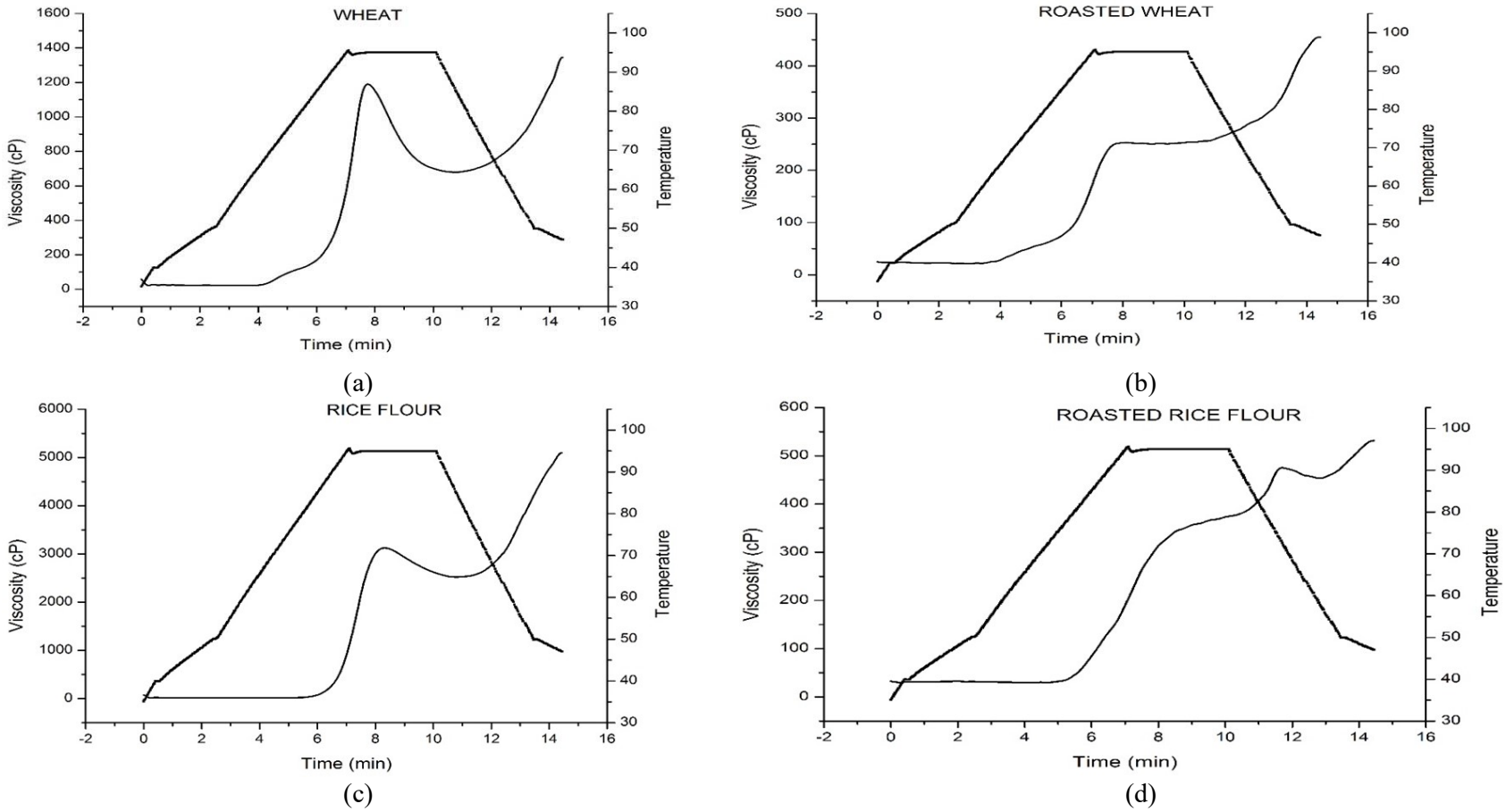

Fig. 4.26 Pasting properties of unroasted and roasted wheat flour and rice flour

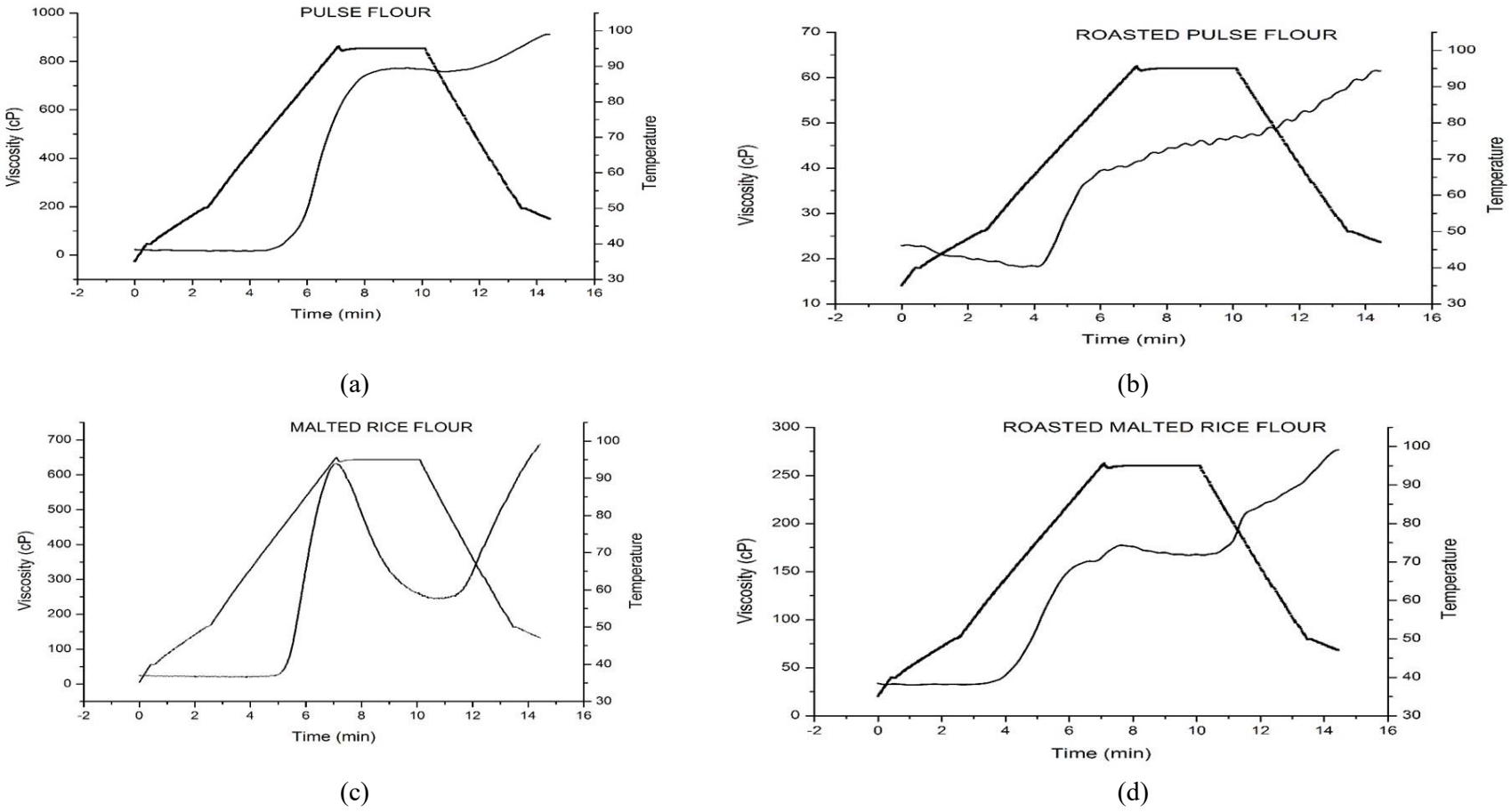

Fig. 4.27 Pasting properties of unroasted and roasted pulse and malted rice flour

Table 4.16 Responses for different weaning combinations

Run	WF	RF	Pulse	WMP	Fruit	MR	Protein	Energy	WAI	WSI
	%	%	%	%	%	%	%	Kcal/100 g	(g/g)	%
1	10.0	15.0	10.0	35.0	20.0	10.0	15.74	755.93	13.25	42.11
2	10.0	10.0	5.0	40.0	30.0	5.0	15.97	851.51	9.31	38.77
3	10.0	10.0	5.0	50.0	20.0	5.0	18.38	775.41	9.32	38.27
4	10.0	10.0	10.0	35.0	30.0	5.0	15.77	845.85	9.83	38.52
5	15.0	10.0	5.0	45.0	20.0	5.0	17.43	770.50	9.16	38.69
6	15.0	10.0	5.0	35.0	30.0	5.0	15.22	846.71	9.87	38.62
7	17.5	17.5	5.0	35.0	20.0	5.0	15.54	756.71	9.06	38.60
8	20.0	10.0	5.0	35.0	25.0	5.0	15.67	803.85	9.93	38.21
9	10.0	20.0	5.0	35.0	20.0	10.0	14.72	753.94	12.07	42.13
10	20.0	10.0	10.0	35.0	20.0	5.0	16.69	760.13	8.87	37.29
11	10.0	20.0	10.0	35.0	20.0	5.0	15.76	754.43	8.47	38.36
12	10.0	15.0	5.0	45.0	20.0	5.0	17.17	767.75	8.69	37.77
13	10.0	10.0	10.0	35.0	25.0	10.0	15.75	801.64	12.96	42.15
14	10.0	10.0	5.0	45.0	20.0	10.0	17.15	769.26	13.97	42.06
15	10.0	10.0	10.0	45.0	20.0	5.0	18.19	769.74	8.99	38.84
16	10.0	10.0	10.0	40.0	20.0	10.0	16.96	763.59	11.51	42.19
17	10.0	15.0	5.0	35.0	25.0	10.0	14.73	799.65	12.73	42.10
18	15.0	10.0	5.0	45.0	20.0	5.0	17.63	770.40	8.99	37.67
19	10.0	15.0	5.0	35.0	30.0	5.0	14.75	843.86	8.88	37.98
20	15.2	11.5	7.2	36.2	21.5	8.4	15.96	772.72	10.53	39.09
21	10.0	20.0	5.0	40.0	20.0	5.0	15.95	760.10	9.73	38.53
22	17.5	17.5	5.0	35.0	20.0	5.0	15.64	756.71	10.33	37.02
23	20.0	10.0	7.5	37.5	20.0	5.0	16.78	762.96	9.32	38.80
24	15.2	11.5	7.2	36.2	21.5	8.4	15.91	772.72	13.01	38.01
25	10.0	15.0	10.0	35.0	25.0	5.0	15.76	800.14	5.81	38.53
26	20.0	10.0	5.0	35.0	20.0	10.0	15.65	759.64	15.00	42.12
27	10.0	10.0	5.0	35.0	30.0	10.0	14.74	845.36	13.56	42.15
28	10.0	20.0	5.0	35.0	25.0	5.0	14.75	798.15	10.13	37.80
29	20.0	10.0	5.0	35.0	20.0	10.0	15.65	759.64	13.78	42.15
30	20.0	10.0	10.0	35.0	20.0	5.0	16.89	760.13	8.56	39.89
31	10.0	10.0	5.0	45.0	25.0	5.0	17.18	813.46	10.11	38.99

4.5.5 Analysis of D-optimal mixture experiment fitting the models

The composition of the different weaning formula and its responses were fitted into the D-optimal mixture design and a total run of 31 was obtained for the formulation. The model incorporated was linear for the measured response. The adequacy of the model is shown in Table 4.17. The models were considered adequate when the R^2 was more than 80% [16]. The R^2 values for the responses i.e. protein content, energy content, water absorption index (WAI) and water sorption index (WSI) are shown in Table 4.18 indicating that the models have satisfactory adequacy in fitting the experimental. Moreover, *P*-value was less than 0.05 which indicated that the model terms are significant. Thus, all the four responses were considered adequate to describe the effect of variables on the quality of weaning mix.

Table 4.17 ANOVA for different responses

Source	Sum of Squares	df	Mean Square	F-Value	p-value Prob > F	
Protein (%)						
Model (Linear Mixture)	31.04	5	6.21	1492.72	< 0.0001	significant
Residual	0.10	25	$4.16x10^{-3}$			
Lack of Fit	0.058	20	$2.87x10^{-3}$	0.31	0.972	not significant
Pure Error	0.046	5	$9.25x10^{-3}$			
Total	31.14	30				
Energy (Kcal/100g)						
Model (Linear Mixture)	31123.64	5	6224.73	$4.21x10^{-3}$	< 0.0001	significant
Residual	0.037	25	$1.48 x10^{-3}$			
Lack of Fit	0.032	20	$1.60x10^{-3}$	1.60	0.318	not significant
Pure Error	$5.00 x10^{-3}$	5	$1.00x10^{-3}$			
Total	31123.68	30				
WAI (g/g)						
Model (Linear Mixture)	113.43	5	22.69	27.66	< 0.0001	significant
Residual	20.50	25	0.82			
Lack of Fit	15.81	20	0.79	0.84	0.649	not significant
Pure Error	4.69	5	0.94			
Total	133.93	30				
WSI (%)						
Model (Linear Mixture)	80.94	5	16.19	22.95	< 0.0001	significant
Residual	17.63	25	0.71			
Lack of Fit	11.90	20	0.59	0.52	0.865	not significant
Pure Error	5.73	5	1.15			
Total	98.57	30				

Table 4.18 Statistical performance parameters for the responses

Responses	Standard deviation	Mean	C.V. %	R^2
Protein	0.064	16.13	0.40	0.997
Energy	0.038	784.60	$4.90x10^{-3}$	0.999
WAI	0.910	10.51	8.62	0.847
WSI	0.840	39.46	2.13	0.821

4.5.6 Effect of mixing ingredients on responses

The observed protein content of the weaning mix with different combinations of the ingredients (Table 4.16) varied between 14.73 to 18.38 % within the combination of variables studied. The maximum protein content was observed for the combination of 1 0 % each of WF and RF, 5 % pulse, 50 % WMP, 20 % fruit and 5 % MR. This was due to the high protein content of WMP (28.58 %). All the variables of the mixture showed positive effect on the protein content. The contour plot (Fig. 4.28) further depicted the effect of the independent variables on the protein content which showed that with increase in the WMP content there was an increase in the protein content. From Eq. 4.4 it was also observed that WMP had major influence on the protein content followed by pulse.

Protein= +0.140xWF +0.047xRF +0.250xPulse +0.283xWMP +0.044xFruit +0.036xMR **Eq. (4.4)**

The energy content of weaning formulation is very important for infants. The energy content of the mixture with different combinations ranged between 753 to 851 kcal/100g. The highest energy content was observed with the combination of 10 % each of WF and RF, 5 % pulse, 40 % WMP, 30 % fruit and 5 % MR. this combination showed high energy value due to the higher percentage of fruit i.e. *Bhim kol* (*Musa balbisiana*). The 100 g of mature fruit pulp of *Bhim kol* was reported to provide 16.8 % of the energy RDA for infants [18]. Moreover, addition of malted rice increases the energy density of the weaning formulation and this was also observed from Eq. 4.5. The contour plot (Fig. 4.29) also depicted similar observations i.e. increase in fruit and WMP content increased the energy content. All the variables showed a positive effect on the energy content.

Energy= +5.637xWF +5.070xRF +5.470xPulse +6.597xWMP +14.211xFruit +5.371xMR **Eq. (4.5)**

Water absorption index (WAI) is mainly an indicator of the ability of the flour to absorb water. Water is absorbed and bound to the starch molecules which induces changes in the molecular structure of starch [34]. The WAI observed for different combinations of the ingredients (Table 4.16) varied between 5.81 to 15 g/g. The maximum absorption of water takes place when the starch granules are sufficiently damaged which imbibes water without disintegration. It was reported that lower water absorption is desirable for weaning formulation which produces low bulk density gruel with high nutrition [16]. The lowest water absorption index was observed for the combination of 10 % WF, 15 % RF, 10 % pulse, 35 % WMP, 25 % fruit and 5 % MR. Water absorption capacities are related to the starch and protein contents and the particle size distribution of the ingredients. Griffith [44] reported that high fat, high protein, low carbohydrate content results in reduced WAI. Therefore, the presence of WMP and pulses might have reduced WAI and the effect of each ingredient on WAI is shown in Eq. 4.6. The contour plot (Fig. 4.30) showed that decrease in WMP resulted in decrease in WAI.

WAI= +0.111xWF +0.022xRF -0.145xPulse +0.057xWMP +0.077xFruit +0.873xMR **Eq. (4.6)**

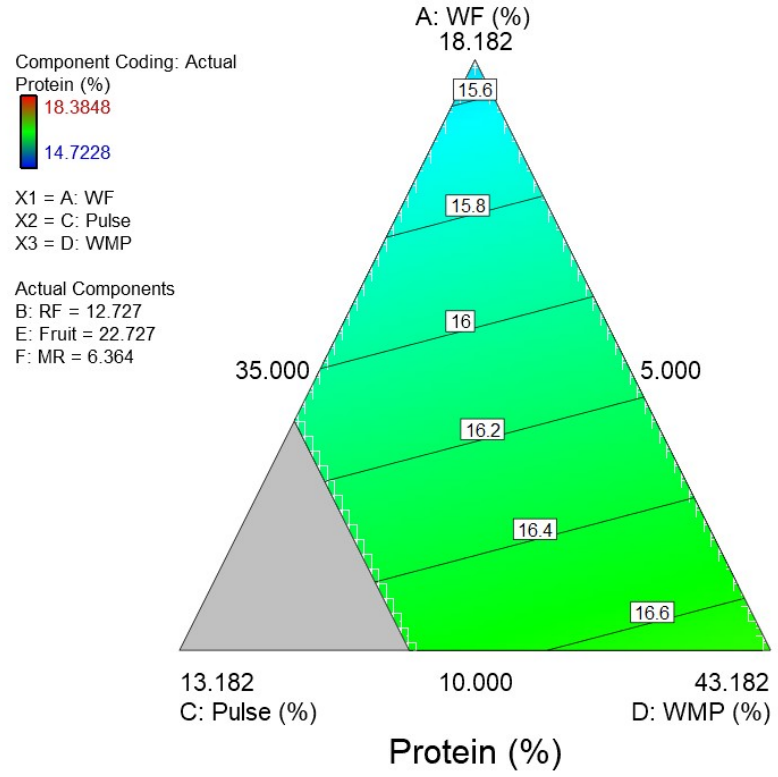

Fig. 4.28 Contour plot showing effect of composition on crude protein

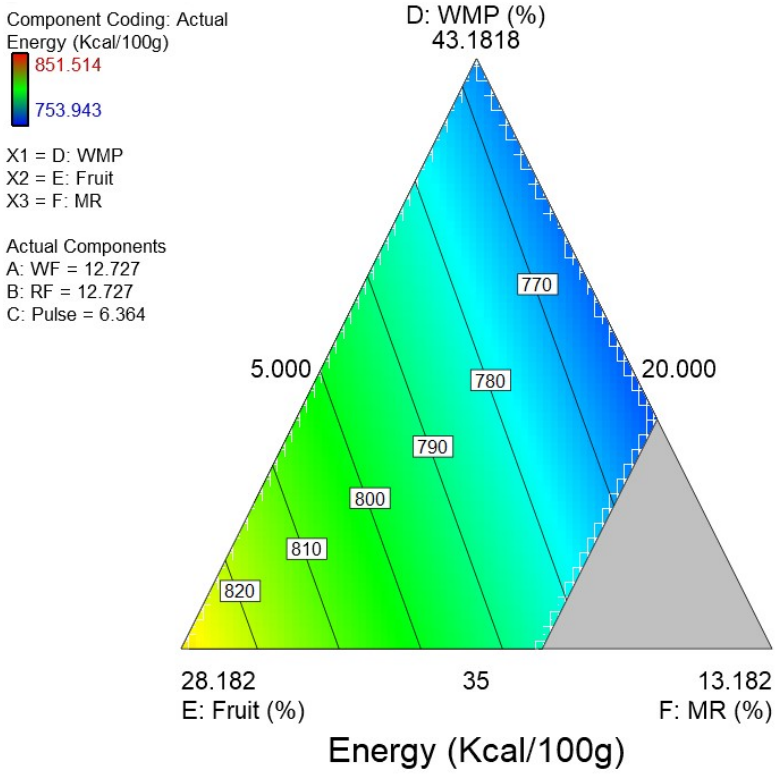

Fig. 4.29 Contour plot showing effect of composition on energy value

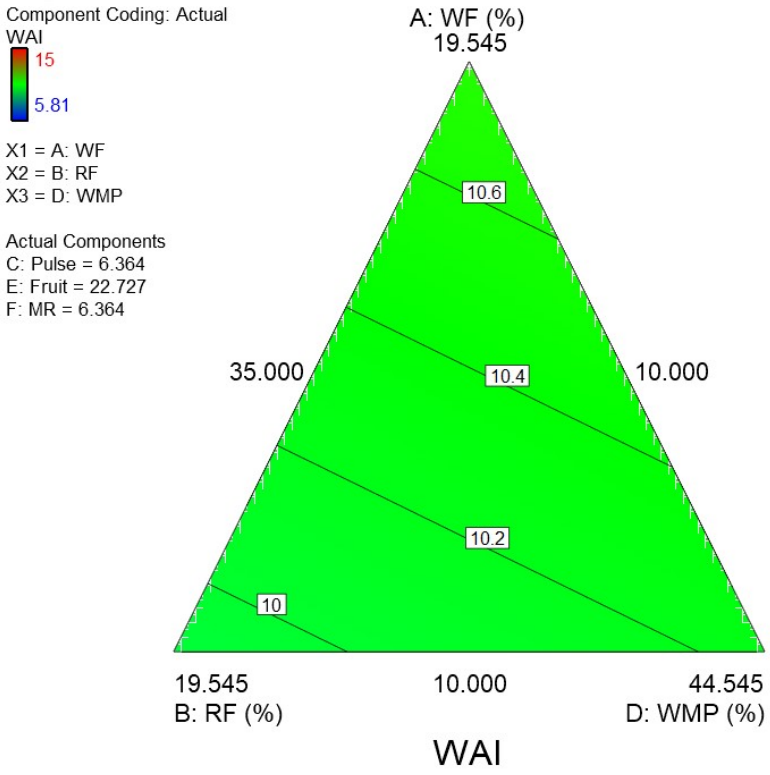

Fig. 4.30 Contour plot showing effect of composition on water absorption index

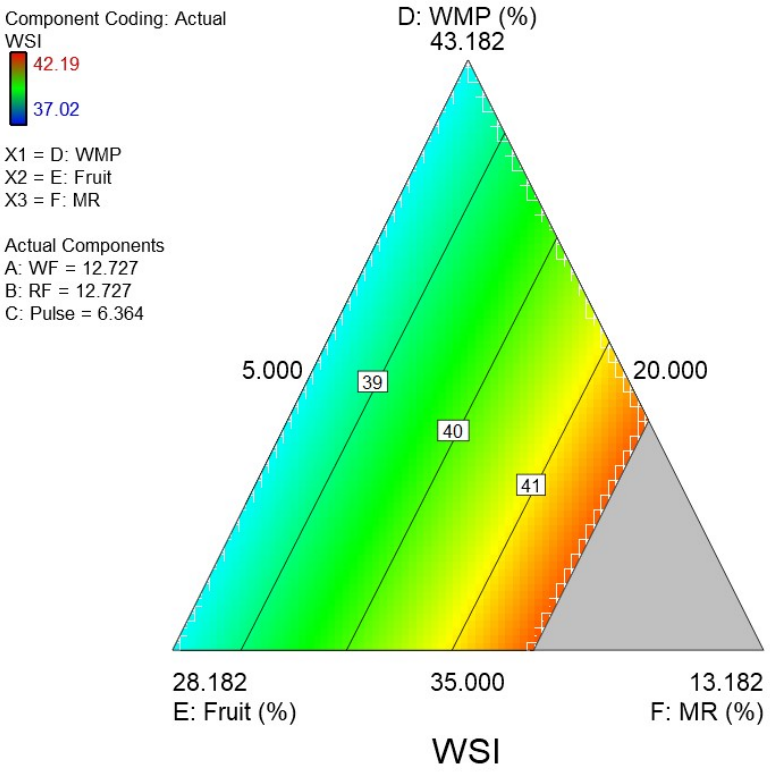

Fig. 4.31 Contour plot showing effect of composition on water solubility index

Water solubility index (WSI) determines the amount of free polysaccharide or polysaccharide released from the granule on addition of excess water. Griffith [44] reported an inverse relationship between WAI and WSI. A high solubility is desirable for weaning food and high WSI indicates that starch underwent extensive conversion. The WSI for different combination of ingredients ranged between 37 to 42 %. From the results it was observed that the mixture with higher malt fraction showed higher WSI. The contour plot (Fig. 4.31) also showed increase in WSI with increase in MR. The Eq. 4.7 showed the effect of ingredients on WSI and MR was observed to have higher effect followed by pulse. This was due to the hydrolysis of storage components such as starch and protein to soluble components i.e. reducing sugars. Moreover, soluble materials such as amylase, amylopectin and amino acids were reported to get released during malting [16]. Similar increase in WSI was observed for brown rice during germination [30]. Griffith [44] also reported that WSI increased by 100 % with malting due to increase in soluble sugars and changes in protein solubility properties.

WSI= +0.323xWF +0.317xRF +0.381xPulse +0.354xWMP +0.361xFruit +1.045xMR **Eq. (4.7)**

4.5.7 Standardization of weaning combinations

Optimization of the levels of variables was performed by selecting the responses i.e. protein content, energy content, WAI and WSI. It was observed that the responses had a direct effect on the quality of the weaning formula as shown by their respective R^2 values and based on this numerical as well as graphical optimization was employed. Table 4.19 depicts the criteria used, upper and lower limit of the responses. The importance level was of 4, 5 and 1 was given to the constraints of protein content, energy content, WAI and WSI respectively. The optimized solution is shown in Table 4.20 and the optimized values were WF 10 %, RF 10 %, pulse 10 %, WMP 35 %, fruit 30 % and MR 5 % each keeping a constant level of 10 % refined vegetable oil. The contour plot (Fig. 4.32) for desirability and each response was drawn by keeping WF, RF and pulse constant as obtained by numerical optimization. The weaning formula was prepared using the recommended level of ingredients and the responses measured. The validation of the standardize combinations were carried out and shown in Table. 4.21. The experimental values were found to be reasonably close to the predicted ones which confirmed the validity and adequacy of the predicted models.

Table 4.19 Optimization conditions

Name	Unit	Goal	Lower Limit	Upper Limit	Importance
WF	%	is in range	10	20	3
RF	%	is in range	10	20	3
Pulse	%	is in range	5	10	3
WMP	%	is in range	35	50	3
Fruit	%	is in range	20	30	3
MR	%	is in range	5	10	3
Protein	%	is in range	14	18	4
Energy	Kcal/100g	maximize	600	851.51	5
WAI	g/g	minimize	5.81	15	1
WSI	%	none	37.02	42	1

Table 4.20 Optimization Solutions

No	WF	RF	Pulse	WMP	Fruit	MR	Protein	Energy	WAI	WSI	Desirability	
1	10.0	10.0	10.0	35.0	30.0	5.0	15.77	845.86	8.54	38.64	0.925	**Selected**
2	10.0	10.0	9.6	35.4	30.0	5.0	15.79	846.26	8.61	38.63	0.922	
3	10.0	10.0	9.1	35.9	30.0	5.0	15.80	846.86	8.72	38.62	0.921	
4	10.0	10.0	8.4	36.6	30.0	5.0	15.83	847.64	8.86	38.60	0.920	
5	10.0	10.0	8.2	36.8	30.0	5.0	15.84	847.92	8.91	38.60	0.919	

Table 4.21 Validation of the standardize combination

PARAMETERS	ACTUAL	PREDICTED	ERROR (%)
Protein (%)	15.77	15.1	4.25
Energy (Kcal/100g)	845.86	845.12	0.09
WAI (g/g)	8.54	7.99	6.44
WSI (%)	38.60	40.36	4.55

4.5.8 Analysis of optimized weaning formula

4.5.8.1 Proximate analysis

The moisture content of the optimized weaning formula was observed to be 6.12±0.02% and similar result was reported in a weaning food based on sorghum and legumes [62]. The energy content was found to be 845.86 kcal per 100 g of the formula which was much higher than the minimum energy density requirement of well-nourished infants i.e. 77 and 116 kcal per 100 g [84]. The minimum protein requirement for infants as suggested by Bureau of Indian Standards [23] is 12% while the protein content in the optimized weaning formula was higher (15.77 ± 0.02). The ash, fat and fibre content measured by standard AOAC method [7] were found to be 3.48±0.60%, 10.10±0.67% and 2.06 ± 0.05% respectively, which were in accordance with the specifications of Bureau of Indian Standards [23].

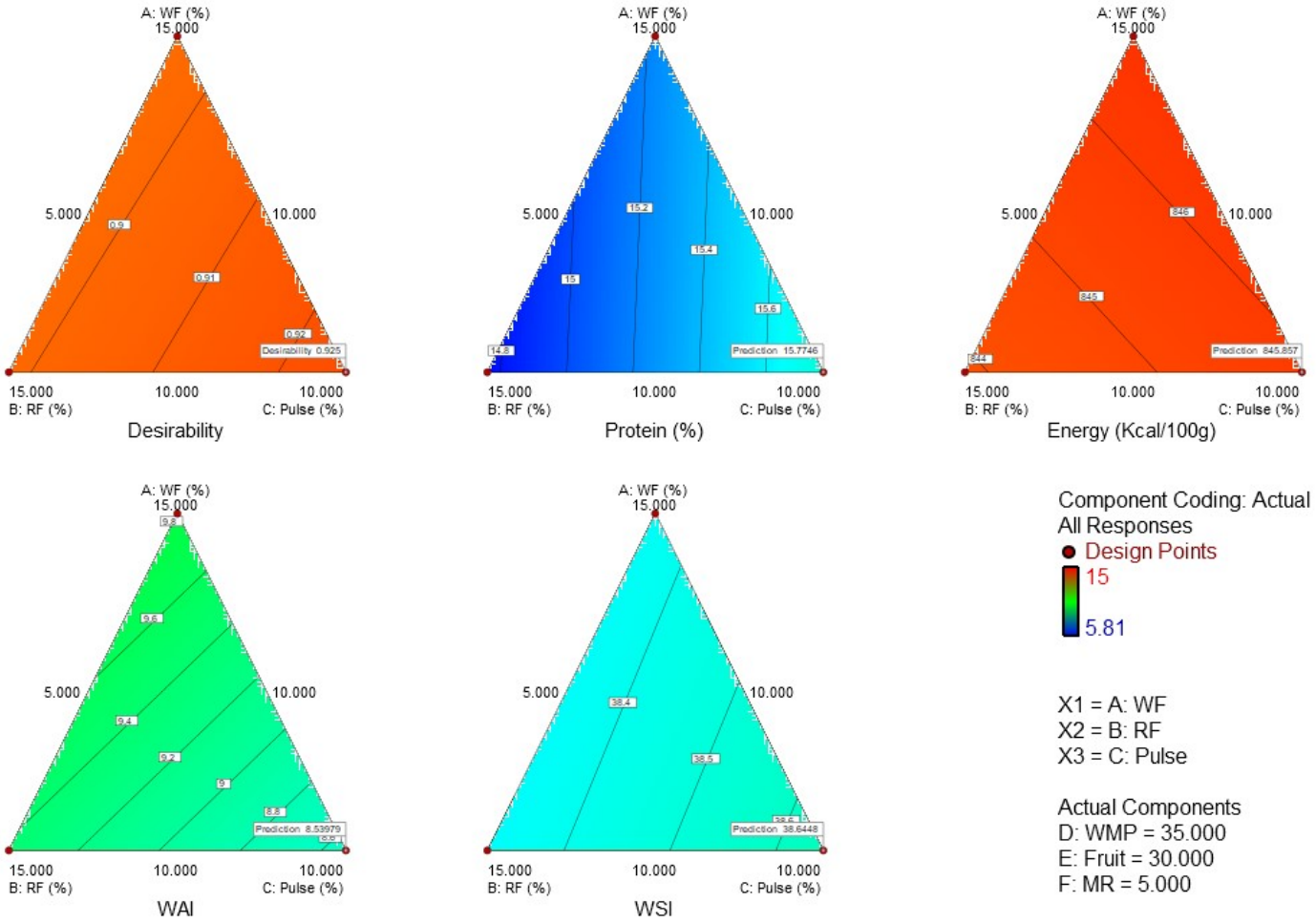

Fig. 4.32 Graphical representation of standardized result

4.5.8.2 Water holding and binding capacity

The water holding capacity of materials is an index of the maximum amount of water that a material can take up and retain under food formulation condition [48]. The water holding capacity of the optimized formulation was found to be 3.37±0.062 g/g and similar range in WHC was reported in a complementary diet prepared from germinated cereals (maize, rice and cowpea) [48]. It was also reported that the hydrolytic enzymes produced during the process of germination causes changes in the WHC of gruels since these enzymes degrades starch which is the main constituent of gel structure of the gruel. The water binding capacity (WBC) is defined as the amount of water retained by the sample but under low-speed centrifugation [30]. The water binding capacity of the optimized weaning formula was observed to be 2.33± 0.27 g/g. Similarly, germinated rice flour shows significant decrease in WBC as reported by [30] and incorporation of germinated rice flour in weaning formulation will affect its properties. The swelling power (SP) of the optimized formula was 9.32±2.04 g/g. Ikujenlola [48] reported similar range of SP in a complementary diet and also found that reduction of SP occurred in the complementary formula prepared from germinated cereal compared to ungerminated flour. This was attributed to the fact that amylase enzymes are released from the scutellum, which hydrolyse starch to dextro-maltose, which do not swell when cooked into gruel.

4.5.8.3 Physical properties

The bulk and tapped density of the optimized weaning formula was found to be 0.50±0.02 g/cm^3 and 0.80±0.02 g/cm^3 respectively and similar bulk density was observed for weaning formula prepared from sorghum and legumes [62]. The particle density and porosity were observed to be 1.04±0.02 g/cm^3 and 3.03±0.15 g/cm^3 respectively. Flow characteristics of powder were judged by the free flowing, semi-free flowing and cohesive flow. Flow behaviour is multidimensional in nature, and it depends on many physical characteristics. Some of the factors that affect flowability of bulk solids and powders include moisture content, humidity, temperature, pressure, fat, particle size, and flow agents [41]. The flowability and cohesion in terms of Carr index (CI) and Hausner ratio (HR) of the optimized weaning formula was observed to be 36.99±0.014 % and 1.58±0.03. As per the categorization of flowability and cohesiveness (Table 3.4), powder with CI greater than 35 and HR greater than 1.4 is treated as very poor. The poor flow behaviour of the formula may be due to the presence of free surface fat which plays a key role in determining the flowability and stickiness of a powder. Jinapong [50] reported that the high fat content of spray-dried soymilks resulted in very poor flowability.

4.5.8.4 Mineral analysis

The mineral content of the optimized weaning formula was obtained by Energy Dispersive X-Ray Spectroscopy (EDS). Highest content of mineral observed was sodium (28.63 %), calcium (27.60 %), phosphorous (20.53 %) and Chlorine (11.52 %) and small amounts of Magnesium (3.17 %), Iron (3.82 %) and zinc (3.86 %). The developed weaning formula was observed to contain all the essential minerals i.e. calcium, magnesium, sodium, potassium, iron, and zinc as reported by Sajilata [84].

4.5.8.5 Amino acid composition analysis

The amino acid composition of the optimized weaning formula are presented in Table 4.22. Nine amino acids such as histidine, isoleucine, leucine, lysine, methionine, phenylalanine, threonine, tryptophan, and valine. These amino acids are not synthesized by mammals and therefore regarded as indispensable nutrients. These are also called the essential amino acids. In this study six essential amino acid were identified in the developed weaning formula and non-essential amino acid detected were alanine, arginine, glutamic acid and cysteine. The recommended dietary allowance (RDA) of amino acids for per 100 gm of the developed formula is shown in Table 4.22. From the results it was observed that the weaning formulation met 33.087 % of the total essential amino acids required for infants. However, the RDA met 49.04 % of the total amino acid that was identified in the formula. The highest amino acid content was observed to be for histidine. Histidine is reported to be an essential amino acid for infants, but not demonstrated to be required by adults [82]. The high histidine content in the weaning formulation may be due to presence of high-protein foods such as dairy, rice, wheat and rye. Histidine levels in the body mainly balances good mental and physical health. Thus, the developed weaning formula can provide the required amino acids in two to three feeding along with breast milk.

4.5.9 Estimation of solid water ratio of the weaning and its effect on viscosity

The increase in calorie density of weaning formula in developing countries is of a major concern. The concentration of ingredients in a prepared formula is a function of the consistency or viscosity of the product that can be fed, which in turn is related to the functionality of the product ingredients, specifically starch [84]. High concentration of starch can lead to thick gruels whereas low concentration of solids will result in low calorie density. Thereby, the effect of solid water ratio on viscosity of the developed weaning formula was estimated. The viscosity was measured at temperature range which was close to the consumption temperatures of infants i.e. 35, 40 and 50°C (Table 4.23). From the result it was observed that with increase in solid content there was an increase in the viscosity at all temperatures. This is due to the swelling of starch granules due to absorption of water which makes the gruel thick and viscous [26]. However, with increase in temperature there was a decrease in the viscosity which might be due to the disruption of the starch granules

and as the number of disrupted interparticle bonds increases, the viscosity drops. The optimum viscosity reported for feeding of infants which is termed as spoonable and have an easy-to-swallow semiliquid consistency ranges from 1 to 3 Pa-s [69, 84]. Therefore, solid water ratio selected for the weaning formula was 50:50 where the viscosity was in the range of 2 Pa-s indicating a semi liquid consistency.

Table 4.22 Essential amino acid (EAA) composition analysis and Percentage of RDA of amino acids met per day

Amino acid	**Quantity of EAA**		**Suggested pattern of requirement of EAA for infants (RDA) (mg/ per day) ***			**% RDA met per day**
	(mg/g of protein)	**mg/100 of WF protein@15%**		mg/ kg wt per day	mg/ per day	
Alanine	7.90	118.50	Arginine	20.00	192.00	103.237
Arginine	18.50	277.50	Histidine	28.00	268.80	119.196
Glutamic acid	13.00	195.00	Isoleucine	70.00	672.00	-
Histidine	21.36	320.40	Leucine	161.00	1545.60	-
Lysine	4.50	67.50	Lysine	103.00	988.80	6.826
Cystine	15.70	235.50	Cystine + Methionine	58.00	556.80	118.534
Methionine	28.30	424.50				
Phenylalanine	22.10	331.50	Phenylalanine + Tyrosine	125.00	1200.00	27.625
Threonine	11.60	174.00	Threonine	87.00	835.20	20.833
Valine	18.40	276.00	Tryptophan	17.00	163.20	
			Valine	93.00	892.80	30.914
Total EAA	**161.36**	**2420.40**	**Total EAA required**	**762.00**	**7315.20**	**33.087**
			Total EAA based on available amino acids		**4934.4**	**49.044**

Body weight of infants (9-12 Months) = 9.6 kg*

***FAO/ WHO [39]**

Table 4.23 Viscosity of weaning formulations with different dilution at different feeding temperature

Solid Water Ratio	**Feeding Temperature (°C)**	**Viscosity (Pa-s)**
50:50	35	02.16 ± 2.1E-04
	40	02.08 ± 4.6E-04
	50	02.01 ± 1.5E-03
55:45	35	08.88 ± 8.8E-04
	40	08.32 ± 7.0E-04
	50	08.21 ± 1.6E-03
60:40	35	15.77 ± 5.0E-04
	40	15.64 ± 7.2E-04
	50	15.29 ± 8.5E-04

4.6 In-vitro starch digestibility and rheological behavior of weaning formulation in simulated human digestive system

4.6.1 In-vitro starch digestibility of weaning food

The *in vitro* starch digestibility of the developed weaning formula was studied with two different particle sizes i.e. 75 and 105 μm (Fig 4.33). The starch digestibility in infants is essential from the nutritional point of view and it was evaluated by measuring the saccharides released during an in vitro starch hydrolysis. From the results (Fig 4.33) it was observed that the starch digestibility increased significantly when it passes through the digestive system i.e. from the mouth to the intestine by the action of enzymes (saliva, pepsin and pancreatic juice). The starch digestibility in the mouth mainly takes place due to the presence of α-amylase in saliva. However, starch digestibility was observed to be lowest due to the short residence of the weaning formulation in the mouth [80]. Salivary amylase which is active in the adult stomach but its presence in infants is very low. However, from the results, it was observed that significant amount of starch was digested in the stomach and intestine which can be attributed to the presence of a significant concentration of glucoamylase or amyloglucosidase in the small intestinal mucosa in infants which possess 50% more activity than that of adults [80]. The enzyme glucoamylase thereby becomes an alternate enzyme for starch digestion in infants. The starch digestibility is also determined by its structure i.e. type A starch (e.g. wheat or rice starch) has an easily digestible, open-helical structure. However, type B starch (e.g. raw potato starch) has lower digestibility due to the densely packed hexagonal pattern of the double helices that reduces access to amylases. On the other hand, C-type starch such as pulses are assumed to be mixture of type A and B [28]. In the developed formula, the presence of wheat and rice might have increased the digestibility. The high starch digestibility of the developed weaning formulation from mouth to stomach can also be attributed to the addition of malted rice flour in weaning formulations. Germination causes increase in digestibility of cereals and legumes due to hydrolysis of starch chains by amylolytic enzymes (α and β amylase) and thereby starch granules become readily digestible [105]. Germination causes the formation of pores on the starch surface leading to penetration of enzymes into the granules which in turn increases the digestibility. Moreover, the easy digestibility of the developed formula may be also be due to the roasting of the ingredients (wheat flour, rice flour, malted rice flour and pulse flour) that causes modification of starch and Christian [28] also reported that all three starch types (A, B, and C) can be rapidly digested in the cooked state. The weaning formulation

prepared from germinated cowpea flour (*Vigna unguiculata*) showed increased starch digestibility and the rate of digestion was highest after 120 min [51].

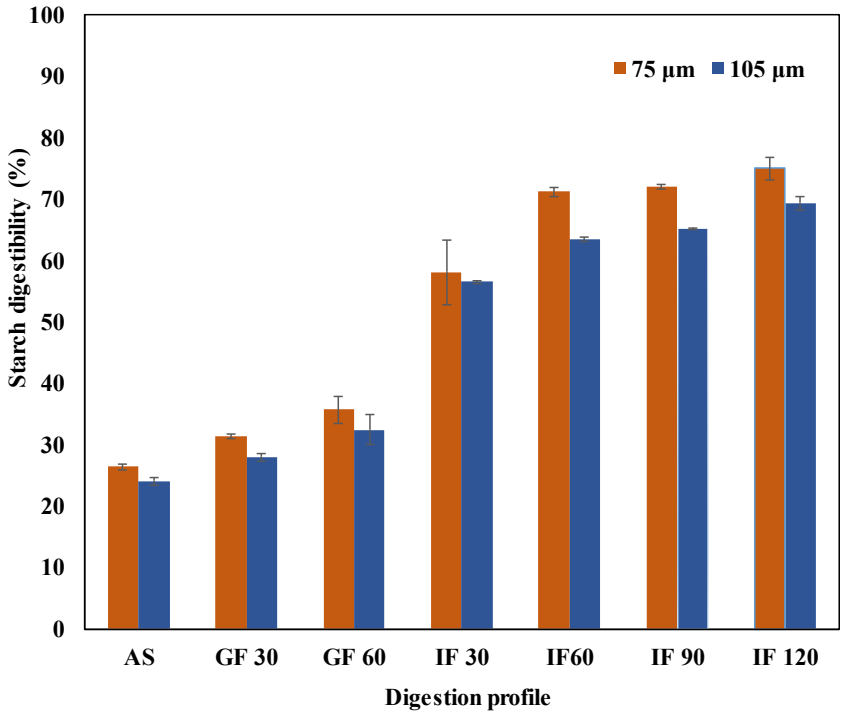

Fig. 4.33 In vitro Starch digestibility of weaning formulation [AS= Artificial saliva; GF= Gastric fluid; IF= Intestinal fluid and 30, 60, 90 and 120 min of digestion]

The particle size of weaning formula also had a significant effect on the starch digestibility. It was observed that the smaller particle size (75 µm) was more easily digested than larger particle size (105 µm). This may be attributed to the fact that larger surface area of the smaller particles increases the chance for enzymes to absorb for digestion. It was reported that starch digestion was dependent on various factors such as granule size, architecture, crystalline pattern, the degree of crystallinity, surface pores or channels and degree of polymerization [61]. The starch granule digestion occurs by the mechanism which was mentioned earlier in this study in section 4.1.4.2 which involves diffusion of enzymes through the capillary action and moves inside the granules where hydrolysis occur at the enzyme-granule contact points. The enzymes generally proceed radially to create additional pores and channels and thereafter spreads from the core inside the granules. However, the weaning formulation also contains non-starch components which might cause a modification in this mechanism.

4.6.2 Rheological changes of weaning food in the simulated human digestive system

The in vitro rheology study of the developed weaning formula was divided into three main stages as described by Prakash [80] (a) flow behaviour in the mouth (b) flow behaviour in the stomach (cumulative to the mouth) (c) flow behaviour in the duodenum (cumulative of the mouth and stomach). However, in this study the viscosity of the weaning food was mainly assigned to the enzyme hydrolysis and residual contents and adsorption of digested ingredients was not taken into consideration**.**

4.6.2.1 *In vitro* mouth incubation

The rheological property in the mouth of infants is essential for the process of swallowing. In the mouth, saliva is secreted which consists of electrolytes (sodium chlorides and sodium bicarbonate), proteins (mucin, α-amylase, lingual lipase and proline-rich proteins) and epithelial cells from the oral mucosa. The weaning formulation remains in the mouth only for few seconds after feeding and mixes immediately with saliva. Therefore, the flow behaviour of weaning formula was estimated immediately after addition of artificial saliva. The viscosity of the sample is shown in Fig.4.34. It was observed that addition of saliva caused dilution of the sample. The viscosity of the sample mixed with saliva was lower when compared to control. Moreover, weaning formulation with the particle size (105 μm) was more viscous than the smaller the particle size (75 μm) during the digestion process which is due to the larger surface area of the smaller particle leading to higher digestibility as mentioned earlier. The α-amylase present in the saliva acts firstly on the carbohydrates of the weaning formula which mainly breaks down starch when it is mixed properly into the food bolus via tongue which in turn reduces the viscosity of the sample [33]. Prakash [80] reported that there was no significant influence in the viscosity of the formula before and after addition of saliva due to short residence time in the mouth. However, in this study, significant changes were observed after addition of saliva which may be due to the presence of malted rice in the formulation which resulted in a higher decrease in viscosity.

4.6.2.2 In vitro stomach incubation

The weaning period is one of the most crucial periods and therefore proper digestion is necessary for utilization and absorption of ingested food. The weaning food was incubated with simulated gastric fluid (GF) after the digestion in the mouth. The food is basically carried from mouth to the stomach by oesophageal peristalsis. The gastric juice produced in the stomach is highly acidic (pH 1-2) as it contains hydrochloric acid (pH ~1), water, salts, pepsin, mucous and bicarbonate ions. The chief cells in the stomach secrete the digestive

enzymes, pepsinogen and gastric lipase. The extremely nature acidic nature of gastric juice retards the action of salivary amylase, but acid hydrolysis of starch takes place in the sample. This hydrolysis of the weaning formula with particle size 75 and 105µm lead to decrease of approximately 84 and 80 % in viscosity from the control as it passes through the gastric simulated conditions for 60 min as shown in Fig 4.34. The particle size of the weaning formula also had a significant effect ($p< 0.05$) on the viscosity during gastric digestion since viscosity of 75 µm weaning formula decreased rapidly as compared to the 105 µm particle size. Prakash [80] reported that factors affecting the viscosity of weaning formula during digestion involve the size of starch granules and the number of chains of amylose and amylopectin (glucose chains) induced by pH change. Moreover, other enzymes present in gastric juice such as pepsin and renin cause protein hydrolysis which also influence the viscosity of the formula [60].

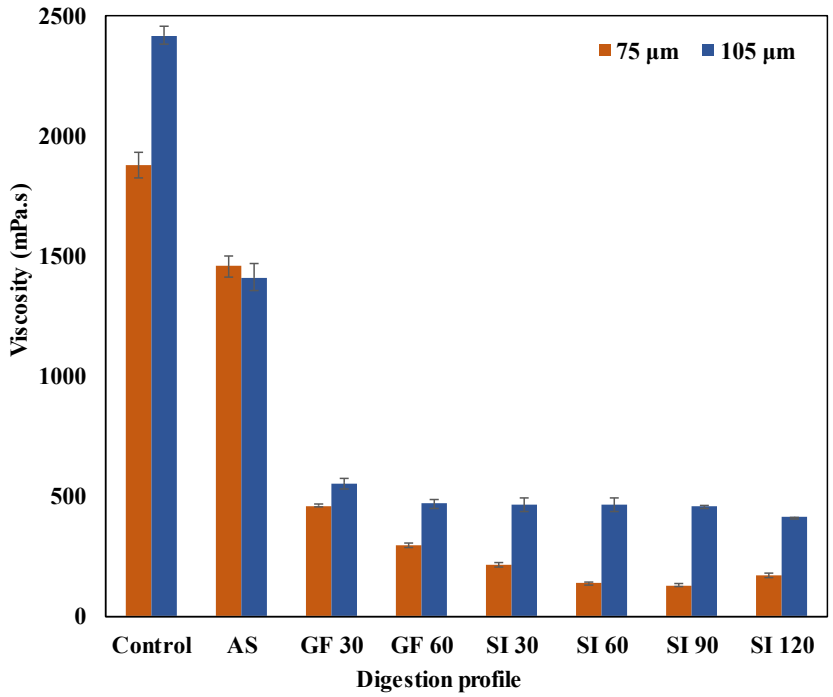

Fig. 4.34 Viscosity of weaning formula in simulated human digestive system [AS= Artificial saliva; GF= Gastric fluid; IF= Intestinal fluid and 30, 60, 90 and 120 min of digestion]

4.6.2.3 In vitro intestine incubation

The ingested infant formula moves from the stomach to the small intestine which consists of the duodenum, jejunum and ileum. The pancreas secretes pancreatic juice into the duodenum and the weaning formula further subjected to digestion in the alkaline environment (pH 7.0–8.5) as the presence of sodium hydrogen carbonate neutralizes the

acidity of the fluid arriving from the stomach. From the results, it was observed that the viscosity decreased initially for both the particle size i.e. 75 and 105 μm during the incubation with simulated intestinal fluid (IF) for 120 min (Fig 4.34). This may be due to the presence of amylase in the pancreatic juice which causes additional breakdown of carbohydrate leading to decrease in viscosity. However, after 30 min of intestinal digestion, there were minimal changes in the viscosity of ingested weaning food and a total decrease of 90 and 83 % was observed from the control. Singh [92] reported that the composition of food matrix also affects the starch digestion. The presence of starch and protein in various cereal products and their interaction significantly affects the digestibility and in turn the viscosity of food. The gastrointestinal lipid digestion occurs in both the stomach and intestine. In the small intestine, pancreatic lipase causes hydrolysis of lipids and duodenal juice causes hydrolysis of casein and α-lactalbumin or β-lactoglobulin present in milk which also had a significant influence on the viscosity of weaning formula [80].

4.6.3 Modelling Rheological behaviour of weaning food in simulated human digestive system

The rheological behaviour of the developed weaning formula was studied and the plot of shear stress over shear rate is shown in Fig. 4.37 and 4.38 for two different particle sizes. From the plot, a decreasing trend of shear stress was observed with increase in shear rate which represented the shear thinning behaviour of the reconstituted weaning formulation at 50% solid concentration.

The developed weaning formula showed decreasing viscosity with increase in shear rate as the food passed from mouth to stomach indicating shear thinning behaviour (Fig. 4.35 and 4.36). This was due to the action of enzymes present in the mouth, stomach and intestine. The smaller particle size (75 μm) showed higher decrease in viscosity as compared to larger particle size (105 μm) which again may be due to the difference in the surface area. Similar observation was made in the rheology of baby foods by Prakash [80]. The author reported that the ingredients have a pronounce effect on the viscosity of the weaning formula since it is prepared mainly from milk, vegetable oils carbohydrate sources which in turn effects the dispersion, concentration and hydration property. Other consideration that can affect the viscosity of weaning formula are pH, temperature and heat treatments of the mixture during the manufacturing process [80].

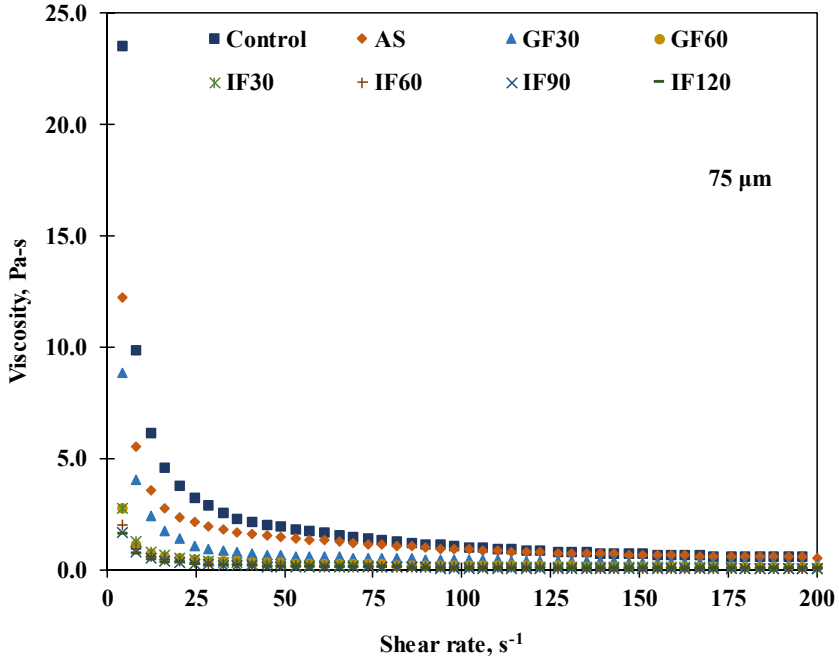

Fig. 4.35 Curves showing the change in viscosity of weaning formula (75µm) during digestion process w.r.t shear rate

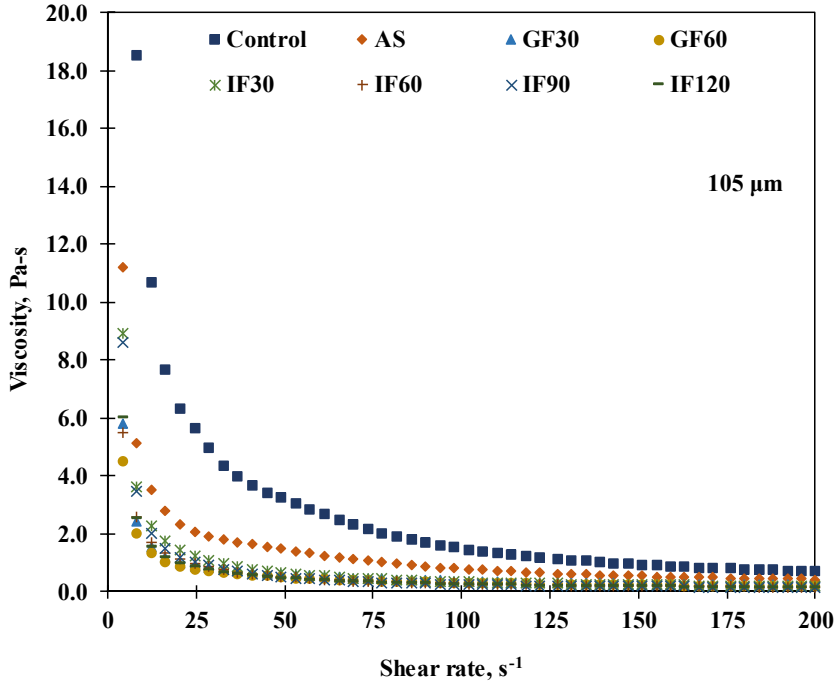

Fig. 4.36 Curves showing the change in viscosity of weaning formula (105µm) during digestion process w.r.t shear rate

The conventional viscous flow rheological models such as power law model and Herschel-Bulkley model were employed for fitting the shear stress-shear rate data. The power law model and Herschel-Bulkley model represented the digestion data of both the particle size (75 and 105 µm) well with high R^2 value ranging from 0.82 to 0.99 with low RMSE. However, the yield stress (σ_0) in Herschel-Bulkley model was very low in case of 75 µm and almost negligible in case of 105 µm particle size. Therefore, Power law model was taken as the best-fitted model. The flow rheological parameters are shown in Table 4.24. The flow behaviour index (n) was observed to be <1 indicating a pseudoplastic shear-thinning behaviour. This may be due to the presence of fluid milk and protein dispersions containing casein, whey protein, and soy protein in the weaning food which exhibit pseudo plastic flow behaviour [80]. The consistency index (*K*) which gives an idea of the viscosity of the sample was observed to decrease with the digestion time. The characteristic viscosity of the weaning formula depends on the ingredients, type of their dispersion, concentration and hydration property [80].

Table 4.24 Model parameters for two rheological models

Particle Size	Sample	Power				Herschel-Bulkley				
		$\sigma = K(\dot{\gamma})^n$				$\sigma = \sigma_0 + K(\dot{\gamma})^n$				
		K	n	R^2	RMSE	K	N	σ_0	R^2	RMSE
75 µm	Control	53.34	0.14	0.921	4.12	40.89	0.17	13.41	0.922	4.13
	AS	24.20	0.28	0.951	4.65	24.19	0.28	0.00	0.951	4.70
	GF30	4.29	0.36	0.973	0.99	1.86	0.49	4.69	0.984	0.78
	GF60	4.26	0.32	0.996	0.29	3.81	0.34	0.69	0.996	0.29
	IF30	5.54	0.19	0.924	0.66	2.13	0.32	4.17	0.934	0.63
	IF60	3.49	0.24	0.955	0.48	2.14	0.31	1.76	0.958	0.47
	IF90	2.69	0.25	0.973	0.30	1.09	0.38	2.25	0.984	0.23
	IF120	2.45	0.26	0.966	0.32	0.72	0.44	2.57	0.985	0.21
105 µm	Control	61.61	0.15	0.825	8.37	61.61	0.15	0.00	0.825	8.46
	AS	30.91	0.19	0.894	4.59	90.92	0.19	0.00	0.894	4.64
	GF30	10.07	0.26	0.975	1.15	10.07	0.26	0.00	0.975	1.15
	GF60	8.22	0.27	0.993	0.54	8.22	0.27	0.00	0.993	0.54
	IF30	7.58	0.13	0.936	0.48	7.58	0.13	0.00	0.936	0.48
	IF60	6.71	0.12	0.925	0.43	6.71	0.12	0.00	0.925	0.43
	IF90	4.91	0.16	0.940	0.41	4.18	0.18	0.81	0.940	0.41
	IF120	3.79	0.20	0.935	0.46	2.17	0.27	1.99	0.941	0.44

[AS = Artificial saliva; GF = Gastric fluid; IF= Intestine fluid]

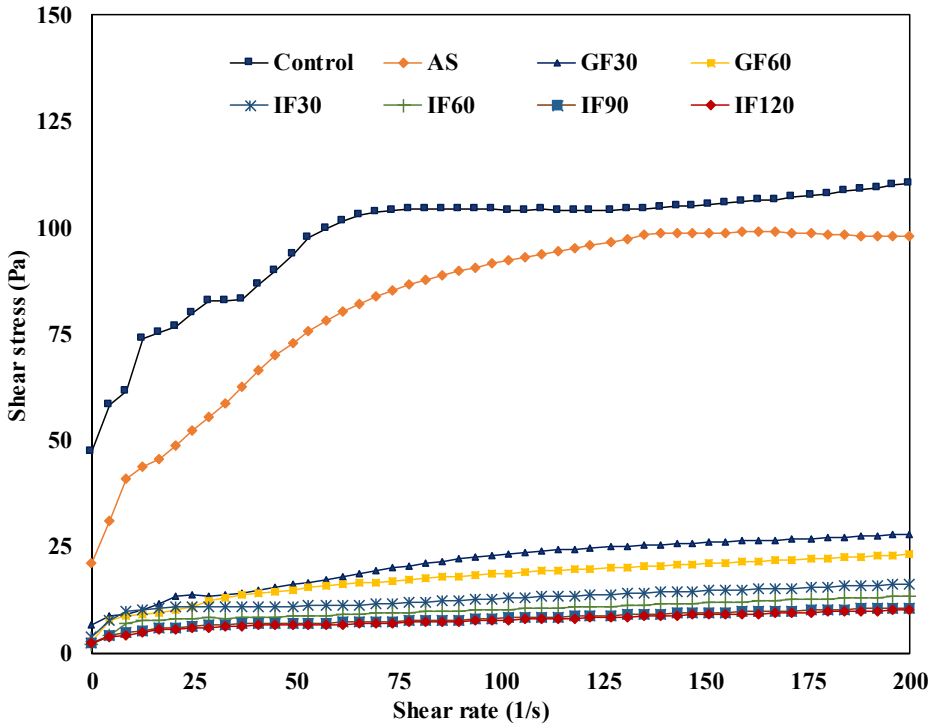

Fig. 4.37 Rheological changes in the weaning food (75µm) during digestion process

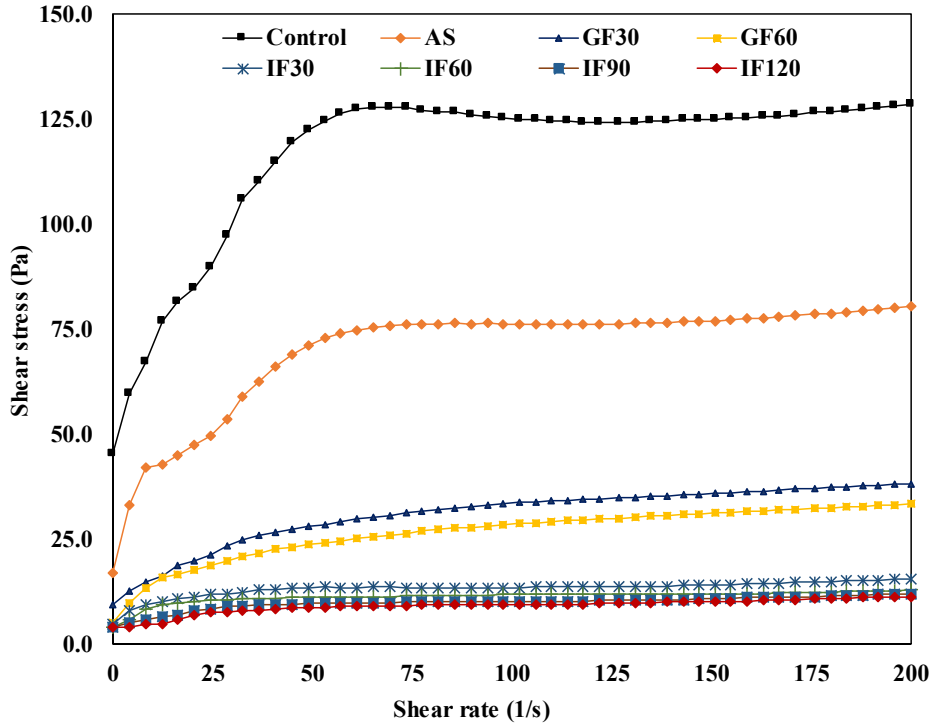

Fig. 4.38 Rheological changes in the weaning food (105 µm) during digestion process

4.7 Cytotoxicity study of developed weaning formula

4.7.1 XTT assay and Trypan blue exclusion assay

Tetrazolium salts have been widely used as detection reagents for many years in histochemical localization studies and cell biology assays [90]. XTT assay can be effectively used to study cell proliferation, cytotoxicity and apoptosis. 2, 3-Bis-(2-methoxy-4-nitro5-sulfophenyl)-2H-tetrazolium-5-carboxanilide salt (XTT) is a colourless or slightly yellow compound which reduces to orange coloured formazan dye, that can be measured by absorbance at 490 (or 450) nm in a microplate reader. It is reported that XTT dye reduction occurs at the cell surface facilitated by trans-plasma membrane electron transport and mitochondrial oxidoreductases contribute to XTT response with their reductants being transferred to the plasma membrane [6]. In this study acute monocytic leukemia cell line (THP-1) were employed and the cell viability analysed. From the results (Fig. 4.39) it was observed that the cell line added with the developed weaning formula showed almost 100% viability as that of the control indicating absence of any cytotoxicity of the formula. The result was also confirmed by the microscopic observation (Fig. 4.40) of the cells which showed similar morphology to that of control which shows absence of cellular necrosis or apoptosis.

Another method employed to determine the cytotoxicity of the weaning formula was trypan blue exclusion assay. This trypan blue (TB) method is a very common assay for evaluating cytotoxicity where dead cells absorb TB into the cytoplasm as the membrane selectivity is lost, whereas live cells remain unstained. Similar to XTT assay, acute monocytic leukemia cell line (THP-1) were employed and incubated with TB solution and the relative number of dead and live cells was obtained by optical microscopy by counting the number of stained (dead) and unstained (live) cells. The results (Fig. 4.41) showed that the cells added with the weaning formula at different concentration had more than 90% viability when compared to the control indicating absence of any cytotoxic effect of the formulation.

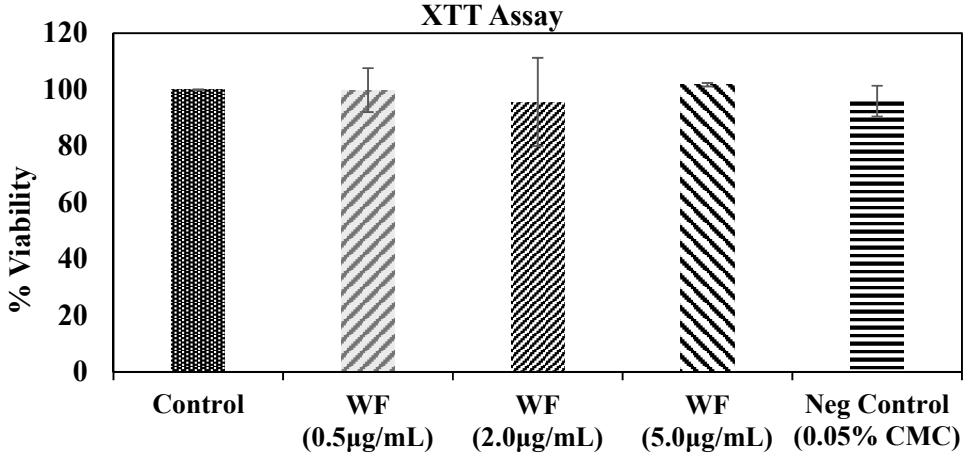

Fig. 4.39 XTT assay of weaning formula

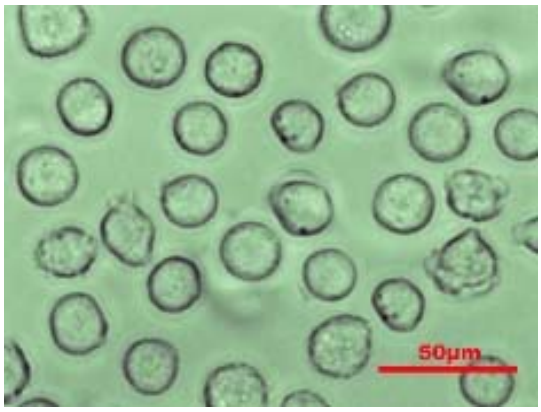

Negative control

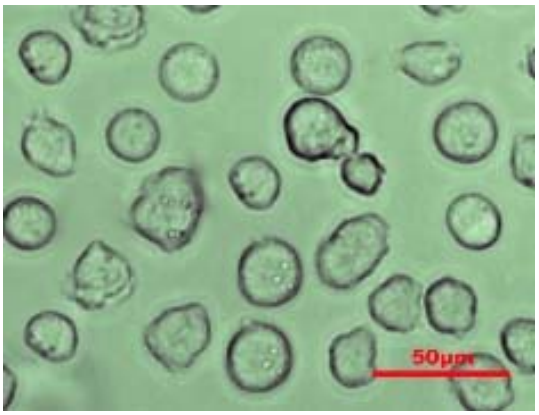

Treated with weaning formula

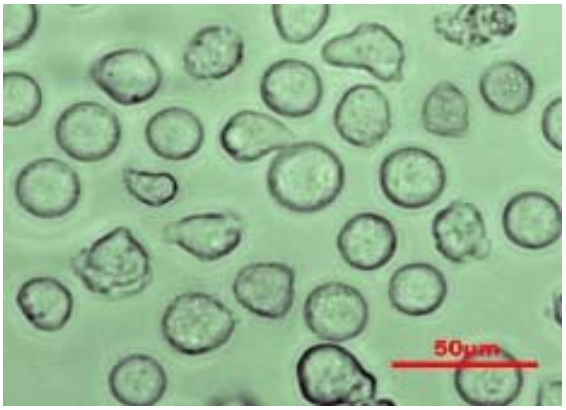

Normal control

Fig. 4.40 Morphology of cells under the light microscope

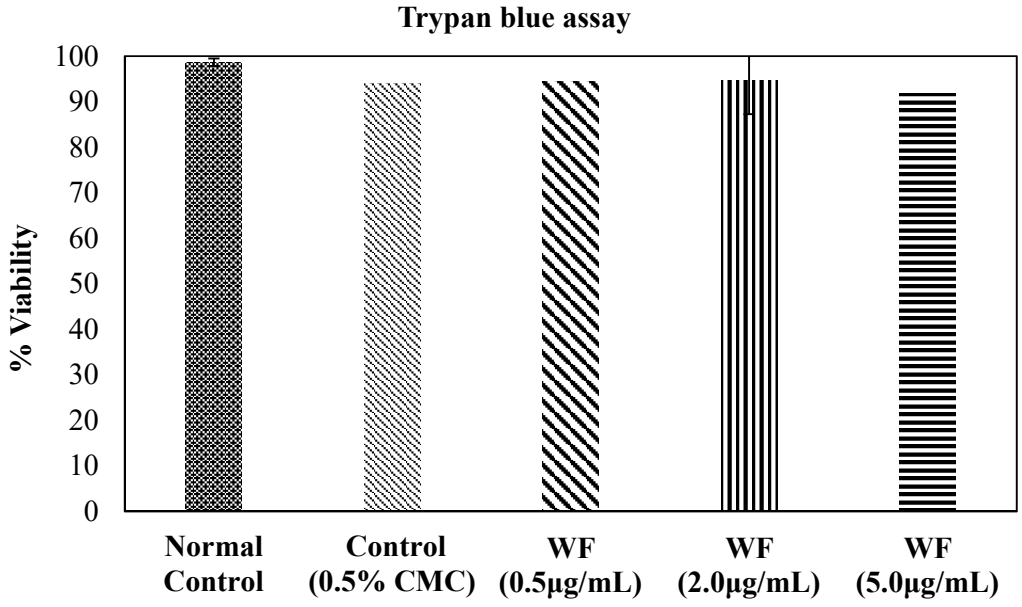

Fig. 4.41 Trypan blue exclusion assay of weaning formula

4.8 Modelling of moisture sorption isotherm and its thermodynamic properties for weaning formula

4.8.1 Moisture sorption isotherms

The moisture adsorption isotherms of the weaning formula were generated at the three different temperatures 20, 30 and 40°C in the water activity (a_w) range of 0.11-0.90. The EMC's of samples at different temperatures were plotted against a_w to obtain a sorption isotherm (Fig. 4.42). The sorption isotherms demonstrated an increase in equilibrium moisture content with increase in water activity, at constant temperature and were sigmoid in shape which showed the characteristics of amorphous materials rich in hydrophilic components [5]. It was also reported that at low and intermediate water activities, known as the multilayer sorption region, moisture content increases linearly with a_w, whereas at high water activity levels, the capillary condensation region, water content rapidly increases with a_w. This nature of the isotherms at low water activities was due to the strong physical sorption on the active sites of proteins since water can be sorbed only to surface –OH sites of crystalline sugar. Moreover, at intermediate a_w, sorption takes place at the less active site where gradual dissolution of sugar leads to a complete elimination of sugars in solutions at a high-water activity [43].

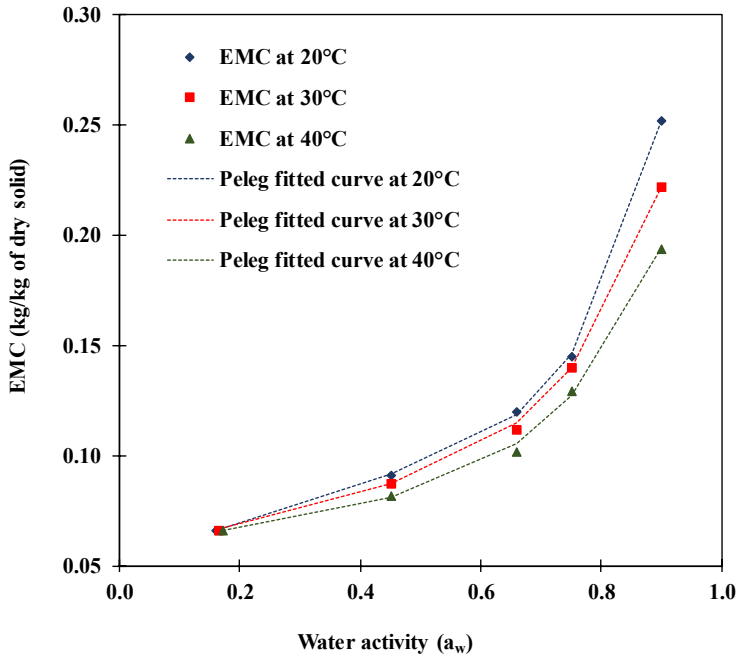

Fig. 4.42 Moisture sorption isotherms of weaning formulation at different temperature showing the fitted curve of Peleg model

The sorption isotherm of the developed weaning formula followed the type-II BET classification shape or a sigmoidal curve which may be due to the high protein content in the formula. The moisture sorption isotherm of a composite weaning formula (Ghavidel & Prakas, 2010) at 25°C represented type-II sorption isotherm, which was prepared from germinated legumes, cereals, vegetables and milk. Similarly, Manoj Kumar [64] estimated the moisture adsorption isotherms of barley-pearl millet-milk based complementary food, generated at the three different temperatures i.e. 28, 37 and 45°C in the a_w range of 0.11-0.92 and found that isotherms resembled type-II according to BET classification.

4.8.2 Temperature dependence of the sorption isotherms

The study of the temperature effect on the sorption isotherm is essential since food products are exposed to a range of temperatures during storage and processing which causes water activity to change with temperature for the same moisture content. It has been reported that temperature affects the mobility of water molecules and the dynamic equilibrium between vapour and adsorbed phases [43]. From the results of sorption isotherm (Fig. 4.42), it was observed that the equilibrium moisture content decreased with increase in temperature at constant water activity. This was due to the fact that the loss of the hydrogen bonds takes place at a higher temperature or breakaway of some water molecules occurs from their sorption sites due to activation to higher energy levels at elevated temperatures [64]. Moreover, it was observed that the presence of large quantities of crystalline sugar, such as glucose, in dry foods can have a different effect of temperature at high a_w levels [43]. Similar findings have also been reported in the literature of sorption isotherm study of complementary food based on barley-pearl millet-milk [64]. The equilibrium moisture content of whey protein isolate powder (WPI) measured at 4, 20, and 37°C did not show temperature dependence but at 50°C EMC was significantly lower [40]. Lal [59] reported that the pearl millet based mineral fortified complementary food showed decreasing trend of moisture adsorption with an increase in temperature.

4.8.3 Mathematical description of the adsorption isotherms

Five different sorption models viz. GAB; Peleg; Henderson; Smith; and Oswin Model (Eq 3.34-3.38) were selected for the fitting of sorption data at different temperatures. The model parameters and statistical analysis of the fitted experimental data of the weaning formula on moisture sorption models are summarized in Table 4.25. The models with minimum *SSE* and maximum R^2 were considered to be the best fit. According to the statistical model indices (R^2 and SSE), the GAB and Peleg model adequately described the experimental data

for developed weaning food. However, the Peleg model was proved to be best fitted among the five selected models with highest R^2 values of greater than 0.998 and low SSE and RMSE.

Table 4.25 Isotherm model parameters with their statistical performance parameters

Model	T (°C)	Model Parameters				R^2	SSE ($x10^{-3}$)	RMSE ($x10^{-2}$)
GAB	20	M_0=0.0516	C= 41.350	K= 0.8559		0.982	0.3	1.15
	30	M_0=0.0512	C= 41.100	K= 0.8185		0.972	0.3	1.19
	40	M_0= 0.0462	C= 90.280	K= 0.9148		0.975	0.5	1.62
Peleg	20	k_1= 0.1153	n_1= 0.3028	k_2= 0.2875	n_2= 6.826	0.998	0.0	0.20
	30	k_1= 0.1040	n_1= 0.2491	k_2= 0.2194	n_2= 5.664	0.997	0.0	0.28
	40	k_1= 0.0890	n_1= 0.1696	k_2= 0.1812	n_2= 5.041	0.998	0.0	0.43
Henderson	20	A= 16.540	B= 1.368			0.915	1.8	2.42
	30	A= 27.310	B= 1.577			0.918	1.2	2.01
	40	A= 49.020	B= 1.791			0.904	1.0	1.80
Smith	20	A= 0.0385	B= -0.087			0.967	0.7	1.50
	30	A= 0.0436	B= -0.074			0.978	0.3	1.03
	40	A= 0.0466	B= -0.061			0.977	0.2	0.87
Oswin	20	A= 0.0977	B= 0.4185			0.975	0.5	1.33
	30	A= 0.0956	B= 0.3719			0.976	0.3	1.08
	40	A= 0.0903	B= 0.3348			0.968	0.3	1.04

The Peleg model is an empirical double power law model (sigmoidal isotherm) that assumes sorption comprises two mechanisms: (i) the sorption rate decreases with the lowering of a_w and (ii) at higher a_w values, free condensation increases [9]. The model was developed to evade the assumption of the BET and GAB models i.e. a specific monolayer moisture content. The Peleg model parameters (K_1 and K_2) decreased as the storage temperature increased. The value of K_2 was 2.04-2.5 times more than the value of K_1. The value of K_1 parameter corresponding to the equilibrium moisture content at lower a_w (0.159-0.660 in the present study) and the values K_2 was close to the equilibrium moisture content for higher a_w (> 0.660 in the present study). The predicted value by Peleg model is presented in Fig. 4.42. The information on monolayer moisture (M_o) of GAB model is essential because it indicates the amount of water that is strongly adsorbed in specific sites, and it is considered to be the value at which a food product is the most stable. It ensures that no associated reaction occurs if the moisture content of foods remains below M_0 since it indicates a strong binding potency of water on the surface [5]. This M_0 parameter was observed to vary between 0.0516 – 0.0462

and it decreased with increase in storage temperature which could be attributed to the activation to higher energy levels at elevated temperatures. It also corresponded to the equilibrium moisture content (5.16-4.62% (db)) at lower a_w (0.159 in the present study). Manoj Kumar [64] reported the adsorption isotherm of barley-pearl millet-milk based mineral fortified complementary food and found that the GAB model was the best fit. Both BET and GAB model showed a decrease in M_0 value with a higher temperature at 28, 37 and 45°C. The similar decreasing trend was observed for fufu flour and tapioca grits [3, 86]. The decreasing trend of monolayer moisture content could be attributed to the fact that increased storage temperature caused a reduction in number of active sorption sites (the sorption capability) of powdered material due to physical and chemical damage. Monolayer moisture is a measure of available active sorption sites for adsorption of water by food materials and it is an essential parameter to attain minimum quality loss in most foods during long storage time [77]. Therefore, from the microbiological point of view, it can be concluded that the safest water activity of food material should correspond to the monolayer moisture content.

The GAB model which is semi-empirical in nature and has been suggested to be the most versatile sorption model which describes sorption behaviour of almost all foods [5]. Therefore, parameters of both the best-fitted model i.e. Peleg model and GAB model were taken for thermodynamic analysis of weaning formula.

4.8.4 Thermodynamic properties

4.8.4.1 Net Isosteric heat of sorption and sorption entropy

The differential heat of sorption is very important since it is an important parameter when designing equipment for dehydration processes. The net isosteric heat (q_{st}) is defined as the heat in excess of the latent heat of vaporization of pure water [1] and it measures the forces for binding energy between water vapour molecules and the solids [77]. Effect of equilibrium moisture content on the net isosteric heat of sorption of weaning formula estimated using Peleg and GAB models are shown in Fig.4.43. From the result, a strong dependency of the net isosteric heat of sorption on EMC was observed as the sorption heat was significantly more at lower moisture content, however, it decreased gently to approach the latent heat of vaporization of pure water (q_{st}=0) as the moisture content increased. A similar trend was also observed for sorption entropy for the weaning food in this study. This could be attributed to the strong interactions between the water molecules and the hydrophilic groups of the food solid such as sugars and protein present in the weaning

formula. The decrease in the isosteric heat with higher amounts of sorbed water was explained by considering the fact that initially sorption occurs on the most active available sites which give rise to high interaction energy [98]. As these sites become occupied, sorption occurs on the less active ones, leading to lower heats of sorption. At high water content, it tilts towards the heat of condensation of pure water [31]. Similar findings were reported for sorghum-based complementary foods [1].

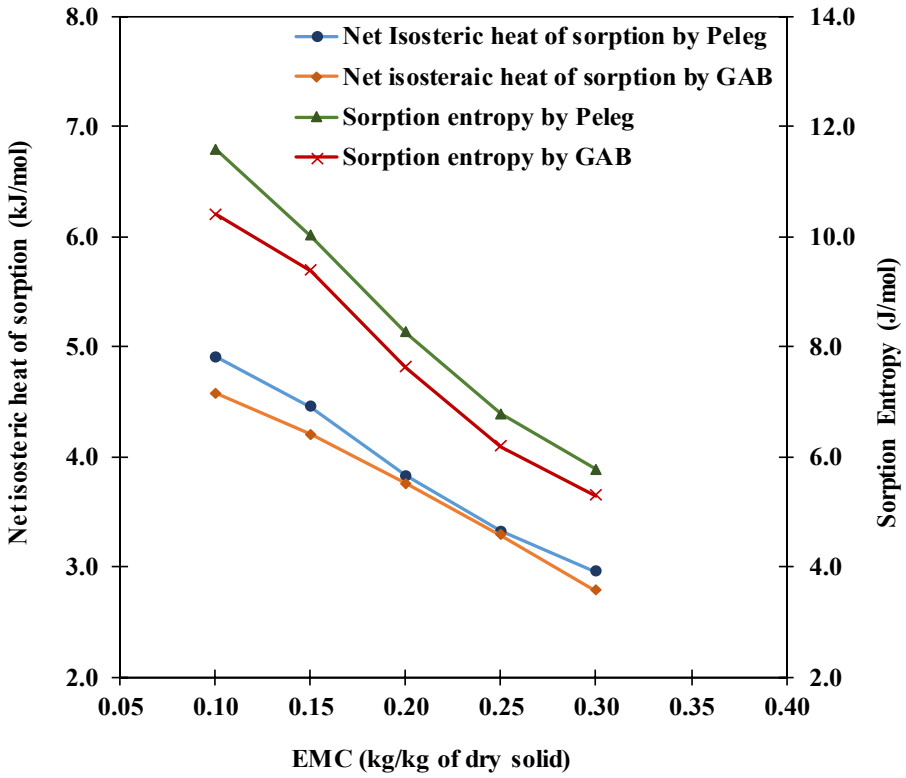

Fig. 4.43 Effect of EMC on the net isosteric heat of sorption and sorption entropy of weaning formulation estimated using Peleg and GAB models output.

The values of net isosteric heat of sorption and sorption entropy were found to be slightly higher (less than 10%) based on Peleg model parameters as compare to GAB model parameters. The values of net isosteric heat of sorption and sorption entropy were assumed to more accurate when estimated based on Peleg model parameters because this model described better to the experimental data.

As reported by Goula [43] the net isosteric heat of sorption is dependent upon EMC. The effect of EMC on the heat of sorption was fitted by Eq. 4.8 and 4.9 for Peleg Model (R^2= 0.994) and GAB model (R^2= 0.985) respectively.

$$q_{st} = 6.428 \exp(-\frac{X}{0.328}) \qquad \text{Eq. (4.8)}$$

$$q_{st} = 5.917 \exp(-\frac{X}{0.419}) \quad \text{Eq. (4.9)}$$

where X is the moisture content in % dry basis and q_{st} is the net isosteric heat of sorption in kJ/mol. Similar effects of moisture content on the heat of sorption were reported by other fruits and vegetables such as for yellow globe onion, sultana raisins, dried currants, figs, prunes, and apricots [65, 88, 96]. The reason for the rapid increase in q_{st} at low EMC may be that there are highly active polar sites on the surface of the food material in the initial stages of sorption, which are covered with water molecules to form a monomolecular layer.

4.8.4.2 Enthalpy-Entropy Compensation Parameters

From the straight lines calculated by Eq. (3.43) at different moisture contents the values of ΔS were obtained (Fig. 4.44). The results showed a strong dependence of differential entropy on moisture content with an exponential trend similar to that exhibited by differential enthalpy. This observation is similar to that obtained by [5] Al-Muhtaseb et al. (2004b), who studied the water sorption thermodynamic properties of the starch powder. A plot of enthalpy versus entropy showed a linear correlation:

For Peleg Model $\Delta q_{st} = 338.12\,\Delta S + 1025.6$ Eq. (4.10)

For GAB Model $\Delta q_{st} = 331.30\,\Delta S + 1145.6$ Eq. (4.11)

As the law of compensation could be applied in the range of moistures studied, the results were correlated in accordance with Eq. (4.10 and 4.11) and the isokinetic temperature of sorption was found to be T_B = 338.12 K and 331.30 K for Peleg and GAB Model respectively. Based on these two values the range of isokinetic temperature may be taken as 58-65°C. The harmonic mean temperature was calculated as T_{hm} = 303 K, a value significantly different from the value of T_B, confirming the suitability of the isokinetic theory for water sorption in the developed weaning formula and since $T_B > T_{hm}$, the process can be characterized as enthalpy driven.

4.8.4.3 The Gibb's free energy change

The variation in Gibb's free energy change (ΔG) with respect to equilibrium moisture content at three temperature levels during adsorption is shown in Fig. 4.45. The graph clearly demonstrated that the ΔG decreased exponentially for both GAB and Peleg model with increasing EMC which indicated that water adsorption was a spontaneous phenomenon. The higher ΔG values in food materials can be described by the fact that

components of food material are hydrophilic in nature that show a greater affinity to water sorption [104]. Moreover, from the graph, it was also observed that the ΔG value decreased with increase in storage temperature for both GAB and Peleg model at a specific moisture content which may be related to greater energy required in making sorption sites available. Hence, it may be concluded that water binding potential is higher at a lower temperature. Moreover, it was also reported that moisture content has greater influence on ΔG when the moisture content is less than the monolayer moisture content (Mo) [104].

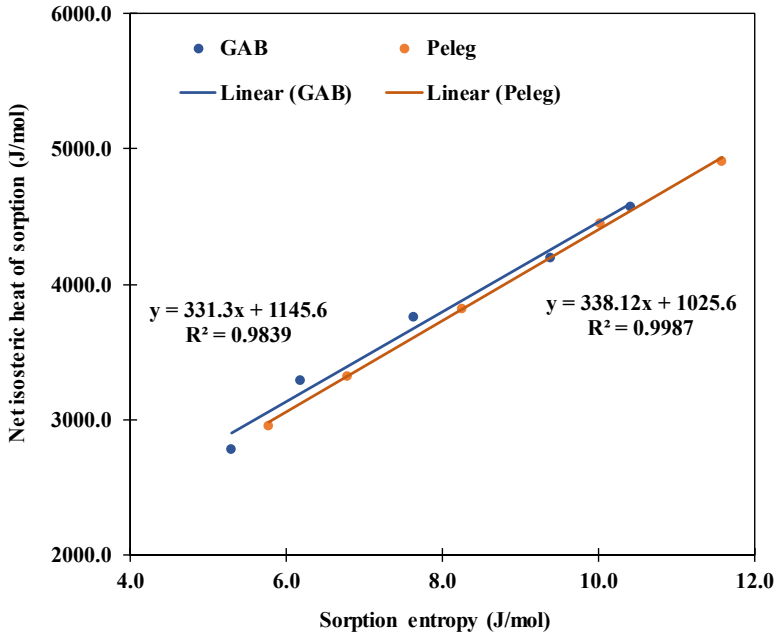

Fig. 4.44 A plot of the net isosteric heat of sorption against the sorption entropy

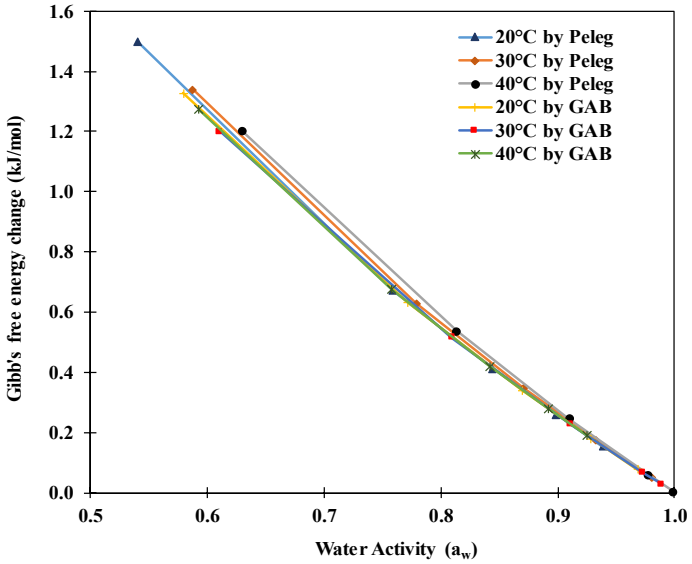

Fig. 4.45 Gibb's free energy change during sorption of moisture in weaning formulation at different temperatures estimated using Peleg and GAB models output

4.9 The sensory attributes and quality evaluation of the weaning formula

4.9.1 Sensory evaluation of the weaning formula

The sensory evaluation determines the organoleptic properties of the food sample. In this study the sensory evaluation of two formulation i.e. developed weaning formula and a commercialized formula (Bhim Shakti) was aby 30 trained and semi trained panellists. The weaning food was reconstituted with warm water based on the optimal solid water ratio obtained in this study while the commercialized formula was reconstituted based on the instructions given in the pack. The samples were provided at room temperature to the panellist.

The results obtained from the sensory evaluation of the reconstituted weaning formula using a 9-point hedonic scale are shown in Fig. 4.46. The attributes evaluated were taste, aroma, consistency and overall acceptability. From the web graph it was observed that all the attributes showed higher rating in case of the developed weaning formula as compared to the commercialized (marketed) formula. Thus, the scores obtained for the sensory attributes showed that the formulated blends were highly acceptable and indicated that the functional properties of the food ingredients used in the blends were very much compatible. Similar observations on sensory evaluation were also observed for a weaning mix based on malted and extruded pearl millet and barley [16]. Bolarinwa et al. [21] reported that malted cereals reduced the viscosity and increased the solubility of the gruel. The gruel produced from 50% malted millet had the most preferred sensory attributes in terms of colour, flavour, mouth feel, appearance and overall acceptability. Moreover, incorporation of malted cereals increases the taste of the product due to the production of sugar during malting [76].

4.9.2 Quality evaluation of developed weaning formula

Peroxide value (PV) and free fatty acid (FFA)

The major constituents of developed weaning formula were starch, sugar, protein and fat. Among these constituents, the fat is more susceptible towards development of off flavour during storage due to oxidation process. Thus, the present study was conducted to evaluate the changes in quality parameters viz. free fatty acid (FFA) and peroxide value (PV) during storage. The weaning formula was stored at 40°C in poly pack with thickness of 64 microns and size of 9 cm X 18 cm and the peroxide vale and free acid content was determined after every 10 days interval up to 30 days. The peroxide value indicates the extent of oxidation in a sample (Table 4.26). Initially the peroxide value of the developed weaning formula was

observed to be 1 meq/kg fat which increased up to 2 meq/kg fat during the 30 days storage. According to FSSAI, the PV of fresh oil should be below 10 meq/kg fat and the peroxide value of the developed weaning formula was well below the recommended value. Similarly, the FFA value of the developed formula was also very low during the storage. Initially the FFA was observed to be 2.80 % which increased only up to 4.24 %. Thus, the low PV and FFA value indicate good quality of the developed weaning formula at high temperature.

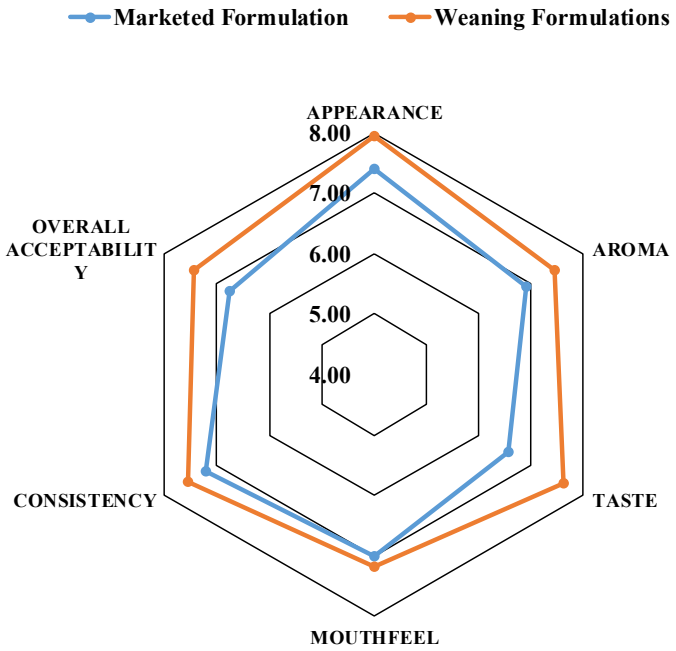

Fig. 4.46 Web plot for sensory evaluation of developed weaning formulations.

Table 4.26 Peroxide value and free fatty acid of developed weaning formula

Storage time (days)	FFA (%)	PV (meq/kg fat)
0	2.80 ±0.46	1.03±0.04
10	3.12± 0.66	1.3± 0.014
20	3.96± 0.33	1.59± 0.17
30	4.24± 0.06	2.05±0.07

Bibliography

[1] Abraham, S. I., Charles, A. C., Oneh, A. J., and Iorwuese, G. D. Moisture adsorption and thermodynamic properties of sorghum-based complementary foods. *International Journal of Food Engineering and Technology*, 2:26-33, 2016.

[2] Adebowale A. A, Sanni S. A, Karim O. R, Ojoawo J. A. Malting characteristics of Ofada rice: chemical and sensory qualities of malt from Ofada rice grains. *International Food Research Journal,* 17:83-88, 2010.

[3] Adebowale, A. S. Effect of cassava varieties on the sorption isotherm of tapioca grits. International Journal of Food Science and Technology, 42:448-452, 2007.

[4] Almeida, M.R., Alves, R.S., Laura B. L. R. N., Stephani, Poppi, R., & de Oliveira, R.J. Determination of amylose content in starch using Raman spectroscopy and multivariate calibration analysis. *Analytical and. Bioanalytical Chemistry,* 397:2693–2701, 2010.

[5] AL-Muhtaseb, A., McMinn, W., and Magee, T. Moisture sorption isotherm characteristics of food products: A review. *Trans IChemE*, 80:118-128, 2002.

[6] American Type Culture Collection. XTT Cell Proliferation Assay Kit, Instruction Manual Catalog Number 30-1011K.

[7] AOAC: Official Methods of Analysis. *Associate of Analytical Chemists,* Washington DC, UK, 1990.

[8] Araujo-Andrade, C., Ruiz, F., Martínez-Mendoza, J. R., & Terrones, H. Infrared and Raman spectra, conformational stability, ab initio calculations of structure, and vibrational assignment of α and β glucose. *Journal of Molecular Structure: THEOCHEM*, 714:143-146, 2005.

[9] Arthur, E. T. Evaluation of theoretical and empirical water vapor sorption isotherm models for soils. *Water Resources Research*, 52:190-205, 2016.

[10] Asante, E., Adjaottor, A. A., and Woode, M. Y. Malting characteristics of *Wita 7* variety of rice. *Peak Journal of Food Science and Technology,* 1:61-67, 2013.

[11] Ashogbon, A.O., and Akintayo, E.T. Morphological, functional and pasting properties of starches separated from rice cultivars grown in Nigeria. *International Food Research Journal*, 19:665-671, 2012.

[12] Association of Official Analytical Chemists. *Official methods of analysis*., Washington DC, 1990.

[13] Atichokudomchai, N., Jane, J. L., & Hazlewood, G. Reaction pattern of a novel thermostable α-amylase. *Carbohydrate polymers*, 64:582-588, 2006.

[14] Ayernor, G. S., and Ocloo, F. C. K. Physico-chemical changes and diastatic activity associated with germinating paddy rice (PSB.Rc 34). *African Journal of Food Science,* 1:037-041, 2007.

[15] Bail, L.P., Bizot, H., Ollivon, M., Keller, G., Bourgaux, C., Buleon, A. Monitoring the crystallization of amylose–lipid complexes during maize starch melting by synchrotron X-Ray diffraction. *Biopolymers*, 50:99–110, 1999.

[16] Balasubramanian, S., Kaur, J., and Singh, D. Optimization of weaning mix based on malted and extruded pearl millet and barley. *Journal of Food Science and Technology*, 51:682–690, 2014.

[17] Barth, A. Infrared spectroscopy of proteins. *Biochimica et Biophysica Acta*, 1767:1073–1101, 2007.

[18] Barthakur, N. N., and Arnold, N. P. Chemical evaluation of Musa 'Bhimkol' as a Baby Food. *Journal of the Science of Food and Agriculture*, 53:497-504, 1990.

[19] Bas, D., Dudak, F. C., and Boyacı, I. H. Modeling and optimization III: Reaction rate estimation using artificial neural network (ANN) without a kinetic model. *Journal of Food Engineering*, 79: 622–628, 2007.

[20] Bijttebier, A., Goesaert, H., & Delcour, J.A. Hydrolysis of amylopectin by amylolytic enzymes: structural analysis of the residual amylopectin population. *Carbohydrate Research*, 345:235–242, 2010.

[21] Bolarinwa, I. F., Olajide, J. O., Oke, M. O., Olaniyan, S. A., and Grace, F. Production and quality evaluation of complementary food from malted millet, plantain and soybean blends. *International Journal of Scientific and Engineering Research*, 7:663-674, 2016.

[22] Briggs, D., Hough, J., Stevens, R., and Young, T. *Malting and Brewing Science: Malt and Sweet Wort, Volume 1*, London, United Kingdom: Chapman and Hall, 1981.

[23] Bureau of Indian Standards. 2nd revision. New Delhi: Government of India, 1985.

[24] Cael, J. J., Koenig, J. L., & Blackwell, J. Infrared and raman spectroscopy of carbohydrates: Part IV. Identification of configuration-and conformation-sensitive modes for D-glucose by normal coordinate analysis. *Carbohydrate Research*, 32:79-91, 1974.

[25] Capanzana, M. V., and Buckle, K. A. Optimisation of Germination Conditions by Response Surface Methodology of a High Amylose Rice (*Oryza sativa*) Cultivar. *Lebensm.-Wiss. u.-Technol,* 30:155–163, 1997.

[26] Carolina, S., and Almeida, M. A. Physicochemical properties, modifications and applications of starches from different botanical sources. *Food Science and Technology*, 35:215-236, 2015.

[27] Chinma, C.E., Adewuyi, O., and Abu, J.O. Effect of germination on the chemical, functional and pasting properties of flour from brown and yellow varieties of tigernut (Cyperusesculentus). *Food Research International*, 42:1004–1009, 2009.

[28] Christian, M., Edwards, C., and Weaver, L. T. Starch digestion in infancy. *Journal of pediatric gastroenterology and nutrition*, 29:116-124, 1999.

[29] Claver, I. P., Zhang, H., Li, Q., Zhu, K., and Zhou, H. Impact of the soak and the malt on the physicochemical properties of the sorghum starches. *International Journal of Molecular Sciences,* 11:3002-3015, 2010.

[30] Cornejo, F., and Rosell, C. M. Influence of germination time of brown rice in relation to flour and gluten free bread quality. *Journal of Food Science and Technology*, 52:6591–6598, 2015.

[31] Correa, P. C., Goneli, A. L., Junior, P. C., de Oliveira, G. H., and Valente, D. S. Moisture sorption isotherms and isosteric heat of sorption of coffee in different processing levels. *International Journal of Food Science and Technology*, 45:2016-2022, 2010.

[32] Damodaran, S., Parkin, K. L., and Fennema, O. R. *Food chemistry* (4th ed.). Unites States: CRC press, 2007.

[33] de Wijk, R. A., Prinz, J. F., Engelen, L., and Weenen, H. The role of a-amylase in the perception of oral texture and flavour in custards. *Physiology and Behavior*, 83:81 – 91, 2004.

[34] Dlamini, N. S., and Solomon, W. K. Effect of ingredients ratio on physicochemical and sensory properties of sorghum, maize and soya protein concentrate blend extrudates. *International Journal of Food Science and Nutrition Engineering*, 6:112-120, 2016.

[35] Dziedzoave, N. T., Graffham, A. J., Westby, A., and Komlaga, G. Comparative assessment of amylolytic and cellulolytic enzyme activity of malts prepared from tropical cereals. *Food Control,* 21:1349–1353, 2010.

[36] Eliasson, A.-C and Ljunger, G. Interactions between amylopectin and lipid additives during retrogradation in a model system. *Journal of Food and Agriculture*, 44:353–361, 1988.

[37] Falade, K.O., and Christopher, A. S. Physical, functional, pasting and thermal properties of flours and starches of six Nigerian rice cultivars. *Food Hydrocolloids*, 44:478-490, 2015.

[38] Fan, D., Ma, W., Wang, L., Huang, J., Zhao, J., Zhang, H., & Chen, W. Determination of structural changes in microwaved rice starch using Fourier transform infrared and Raman spectroscopy. *Starch*, 64:598–606, 2012.

[39] FAO/WHO (1973). Ad Hoc Expert Committee, Energy and Protein Requirements, *WHO Technical Report Series, No. 522*; *FAO Nutrition Meetings Report Series, No. 52*; WHO, Geneva; FAO, Rome, Italy.

[40] Foster, K. D., Bronlund, J. E., and Paterson, A. The prediction of moisture sorption isotherms for dairy powders. *International Dairy Journal*, 15:411-418, 2005.

[41] Ganesan, V., Rosentrater, K., and Muthukumarappan, K. Flowability and handling characteristics of bulk solids and powders – a review with implications for DDGS. *Biosystems Engineering*, 101:425–435, 2008.

[42] Ghavidel, R. A., and Prakas, J. Composite weaning mixes: Formulation and quality characteristics. *Food Science and Technology Research*, 16:65-70, 2010.

[43] Goula, A. M., Karapantsios, T. D., Achilias, D. S., and Adamopoulos, K. G. Water sorption isotherms and glass transition temperature of spray dried tomato pulp. *Journal of Food Engineering*, 85:73-83, 2008.

[44] Griffith, L., and Castell-Perez, M. Effects of roasting and malting on physicochemical properties of select cereals and legumes. *Cereal Chemistry*, 75:780–784, 1998.

[45] Houghs, J. S., Briggs, D. E and Stevens, R. *Malting and brewing science*. Chapman and Hall Ltd, London, 1982.

[46] Ibrahim, M., Alaam, M., El-Haes, H., Jalbout, A.F., & Leon, A. Analysis of the structure and vibrational spectra of glucose and fructose. *Ecletica Quimica*, 3:15-21, 2006.

[47] Iizuka, K., & Aishima, T. J. Starch gelation process observed by FT-IR/ATR spectrometry with multivariate data analysis. *Journal of Food Science*, 64:653-658, 1999.

[48] Ikujenlola, V. A., and Fashakin, J. B. The physico-chemical properties of a complementary diet prepared from vegetable proteins. *Journal of Food, Agriculture and Environment*, 3:23-26, 2005.

[49] Jang, E-H., Lee, S-J., Hong, J-Y., Chung, H-J., Lee, Y-T., Kang, B-S., and Lim, S-T. Correlation between physicochemical properties of japonica and indica rice starches. *LWT - Food Science and Technology*, 66:530-537, 2016.

[50] Jinapong, N., Suphantharika, M., and Jamnong, P. Production of instant soymilk powders by ultrafiltration, spray drying and fluidized bed agglomeration. *Journal of Food Engineering*, 84:194–205, 2008.

[51] Jirapa, P., Normah, H., Zamaliah, M. M., Asmah, R., and Mohamad, K. Nutritional quality of germinated cowpea flour (Vigna unguiculata) and its application in home prepared powdered weaning foods. *Plant Foods for Human Nutrition*, 56:203–216, 2001.

[52] Juhasz, R., Gergely, S., Gelencser, T., & Salgo, A. Relationship between NIR spectra and RVA parameters during wheat germination. Cereal Chemistry, 82:488-493, 2005.

[53] Juliano, B. O., Perez, C. M., Blakeney, A. B., Castillo, D. T., Konngseree, N., Laignelet, B., et al. International Cooperative Testing on the Amylose Content of Milled Rice. *Starch/ Staerke,* 33:157-162, 1981.

[54] Kalita, D., Sarma, B., & Srivastava, B. Influence of germination conditions on malting potential of low and normal amylose paddy and changes in enzymatic activity and physico chemical properties. *Food Chemistry,* 220:67–75, 2017.

[55] Kapoor, R., and Metzger, L. E. Small-scale manufacture of process cheese using a rapid visco analyzer. *Journal of Dairy Science,* 88:3382-3391, 2005.

[56] Kizil, R., Irudayaraj, J., & Seetharaman, K. Characterization of irradiated starches by using FT-Raman and FTIR spectroscopy. *Journal of Agricultural and Food Chemistry*, 50:3912-3918, 2002.

[57] Kong, X., Zhu, P., Sui, Z., and Bao, J. Physicochemical properties of starches from diverse rice cultivars varying in apparent amylose content and gelatinisation temperature combinations. *Food Chemistry*, 172:433–440, 2015.

[58] Labuschagne, M., Phalafala, L., Osthoff, G., and van Biljon, A. The influence of storage conditions on starch and amylose content of South African quality protein maize and normal maize hybrids. *Journal of Stored Products Research*, 56:16-20, 2014.

[59] Lal, M. D. Conventional empirical modelling of moisture sorption isotherms of 'Nutrimix' powder. *Research Journal of Animal Husbandry and Dairy Science*, 4:54-57, 2013.

[60] Lamsal, B., Jung, S., and Johnson, L. Rheological properties of soy protein hydrolysates obtained from limited enzymatic hydrolysis. *LWT — Food Science and Technology*, 40:1215–1223, 2007.

[61] Mahasukhonthachat, K., Sopade, P., and Gidley, M. Kinetics of starch digestion in sorghum as affected by particle size. *Journal of Food Engineering*, 96:18–28, 2010.

[62] Mahgoub, S. Production and evaluation of weaning foods based on sorghum and legumes. *Plant Foods for Human Nutrition*, 54:29–42, 1999.

[63] Man, J., Yang, Y., Huang, J., Zhang, C., Zhang, F., Wang, Y., Gu, M., Liu, Q., & Wei, C. Morphology and structural properties of high-amylose rice starch residues hydrolysed by amyloglucosidase. *Food Chemistry*, 138:2089–2098, 2013.

[64] Manoj Kumar, C., Raju, P. N., and Singh, A. K. Barley-pearl millet-milk based mineral fortified complementary food: moisture adsorption isotherms. *Indian Journal of Dairy Science*, 68:218-222, 2015.

[65] Mazza, G. L. Water sorption properties of yellow globe onion. *Canadian Institute of Food Science and Technology Journal*, 11:189-193, 1978.

[66] Mohan, B. N., Malleshi, N. G., and Koseki, T. Physico-chemical characteristics and non-starch polysaccharide contents of *Indica* and *Japonica* brown rice and their malts. *LWT - Food Science and Technology,* 43:784–791, 2010.

[67] Moongngarm, A., and Saetung, N. Comparison of chemical compositions and bioactive compounds of germinated rough rice and brown rice. *Food Chemistry,* 122:782–788, 2010.

[68] Morrison, W. R., and Azudin, M. N. Variation in the amylose and lipid contents and some physical properties of rice starches. *Journal of Cereal Science*, 5:35–44, 1987.

[69] Mouquet, C., and Treche, S. Viscosity of gruels for infants: a comparison of measurement procedures. *Journal of Food Sciences arid Nutrition*, 52:389-400, 2001.

[70] Muralikrishna, G., & Nirmala, M. Cereal α-amylases—an overview. *Carbohydrate Polymers*, 60:163–1, 2005.

[71] Musa, A. S. N., Umar, I. M., and Ismai, M. (). Physicochemical properties of germinated brown rice (*Oryza sativa* L.) starch. *African Journal of Biotechnology,* 10:6281-6291, 2011.

[72] Nelles, E. M., Dewar, J., Bason, M. L., and Taylor, J. R. N. Maize starch biphasic pasting curves. *Journal of Cereal Science*, 31:287-294, 2000.

[73] Noda, T., Nishiba, Y., Sato, T., and Suda, I. Properties of Starches from Several Low-Amylose Rice Cultivars. *Cereal Chemistry*, 80:193–197, 2003.

[74] Nonogaki, H., Bassel, G. W., and Bewley, J. D. Germination—Still a mystery. *Plant Science,* 179:574–581, 2010.

[75] Olugbile, A. O., Obadina, A. O., Atanda, A. O., Omemu, O. B., and Olatope, S. O. A. Physicochemical Changes and Diastatic Activity Associated with Germination of 'Boromo', a Paddy Rice Variety from Western Nigeria. Journal of Food Processing and Preservation, 39:116-122, 2015.

[76] Onyeka, U., and Dibia, I. (2002). Malted weaning food made from maize, soybean, groundnut and cooking banana. Journal of the Science of Food and Agriculture, 82:513-516, 2002.

[77] Owo, H., Adebowale, A., Sobukola, O., Obadina, O., Kajihausa, O., Adegunwa, M., . . . Tomlins, K. Adsorption isotherms and thermodynamics properties of water yam flour. *Quality Assurance and Safety of Crops and Foods*, 9:221-227, 2017.

[78] Park, I-M., Ibanez, A.M., Zhong, F., and Shoemaker, C.F. Gelatinization and pasting properties of waxy and non-waxy rice starches. *Starch*, 59:388–396, 2007.

[79] Patindol, J., Gu, X., and Wang, Y-J. Chemometric analysis of the gelatinization and pasting properties of long-grain rice starches in relation to fine structure. *Starch*, 61:3–11, 2009.

[80] Prakash, S., Ma, Q., and Bhandari, B. Rheological behaviour of selected commercially available baby formulas in simulated human digestive system. *Food Research International*, 64:889–895, 2014.

[81] Quadir, N., Wani, S. A., Bhat, B. A., Wani, T. A., and Quraazah, A. Germination Behavior of Some Kashmiri Paddy Cultivars. *Journal of Chemical, Biological and Physical Sciences,* 2:1820-1829, 2012.

[82] Recommended Dietary Allowances: Subcommittee on the Tenth Edition of the RDAs Food and Nutrition Board Commission on Life Sciences National Research Council, National Academy Press, Washington, D.C, 1989.

[83] Rygula, A., Majzner, K., Marzec, K.M., Kaczor, A., Pilarczyka, M., & Baranskaa, M. J. Raman spectroscopy of proteins: a review. *Journal of Raman Spectroscopy*, 44:1061–1076, 2013

[84] Sajilata, G., Singhal, R. S., and Kulkarni, P. R. Weaning foods: A review of the Indian experience. *Food and Nutrition Bulletin*, 23:208-226, 2002.

[85] Saman, P., Vazquez, J. A., and Pandiella, S.S. Controlled germination to enhance the functional properties of rice. *Process Biochemistry*, 43:1377–1382, 2008.

[86] Sanni, L. A. Moisture sorption isotherms of fufu and tapioca at different temperatures. *Journal of Food Engineering*, 34:203-212, 2007.

[87] Saqib, A. A. N., and Whitney, P. J. Differential behaviour of the dinitrosalicylic acid (DNS) reagent towards mono- and di-saccharide sugars. *Biomass and Bioenergy,* 35:4748- 4750, 2011.

[88] Saravacos, G. D. Effect of temperature on the water adsorption isotherms of Sultana raisins. *Journal of Food Science*, 51:381-383, 1986.

[89] Schuster, K.C., Ehmoser, H., Gapes, J.R., & Lendl, B. On-line FT-Raman spectroscopic monitoring of starch gelatinisation and enzyme catalysed starch hydrolysis. *Vibrational Spectroscopy*, 22:181–190, 2002.

[90] Scudiere, D. A., Shoemaker, R. H., and Paul, K. D. Evaluation of a soluble tetrazolium/formazan assay for cell growth and drug sensitivity in culture using human and other tumor cell lines. *Cancer Research*, 48:4827-4833, 1988.

[91] Sharma, P., Gujral, H. S., and Rosell, C. M. Effects of roasting on barley b-glucan, thermal, textural and pasting properties. *Journal of Cereal Science*, 53:25-30, 2011.

[92] Singh, J., Kaur, L., and Singh, H. Food microstructure and starch digestion. *Advances in Food and Nutrition Research*, 70:138-173, 2013.

[93] Sun, J., Wu, D., Xu, J., Rasmussen, S.K., and Shu, X. Characterisation of starch during germination and seedling development of a rice mutant with a high content of resistant starch. *Journal of Cereal Science,* 62:94-101, 2015.

[94] Sun, Q., Gong, M., Li, Y., and Xiong, L. Effect of dry heat treatment on the physicochemical propertiesand structure of proso millet flour and starch. *Carbohydrate Polymers*, 110:128–134, 2014.

[95] Tian, B., Xie, B, Shi, J., Wua, J., Cai, Y., Xu, T., Xue, S., and Deng, Q. Physicochemical changes of oat seeds during germination. *Food Chemistry,* 119:1195–1200, 2010.

[96]. Tsami, E. Net isosteric heat of sorption in dried fruits. Journal of Food Engineering, 14:327–335, 1991

[97] Varavinita, S., Shobsngob, S., Varanyanond, W., Chinachotid, P., and Naivikule, O. Effect of amylose content on gelatinization, retrogradation and pasting properties of flours from different cultivars of Thai rice. *Starch*, 55:410–415, 2003.

[98] Wang, N. B. Moisture sorption isotherms characteristics of potatoes at four temperatures. *Journal of Food Engineering*, 14:269-282, 1991.

[99] Warren, F.J., Gidley, M.J., & Flanagan, B.M. Infrared spectroscopy as a tool to characterise starch ordered structure—a joint FTIR–ATR, NMR, XRD and DSC study. *Carbohydrate Polymers*, 139:35-42, 2016.

[100] Woo, H.-D., We, G.N., Kang, T.-Y., Shon, K.H., Chung, H.-W., Yoon, M.-R., Lee, J.-S. and Ko, S. Physicochemical and gelatinization properties of starches separated from various rice cultivars. *Journal of Food Science*, 80:2208-2216, 2015.

[101] Wu, F., Chen, H., Yang, N., Wang, J., Duan, X., Jin, Z., and Xu, X. Effect of germination time on physicochemical properties of brown rice flour and starch from different rice cultivars. *Journal of Cereal Science,* 58:263-271, 2013.

[102] Yang, Y., & Tao, W.-Y. Effects of lactic acid fermentation on FT-IR and pasting properties of rice flour. *Food Research International*, 41:937–940, 2008.

[103] Ye, L., Wang, C., Wang, S., Zhou, S., and Liu, X. Thermal and rheological properties of brown flour from Indica rice. *Journal of Cereal Science*, 70:270-274, 2016.

[104] Yogendrarajah, P., Samapundo, S., Devlieghere, F., de Saeger, S., and de Meulenaer, B. Moisture sorption isotherms and thermodynamic properties of whole black peppercorns (Piper nigrum L.). *LWT - Food Science and Technology*, 64:177-188, 2015.

[105] You, S.-Y., Oh, S.-G., Han, H. M., Jun, W., and Chung, H.-J. Impact of germination on the structures and in vitro digestibility of starch from waxy brown rice. *International Journal of Biological Macromolecules*, 82:863–870, 2016.

[106] Yu, S., Ma, Y., Menager, L., and Sun, D.-W. Physicochemical properties of starch and flour from different rice cultivars. *Food Bioprocess Technol, 5*:626–637, 2012.